NATIONAL ADVISORY COMMITTEE FOR AERONAUTICS

WARTIME REPORT

ORIGINALLY ISSUED

April 1946 as
Memorandum Report A6D03

HIGH-SPEED WIND-TUNNEL TESTS OF A TWIN-FUSELAGE PURSUIT AIRPLANE

By Joseph L. Anderson and Victor B. Tkac

Ames Aeronautical Laboratory
Moffett Field, California

NACA

WASHINGTON

MR No. A6D03

NATIONAL ADVISORY COMMITTEE FOR AERONAUTICS

MEMORANDUM REPORT

for the

Air Technical Service Command, U. S. Army Air Forces

HIGH-SPEED WIND-TUNNEL TESTS OF A TWIN-FUSELAGE PURSUIT AIRPLANE

By Joseph L. Anderson and Victor B. Tkac

SUMMARY

At the request of the Air Technical Service Command, U. S. Army Air Forces, a 0.22-scale model of a twin-fuselage pursuit airplane was built and tested at the Ames Aeronautical Laboratory. The tests of this model were made in order that the aerodynamic characteristics of the airplane, especially at high speed, might be predicted.

The results shown in this report consist of force data for the model and critical Mach numbers of parts of the model as determined from pressure-distribution measurements. The results indicate that a diving tendency of the airplane can be expected at Mach numbers above 0.70 at lift coefficients from 0 to 0.4. There is an indication that the Mach number at which the airplane would first experience a diving tendency for lift coefficients from 0 to 0.2 can be increased if the critical speed of the radiator enclosures is increased, and the wing-fuselage-juncture fillets are improved.

INTRODUCTION

At the request of the Air Technical Service Command, U. S. Army Air Forces, a twin-fuselage, twin-engine, pursuit airplane (fig. 1) was built by the Ames Aeronautical Laboratory and tested in the Ames 16-foot high-speed wind tunnel. (See fig. 2.)

The high-speed wind-tunnel tests of the model were desired in order that the stability, control, and performance characteristics of the airplane, particularly in the high-speed range, might be predicted. This report is the first of a series covering the tests and presents the aerodynamic characteristics of the airplane, particularly in the high-speed range, might be predicted. This report is the first of a series covering the tests and presents the aerodynamic characteristics of the model and the critical Mach numbers of various components of the model with the control surfaces fixed in their neutral positions.

DESCRIPTION OF MODEL

The wing of the model had a steel spar covered with mahogany contoured to the wing surface. An aluminum-alloy aileron was mounted in the right wing only. In order that the model could be pitched in the air stream, booms (fig. 3) were attached to the wing spar, one on each outer wing panel. The fuselages consisted of hollow-steel box spars covered with mahogany finished to the fuselage contour. The carburetor air scoops, engine exhaust stacks, radiator ducts, pilots' enclosures, and empennage were removable and replaceable by wooden blocks to form the basic fuselage contour.

The air flowing into the entrances of the carburetor air scoops was ducted to the engine exhaust stacks through which it passed back into the wind-tunnel air stream. The air flowing into the radiator air scoops passed through the radiator ducts and was exhausted out the exits of the ducts. The internal shape of the model radiator ducts was identical to that of the airplane for several inches aft of the entrances and from the hinges of the exit doors to the exits of the ducts. Rakes of pitot tubes were installed in the ducts of the right fuselage so that the flow of air in the ducts might be measured.

All components of the empennage were metal. The two vertical stabilizers and dorsal fins were aluminum-alloy castings; and the horizontal stabilizer, elevator, tab, and the two rudders were machined from wrought aluminum alloy. Two horizontal tails were tested, one with a 20-percent-chord elevator and one with a 32.8-percent-chord elevator. There were no trim tabs in any of the control surfaces except the

32.8-percent-chord elevator.

The airplane armament includes six .50-caliber machine guns submerged in the wing center panel and firing forward between the propellers. Before the guns are fired the gun ports are covered, but the first shot from each gun opens its port. In order to simulate the open gun ports, holes were drilled in the leading edge of the model wing. (See fig. 2.) A scale model of the droppable gas tank was attached to the lower surface of the wing at the center of the span for some of the tests. For other tests, a scale model of an eight-gun nacelle was attached at the same location. From figure 4, a comparison may be made of the relative size and shape of the gas tank and the gun nacelle.

Two sets of wing-fuselage fillets were used. The first set of fillets was developed at the Ames Laboratory and was used for all tests of the model with the 20-percent-chord elevator. The second set, developed by the manufacturer, was used for all tests of the model with the 32.8-percent-chord elevator. Sections of the Ames and manufacturer's fillets are shown at several locations along the wing chord in figure 5.

Pressure orifices (fig. 6) were located only in the right side of the model in the wing surface, empennage surfaces, canopy, and air intakes. Since there was not sufficient room in the mounting struts to take the tubes from the pressure orifices, a pressure-tube strut (fig. 7) extended from the left wing tip to the wind-tunnel wall in order to carry the pressure tubes from the model to the manometers. This strut was used only during the pressure-distribution tests and was removed during the force tests.

Pertinent dimensions of the 0.22-scale model and the airplane are as follows:

Wing	Model	Airplane
Area, sq ft	19.774	408.550
Span, ft	11.270	51.230
Aspect ratio	6.440	6.440
Mean aerodynamic chord, ft	1.809	8.221

	Model	Airplane
Section profile		
Root	NACA 66,2-215 (a=0.6)	
Tip	NACA 66,1-212 (a=0.6)	
Horizontal tail plane		
Area, sq ft	3.194	66.000
Distance between quarter-chord point of tail plane and design center of gravity, ft	4.655	21.158
Span, ft	3.071	13.960
Section profile		NACA 65_1-011
Stabilizer area		
20-percent-chord elevator, sq ft	2.556	52.800
32.8-percent-chord elevator, sq ft	2.309	47.710
Elevator		
Span		
20 percent chord, ft	3.000	13.648
32.8 percent chord, ft	3.070	13.954
Root-mean-square chord aft of hinge line		
20 percent chord, ft	0.201	0.912
32.8 percent chord, ft	0.343	1.557
Aileron		
Chord aft of hinge line, percent of wing chord	17.5	17.5

	Model	Airplane
Geometric balance, percent	53.8	53.8
Span, one aileron, ft	2.587	11.735
Root-mean-square chord aft of hinge line, ft	0.255	1.157
Vertical tail plane		
Area (each), sq ft	1.418	29.3
Stabilizer area excluding dorsal (each), sq ft	1.050	21.7
Section profile	NACA 651-010	
Rudder		
Area (each), sq ft	0.366	7.56
Span, ft	1.553	7.06
Root-mean-square chord aft of hinge line, ft	0.247	1.124
General		
Design gross weight, lb	-----	19,100
Design wing loading, lb per sq ft . .	-----	46.8
Design center-of-gravity position		
Horizontal, percent M.A.C.	-----	24.74
Vertical, inches below fuselage reference plane	-----	10.10

The horizontal-stabilizer chord line is parallel to the wing and fuselage reference planes.

COEFFICIENTS AND SYMBOLS

The following are the aerodynamic coefficients, symbols, and subscripts used in this report:

Coefficients

C_L	lift coefficient $\left(\frac{L}{qS}\right)$
C_D	drag coefficient $\left(\frac{D}{qS}\right)$
$C_{m_{c.g.}}$	pitching-moment coefficient about the center of gravity $\left(\frac{M_{c.g.}}{qS \text{ M.A.C.}}\right)$
R	Reynolds number $\left(\frac{\rho V \text{ M.A.C.}}{\mu}\right)$
M	Mach number (V/a)
L	lift, pounds
D	drag, pounds
$M_{c.g.}$	pitching moment about the center of gravity, pound-feet
S	wing area, square feet
M.A.C.	mean aerodynamic chord, feet
q	dynamic pressure of the free air stream $(\frac{1}{2}\rho V^2)$, pounds per square foot
ρ	density of the free-air stream, slugs per cubic foot
V	velocity of the free-air stream, feet per second
a	speed of sound in the free-air stream, feet per second
μ	viscosity of the free-air stream, pound-seconds per square foot

α angle of attack of model, degrees (The angle is measured relative to the wing reference plane.)

δ deflection of control surface, degrees

Subscripts

cr critical, used to indicate the Mach number at which the speed of sound is reached locally on the model

u uncorrected, used to indicate that the angle of attack is not corrected for wind-tunnel-wall or mounting-strut interference

e elevator, positive deflection with the trailing edge down

r rudder, positive deflection with the trailing edge to the left

a aileron, positive deflection with the trailing edge down

RESULTS

Wind-Tunnel Calibration and Correction of Data

The Mach number and dynamic-pressure calibration of the free-air stream, as well as the correction due to blocking of the air stream by the model and the wake of the model, were evaluated by the methods outlined in reference 1. The corrections due to air-stream inclination caused by the mounting system were evaluated by comparison of results obtained with the model mounted erect and inverted in the wind tunnel. No corrections were made for the interference between the mounting system and the model, but the data were corrected for the lift, drag, and pitching moment of the mounting system with the model not mounted on the struts.

As determined by the method outlined in reference 2, the corrections for wind-tunnel-wall interference were made

by adding the following:

$$\Delta\alpha \quad (\text{deg}) = 0.73 C_L$$

$$\Delta C_D = 0.0128 C_L^2$$

$$\Delta C_{m_{c.g.}} = 0.0092 C_L$$

Presentation of Results

The test results are presented in this report in the following groups:

1. Average Reynolds number of tests compared with flight Reynolds number of airplane. (See fig. 8.)

2. Lift, drag, and pitching-moment characteristics of the model with the Ames fillets for several model arrangements. Figures 9 through 35 show the results of force measurements for the model as various components were added.

3. Lift, drag, and pitching-moment characteristics of the model with the manufacturer's fillets. Results of force measurements are shown in figures 36 through 38.

4. Comparison of various model arrangements. Figures 39 through 41 show drag data for various arrangements of the model with the Ames fillets, and figures 42 through 44 show the drag and pitching-moment data for the complete model with the Ames and the manufacturer's fillets.

5. Critical Mach numbers of the surfaces of the model. The critical Mach numbers for the wing pressure stations are shown in figures 45 through 50. The critical Mach numbers for the pressure stations of the horizontal- and vertical-tail surfaces are shown in figures 51 through 58, and for the canopy and the entrance of the radiator duct in figures 59 and 60, respectively.

DISCUSSION

At the time the 0.22-scale model of the XP-82 airplane was being designed and built by the Ames Aeronautical Laboratory, the airplane was being designed and lofted by the manufacturer. With the airplane in such a fluid state of design while the model was being built, some minor differences between the contour of the model and airplane resulted. However, since the differences are of minor detail, it is felt that their effect on the predicted aerodynamic characteristics of the airplane derived from these data is inconsequential.

Previous to obtaining the force data and pressure-distribution measurements, the ducts for the carburetor and radiator were constricted so that the air flow through the scoop entrances corresponded approximately to that for high-speed level flight. At a Mach number of 0.65 and an angle of attack of 0° the ratio of the velocity of the air in the duct entrance to the velocity of air in the free stream was 0.48 for the carburetor and 0.53 for the radiator. The air-flow measurements were made in the ducts on the right fuselage only, but the ducts on the left fuselage were constricted identically to those on the right fuselage. Changing the angle of attack $\pm 4^\circ$ or the Mach number to either the maximum or minimum test value did not change these inlet-velocity ratios by more than 0.025.

A complete study of suitable fillets for the wing-fuselage junctures was not made. For tests of the model with the 20-percent-chord elevator, fillets (Ames fillets) that gave fairly satisfactory model stall characteristics at low speeds were developed in the wind tunnel. Study of tuft pictures showing the flow over these fillets indicated that some separation occurred over the trailing edges of the inboard fillets at low angles of attack and high Mach numbers. No further studies were made of these fillets as the manufacturer was developing the fillets for the airplane in their wind tunnel. For tests of the model with the 32.8-percent-chord elevator, the fillets developed by the manufacturer were used. No tuft studies of these fillets were made at the Ames Laboratory. Figures 42, 43, and 44 show that the Mach number of divergence of the model with these fillets was about 0.015 greater than that of the model with the Ames fillets. At low Mach numbers (0.30 and 0.45) the drag coefficient of the model with the manufacturer's fillets

was 0.0010 greater than with the Ames fillets. The maximum lift coefficient measured for the complete model at a Mach number of 0.30 with the Ames fillets was 1.100 (fig. 25) and with the manufacturer's fillets it was 1.115 (fig. 37). Tuft studies of the model with the Ames fillets showed that there was some separation of the flow over these fillets, and yet force tests show (fig. 42) that the drag of the model with these fillets was less at low Mach numbers than the drag of the model with the manufacturer's fillets. Further study of the wing-fuselage fillets might be desirable for it may be possible to reduce the drag coefficient of the airplane at Mach numbers below the Mach number of divergence and also to increase the Mach number of divergence.

Figure 39 shows that the addition of the radiator enclosures not only added a large drag-coefficient increment (0.0035 at a lift coefficient of zero) but it also decreased the Mach number of divergence. The Mach number of divergence of the model without the radiator enclosures (figs. 39 and 40) was about 0.725 and 0.720 at lift coefficients of 0 and 0.2, respectively. With the addition of the radiator enclosures, the Mach number of divergence was reduced to about 0.700 and 0.710 at the same respective lift coefficients. At these lift coefficients, the drag coefficient of the right radiator duct, as calculated from measured air flow and pressure losses in the duct, was 0.0010 (0.0020 for both ducts) and was constant for the Mach number range from 0.3 to 0.8. The addition of the other components (armament and droppable gas tank excluded) to the model changed the Mach number of divergence very little. Figure 60 shows that the critical Mach number of the radiator enclosures near the duct entrances was about 0.675 and 0.700 at angles of attack of -2° and 0° (lift coefficients of 0 and 0.2), respectively. Since the critical Mach number of the radiator enclosures is less than the Mach number of divergence of the complete model and it appears to be the factor that largely determines the Mach number of divergence of the complete model, it seems probable that changing the shape of the radiator enclosures so as to increase their critical Mach number would result in an increase in the Mach number of divergence.

For the complete model with either the Ames fillets or the manufacturer's fillets, the Mach number of divergence was about 0.70 for lift coefficients from 0 to 0.4. Below the Mach number of divergence, figures 25 and 37 show that the angle of attack corresponding to a given lift coefficient was

practically constant with change in Mach number, but above the Mach number of divergence, the angle of attack had to be increased with an increase in Mach number in order to maintain a constant lift coefficient. Figures 26 and 38 show that, above a Mach number of 0.70 at zero lift coefficient, both the value of the pitching-moment coefficient and the slope of the pitching-moment curve became more negative with an increase in Mach number. If the Mach number of the airplane in flight exceeds the Mach number of divergence, an increase in the angle of attack will be necessary to maintain the airplane in a steady condition. Since the average down-wash angle is constant with constant lift coefficient for moderate Mach number changes, this increase in the angle of attack of the airplane produces a corresponding increase in the angle of attack of the horizontal tail, which results in a diving moment on the airplane. As is indicated by the model data, this diving moment would be accompanied by an increase in the static longitudinal stability of the airplane, thus making it more difficult for the pilot to change the attitude of the airplane.

The outer wing panels have a washout of 2° between the root and tip, the outer panels also vary linearly in thickness from 15 percent of the chord at the root to 12 percent of the chord at the tip. The variation of the critical Mach number across the right span of the wing is shown in figure 45. This figure shows that for a constant angle of attack the critical Mach number of the outer panel decreased from the root to the tip, and that the angle of attack at which the maximum critical Mach number occurred increased across the panel from the root to the tip. Figures 47 through 50 show that aileron deflections of up to 10° changed the critical Mach number of the wing outer panel a small amount (about 0.015 at an angle of attack of 0°). The addition of the gun nacelle (fig. 46) had very little effect on the critical Mach number of the wing center panel at low angles of attack, but at higher angles of attack (3° to 6°) it increased the critical Mach number somewhat. This increase was probably due to the nacelle destroying some of the circulation over the center wing section, which, in turn, lowered the value of the peak-pressure coefficient and thus increased the critical Mach number.

Figures 51, 52, 53, 57, and 58 show that even with considerable deflection of the elevator or rudders the

critical Mach numbers of the empennage were either equal to or greater than those of the wing. The small change in the critical Mach number of the horizontal tail (figs. 54 and 55) with change in elevator chord was caused by the leakage of air through the elevator gap altering the pressure distribution.

CONCLUDING REMARKS

The results of tests of the 0.22-scale model indicate that the Mach number of divergence of the airplane will be about 0.70 (475 mph at 30,000 ft altitude). If the Mach number exceeds 0.70, the airplane will probably experience a diving tendency. The test results indicate that the Mach number of divergence of the airplane might be increased slightly if some modifications are made to the wing-fuselage fillets and the external shape of the radiator enclosures.

Ames Aeronautical Laboratory,
National Advisory Committee for Aeronautics,
Moffett Field, Calif.

REFERENCES

1. Missen, James M., Gadeberg, Burnett L., and Hamilton, William T.: Correlation of the Drag Characteristics of a P-51B Airplane Obtained from High-Speed Wind-Tunnel and Flight Tests. NACA ACR No. 4K02, 1945.

2. Silverstein, Abe, and White, James A.: Wind-Tunnel Interference with Particular Reference to Off-Center Positions of the Wings and to the Downwash at the Tail. NACA Rep. No. 547, 1935.

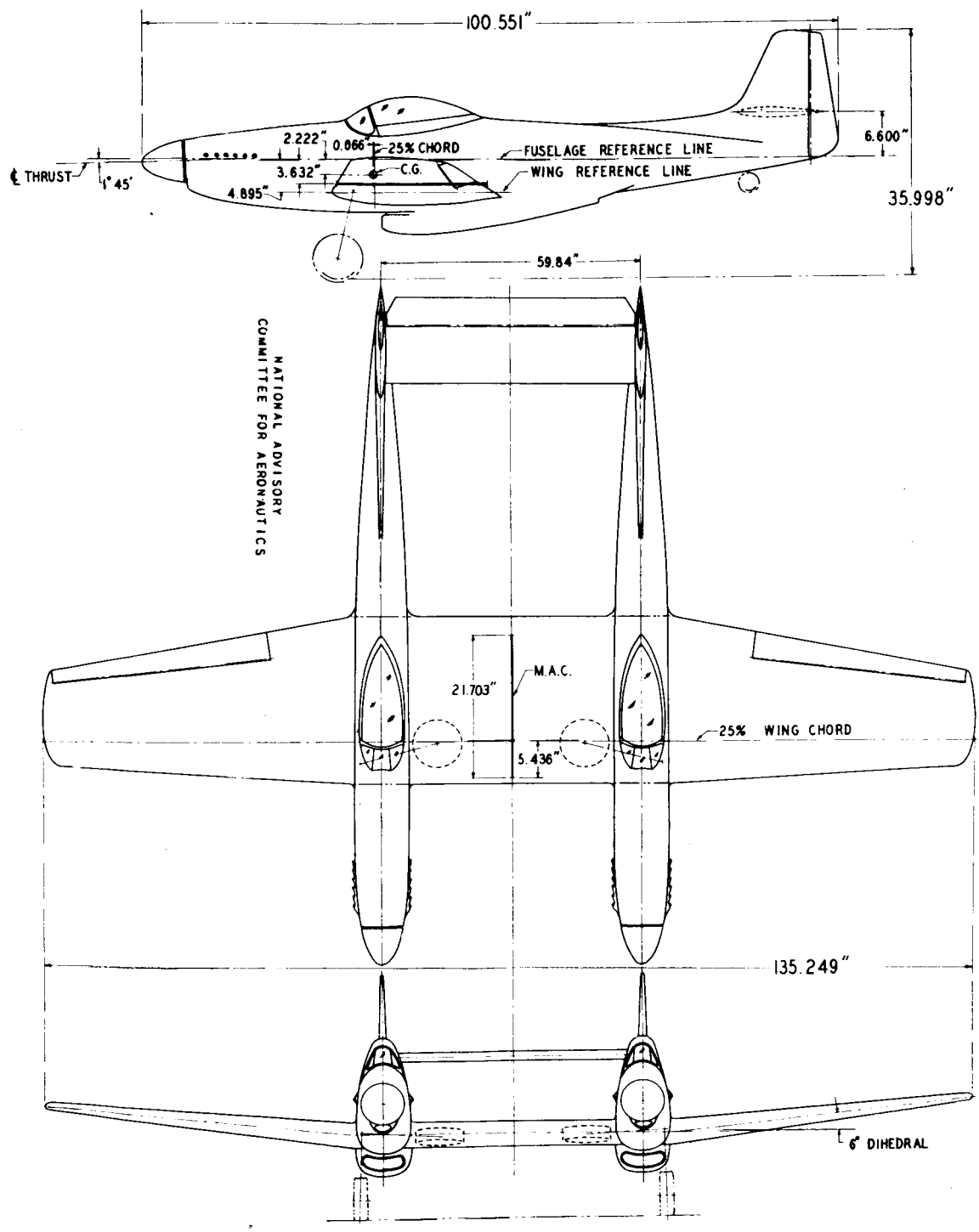

FIGURE 1:- THE 0.22-SCALE MODEL OF A TWIN-FUSELAGE PURSUIT AIRPLANE.

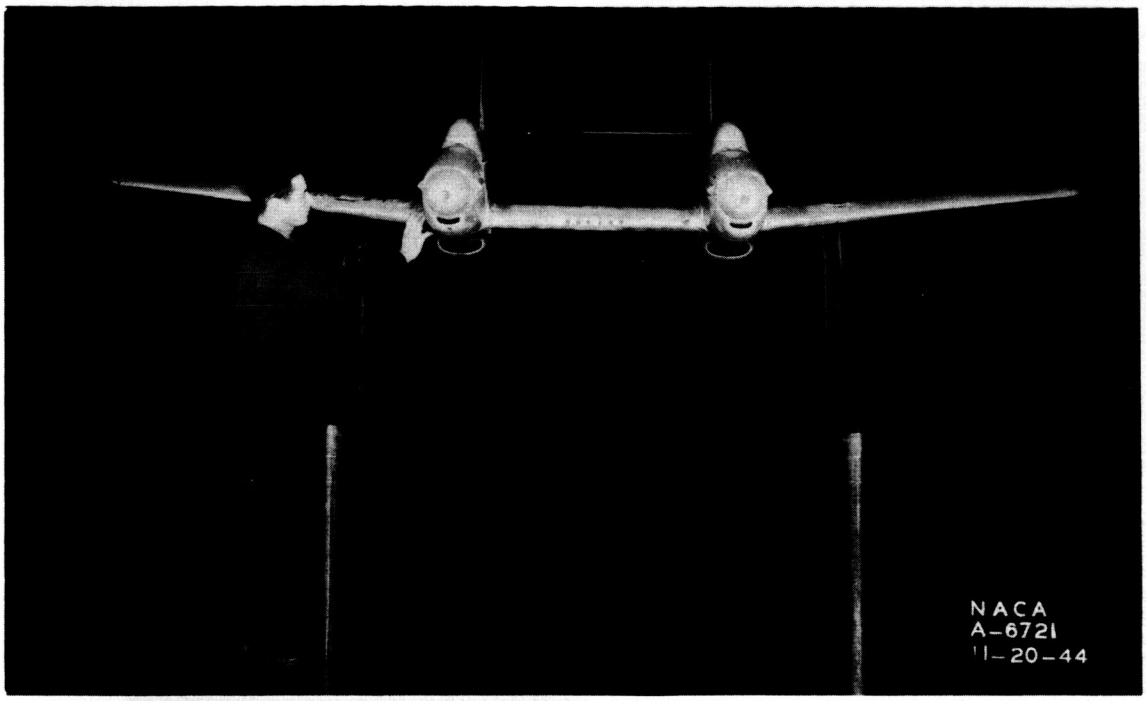

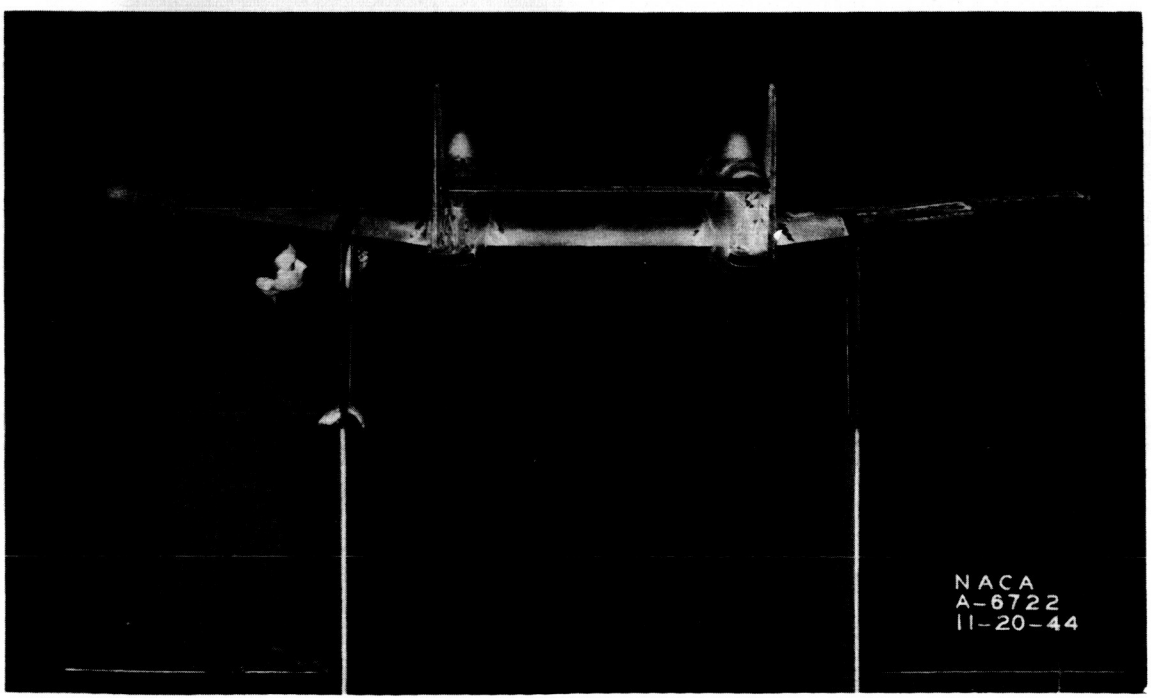

Figure 2.- Complete model of the 0.22-scale model of the airplane with wing armament.

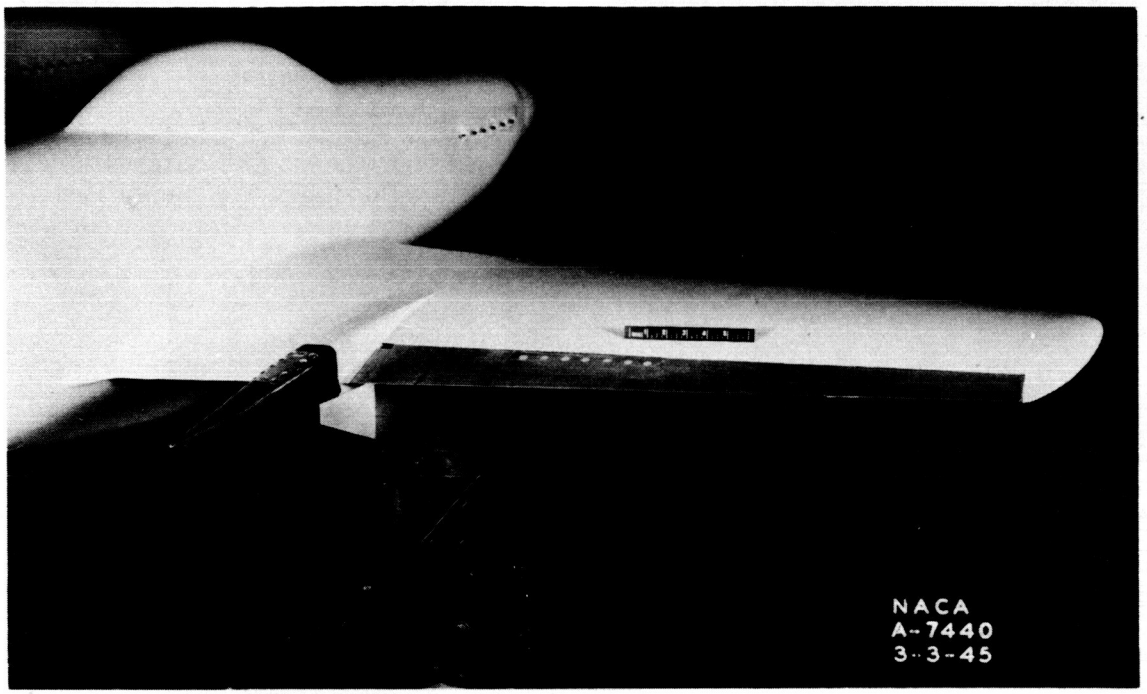

Figure 3.- Right wing span showing one of the pitch booms on the 0.22-scale model of the airplane.

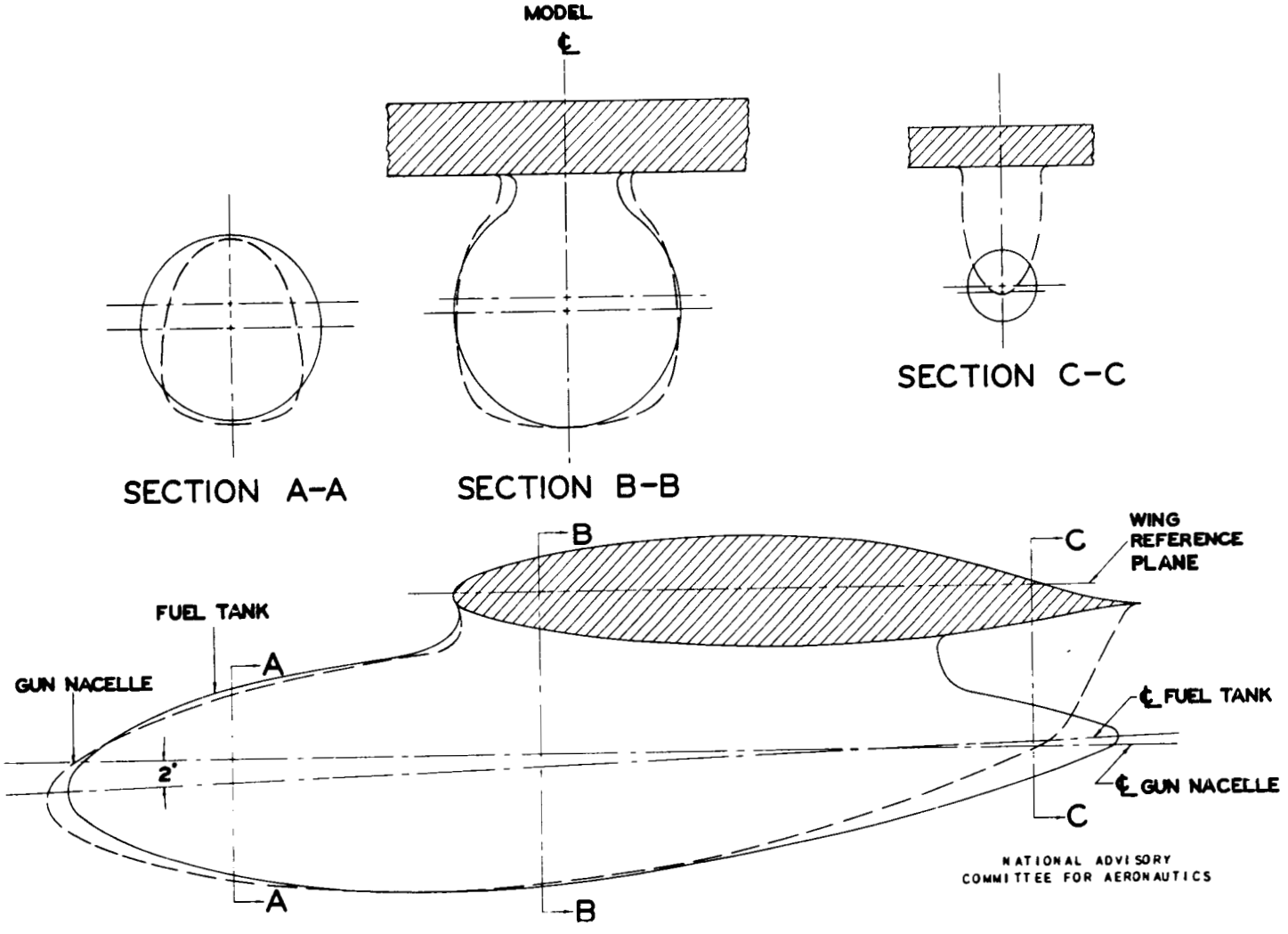

FIGURE 4:- DROPPABLE FUEL TANK AND EIGHT-GUN NACELLE ATTACHED TO THE WING.

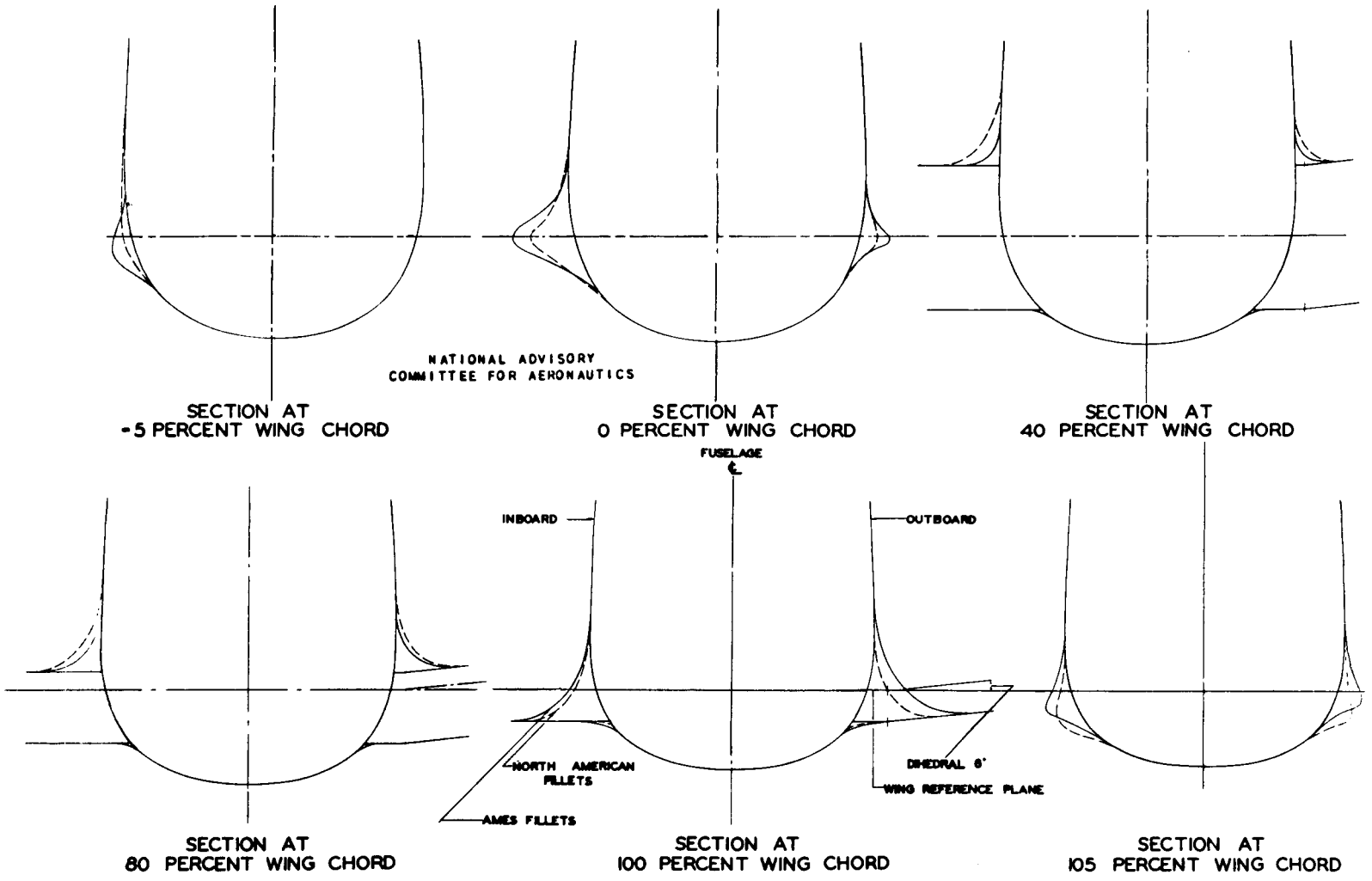

FIGURE 5:- COMPARISON OF MANUFACTURER'S AND AMES FILLETS AT SEVERAL STATIONS ALONG THE WING CHORD.

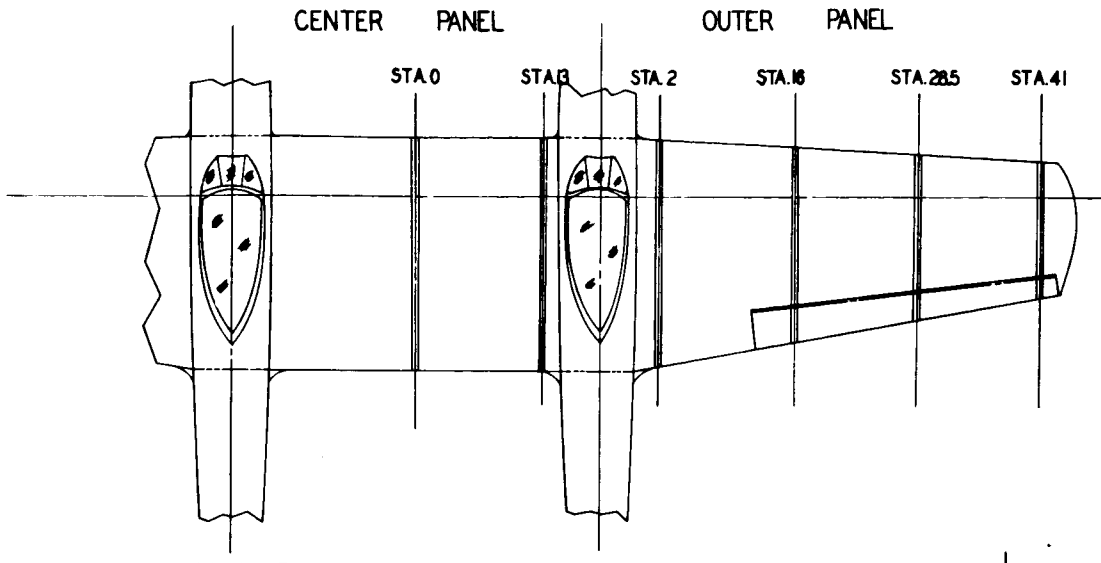

WING PRESSURE ORIFICE STATION LOCATIONS

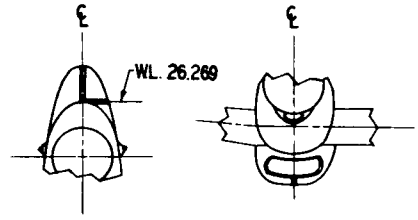

-CANOPY PRESSURE ORIFICE STATIONS-

RADIATOR PRESSURE -ORIFICE STATIONS-

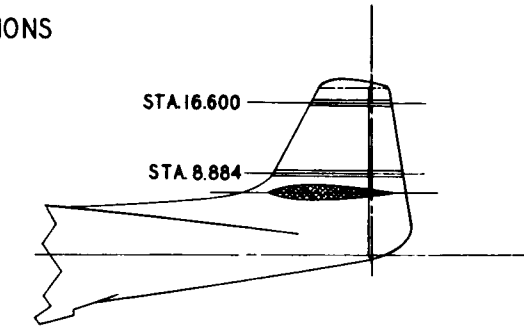

VERTICAL STABILIZER AND RUDDER -PRESSURE ORIFICE STATIONS-

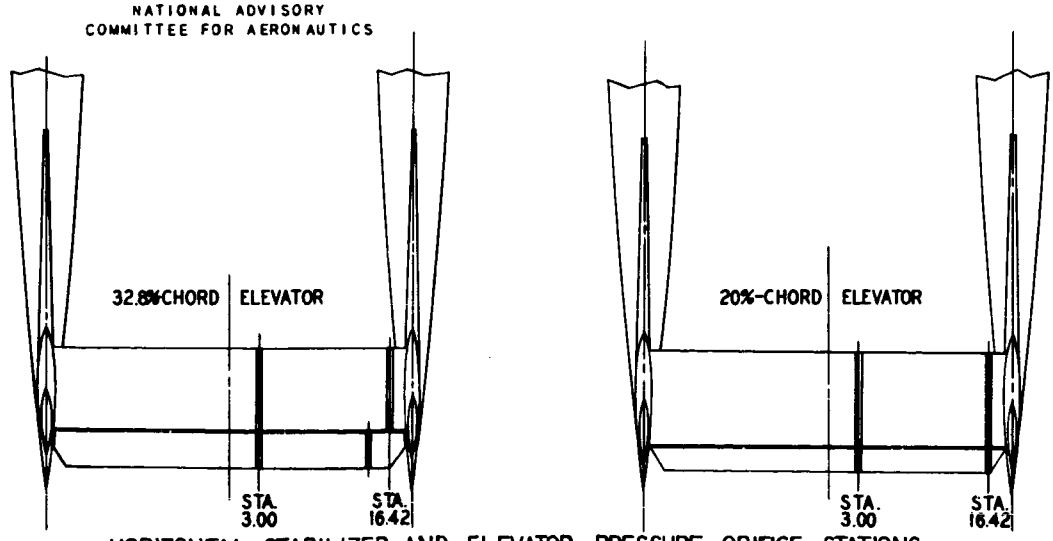

HORIZONTAL STABILIZER AND ELEVATOR PRESSURE ORIFICE STATIONS

FIGURE 6:- THE LOCATION OF THE PRESSURE ORIFICES.

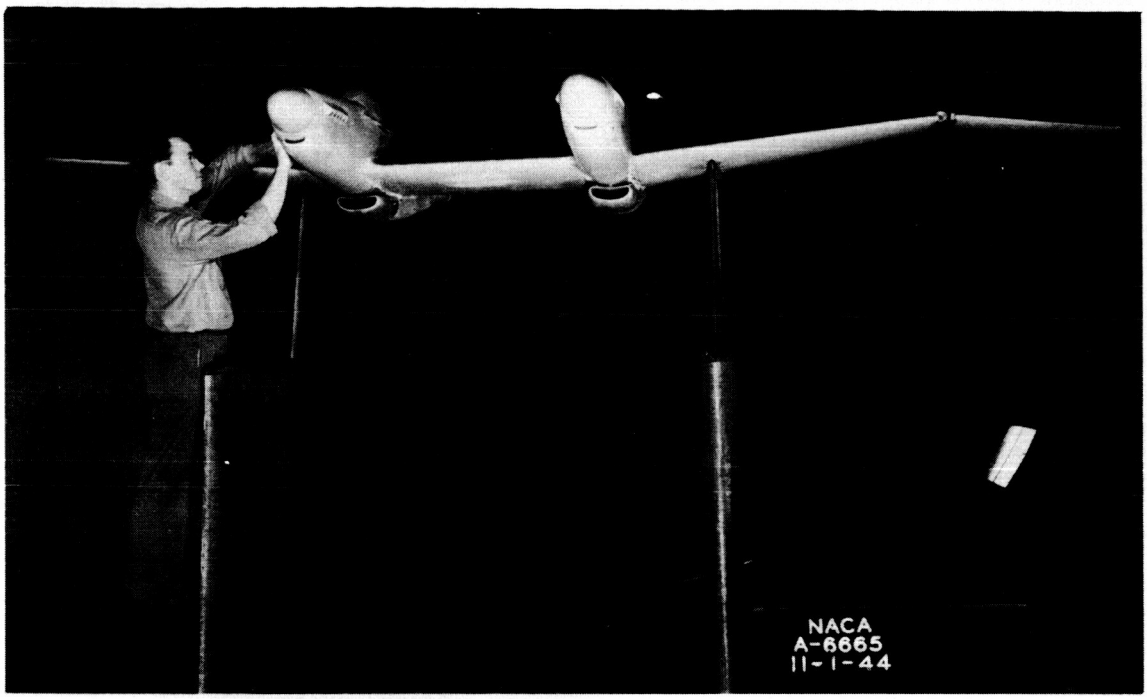

Figure 7.- Pressure-tube strut connected to the left wing of the 0.22-scale model of the airplane.

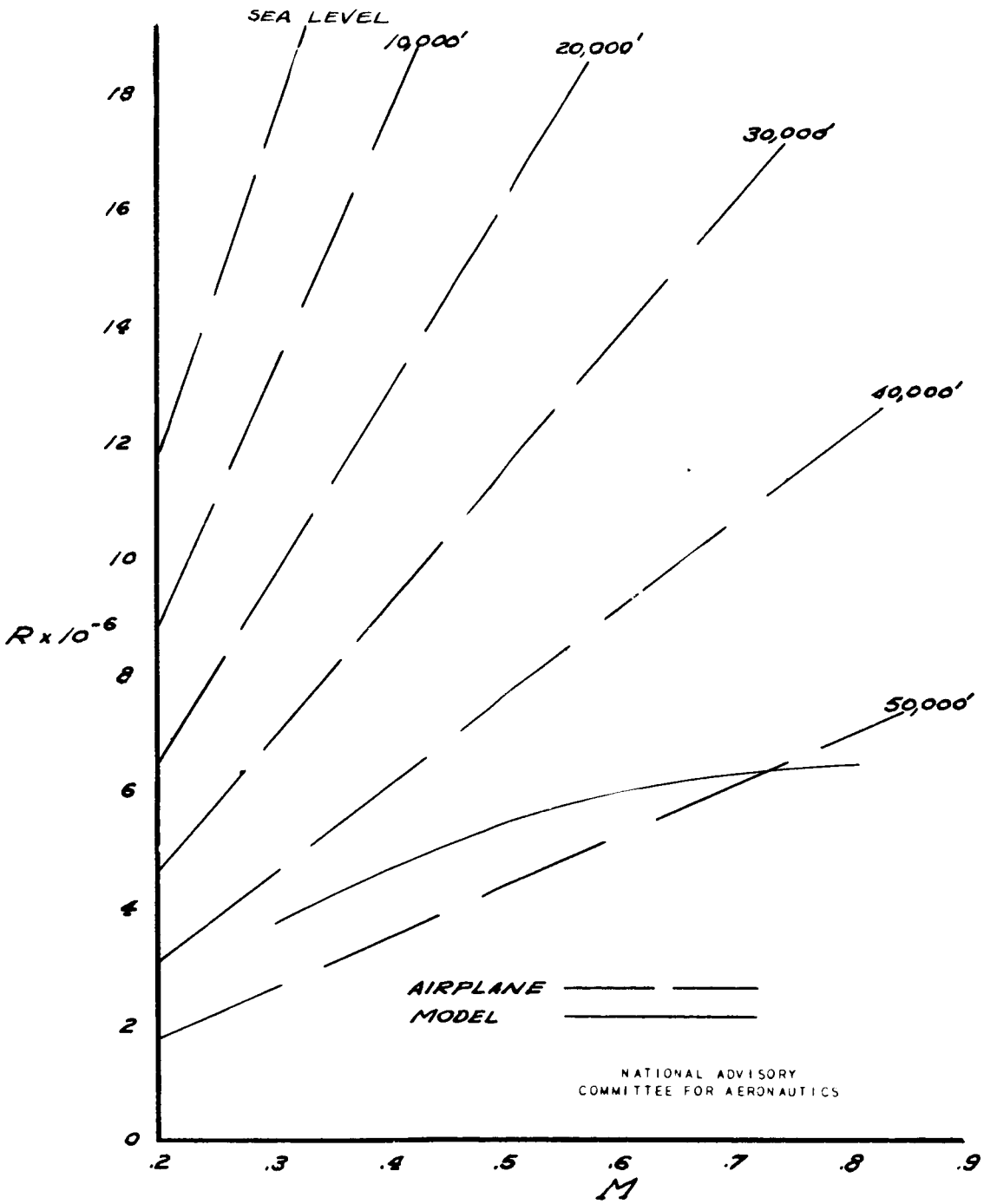

FIGURE 8.—AVERAGE REYNOLDS NUMBER OF MODEL TEST COMPARED WITH FLIGHT REYNOLDS NUMBER OF THE AIRPLANE.

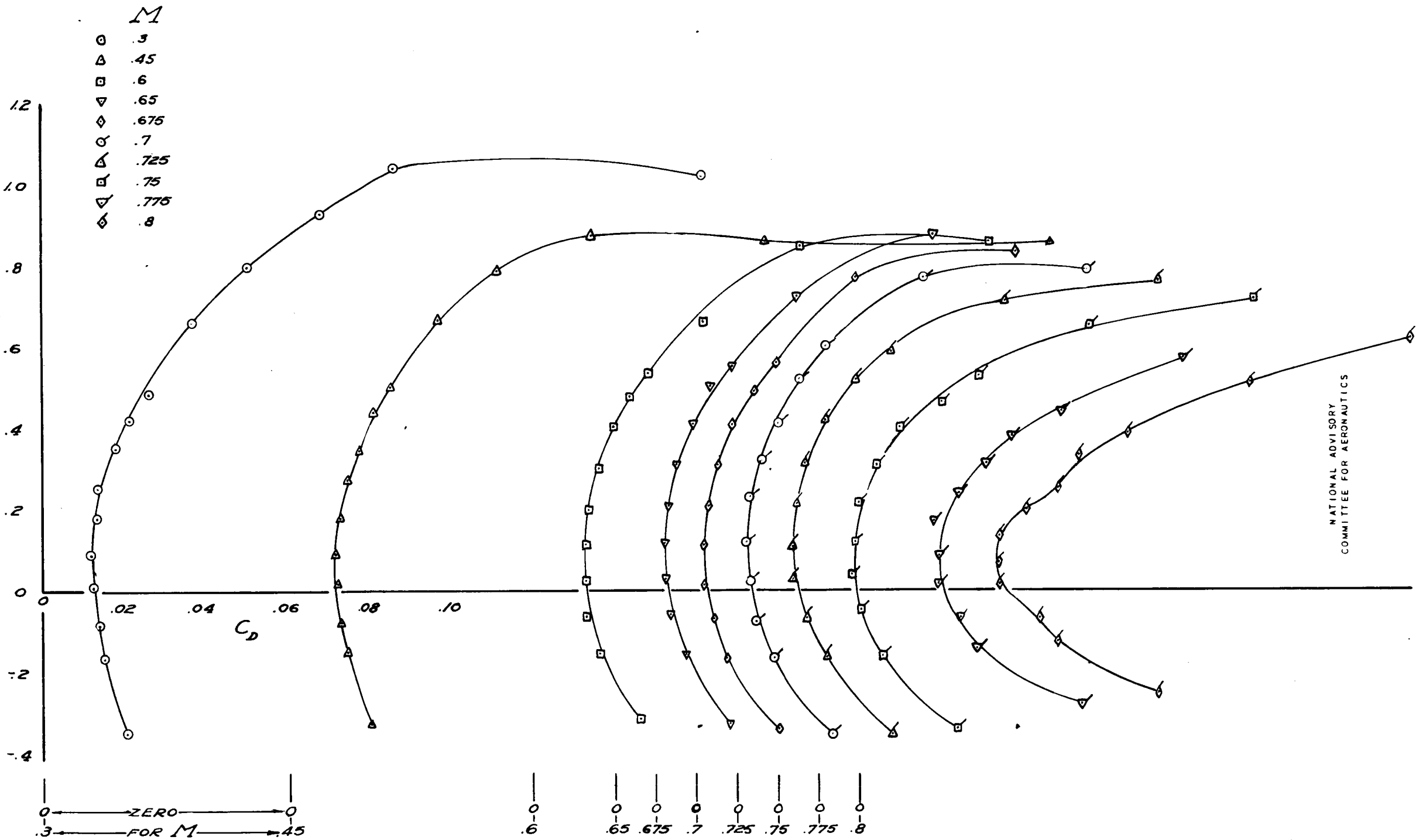

NATIONAL ADVISORY
COMMITTEE FOR AERONAUTICS

FIGURE 9:- VARIATION OF LIFT COEFFICIENT WITH DRAG COEFFICIENT FOR THE MODEL WITH AMES FILLETS MINUS THE HORIZONTAL TAIL, TWO VERTICAL TAILS, CANOPIES, EXHAUST STACKS, CARBURETORS AND COOLANT-RADIATOR DUCTS.

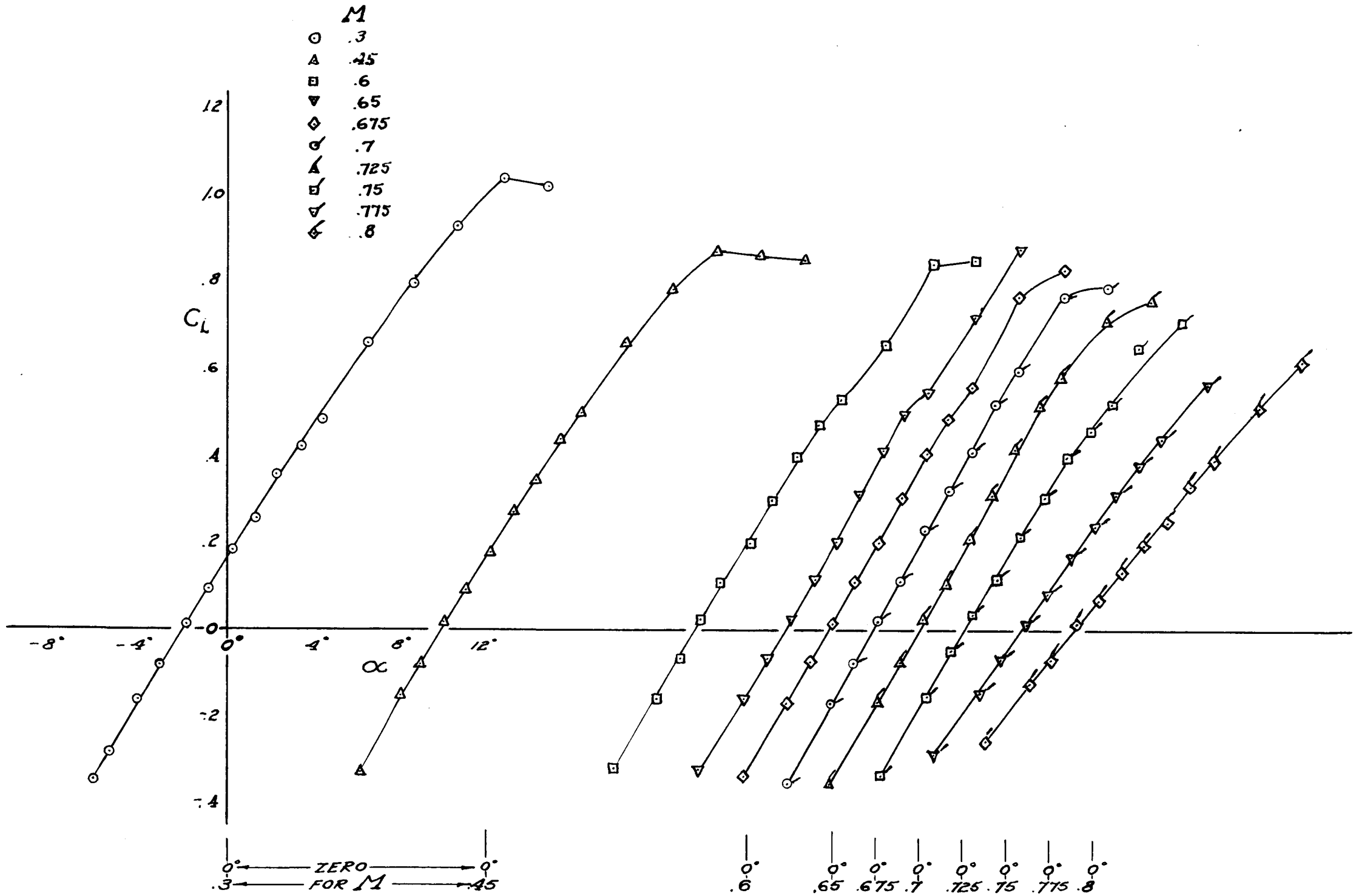

NATIONAL ADVISORY
COMMITTEE FOR AERONAUTICS

FIGURE 10:- VARIATION OF LIFT COEFFICIENT WITH ANGLE OF ATTACK FOR THE MODEL WITH AMES FILLETS MINUS THE HORIZONTAL TAIL, TWO VERTICAL TAILS, CANOPIES, EXHAUST STACKS, CARBURETORS, AND COOLANT-RADIATOR DUCTS.

MR No. A6D03

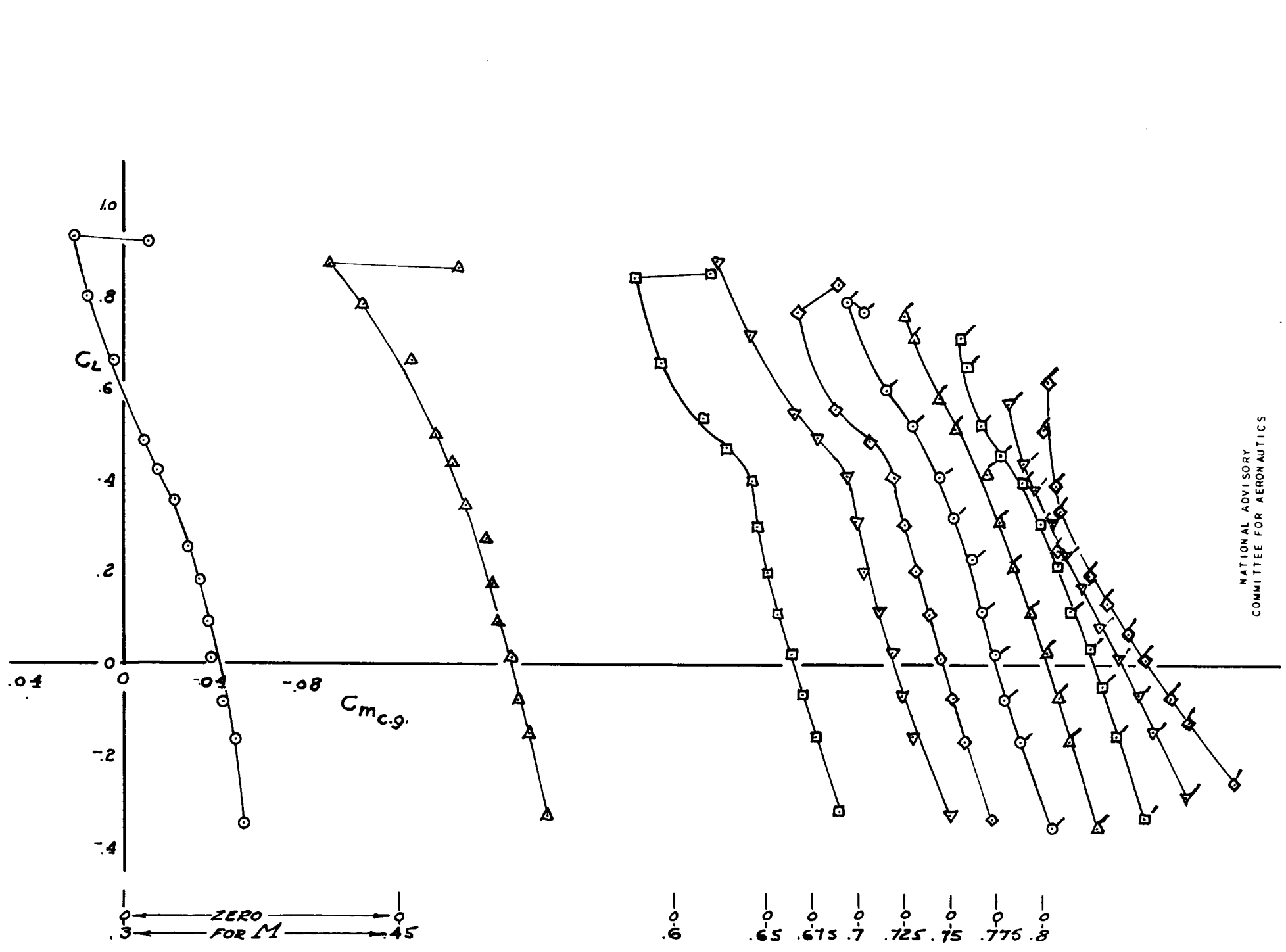

NATIONAL ADVISORY
COMMITTEE FOR AERONAUTICS

FIGURE 11.- VARIATION OF LIFT COEFFICIENT WITH PITCHING-MOMENT COEFFICIENT FOR THE MODEL WITH AMES FILLETS MINUS THE HORIZONTAL TAIL, TWO VERTICAL TAILS, CANOPIES, EXHAUST STACKS, CARBURETORS AND COOLANT-RADIATOR DUCTS.

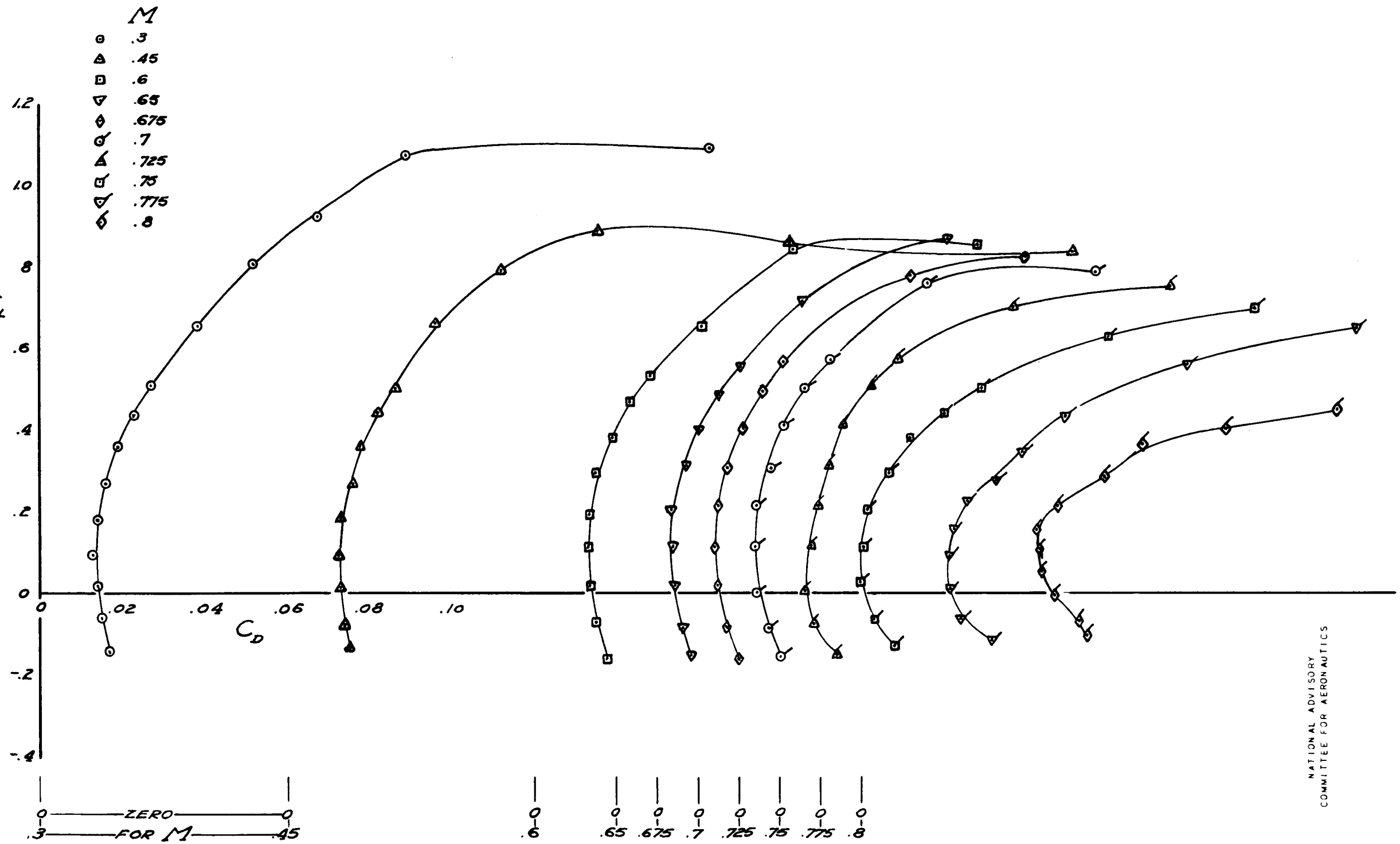

FIGURE 12:- VARIATION OF LIFT COEFFICIENT WITH DRAG COEFFICIENT FOR THE MODEL WITH AMES FILLETS MINUS THE HORIZONTAL TAIL, TWO VERTICAL TAILS, CANOPIES, AND COOLANT-RADIATOR DUCTS.

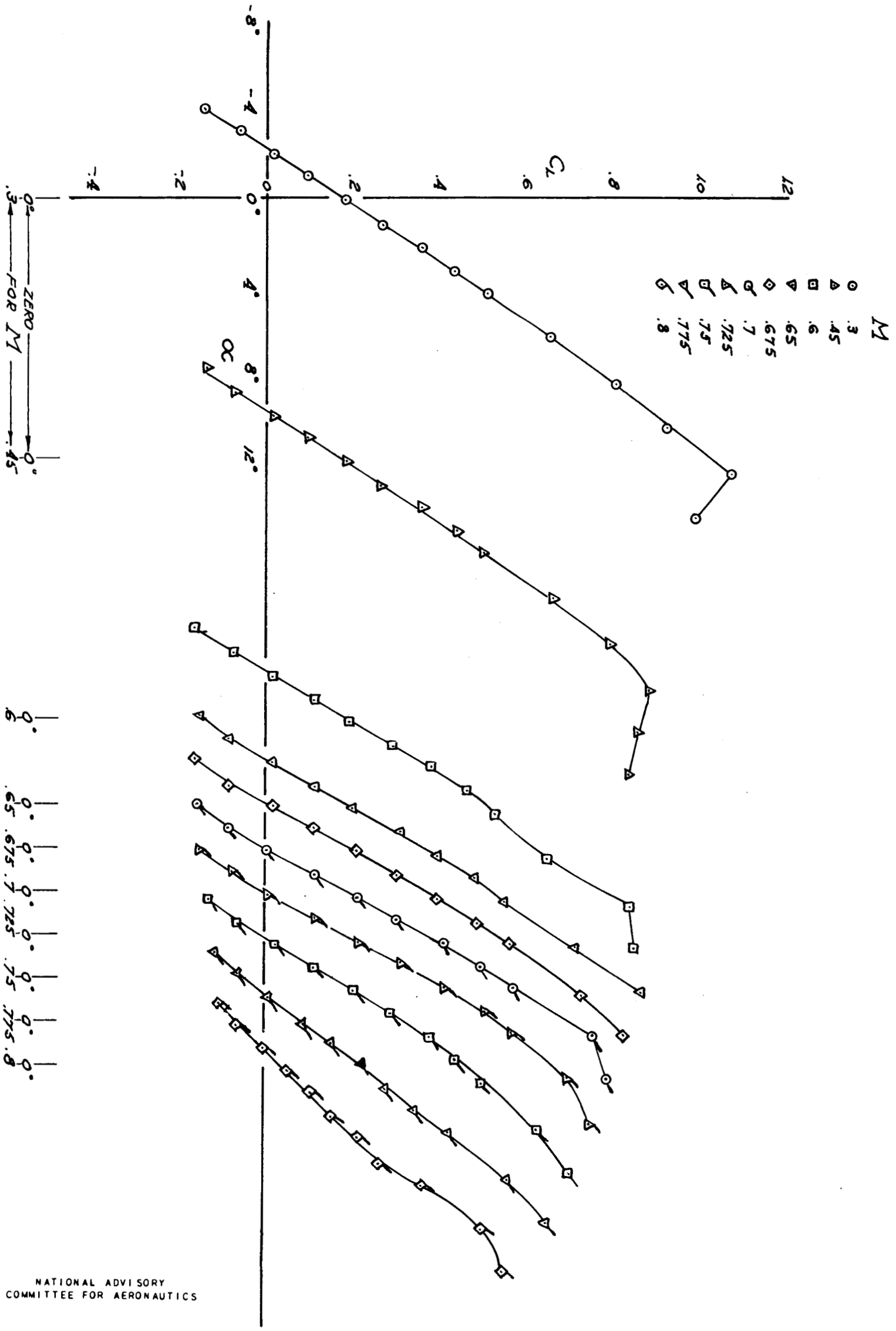

FIGURE 13:- VARIATION OF LIFT COEFFICIENT WITH ANGLE OF ATTACK FOR THE MODEL WITH AMES FILLETS MINUS THE HORIZONTAL TAIL, TWO VERTICAL TAILS, CANOPIES, AND COOLANT-RADIATOR DUCTS.

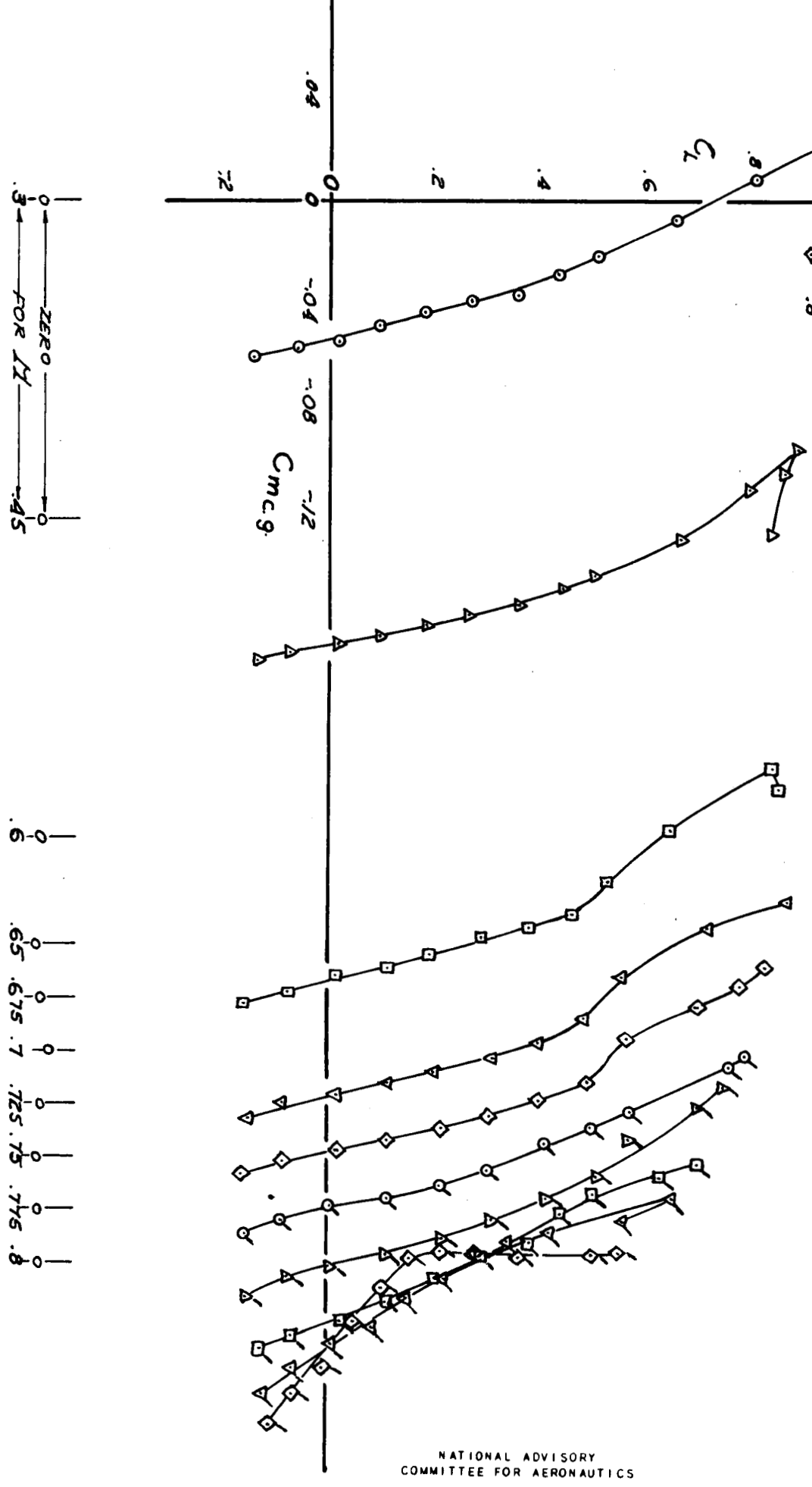

FIGURE 14:- VARIATION OF LIFT COEFFICIENT WITH PITCHING-MOMENT COEFFICIENT FOR THE MODEL WITH AMES FILLETS MINUS THE HORIZONTAL TAIL, TWO VERTICAL TAILS, CANOPIES, AND COOLANT-RADIATOR DUCTS.

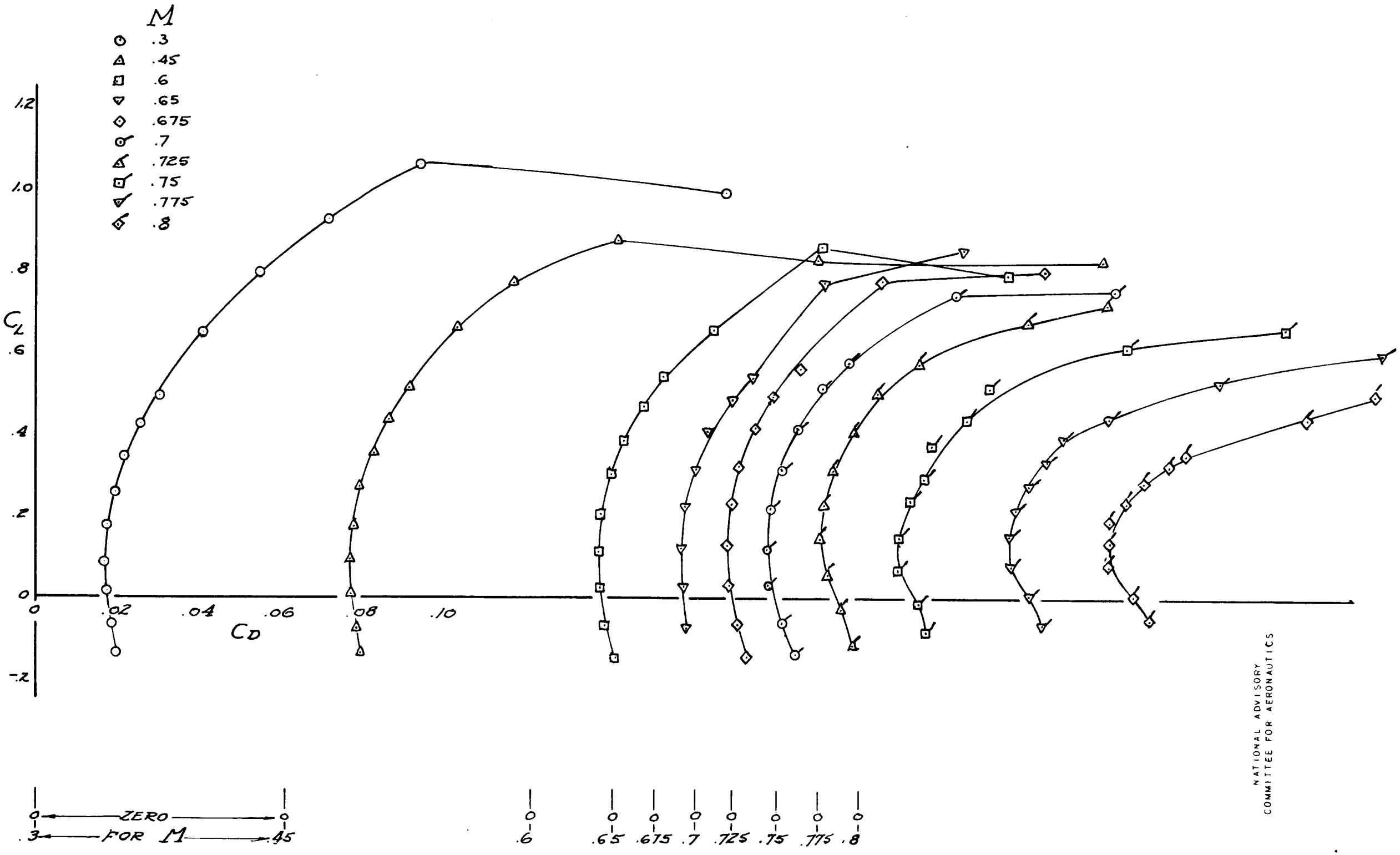

NATIONAL ADVISORY
COMMITTEE FOR AERONAUTICS

FIGURE 15 :- VARIATION OF LIFT COEFFICIENT WITH DRAG COEFFICIENT FOR THE MODEL WITH AMES FILLETS MINUS THE HORIZONTAL TAIL, TWO VERTICAL TAILS, AND CANOPIES.

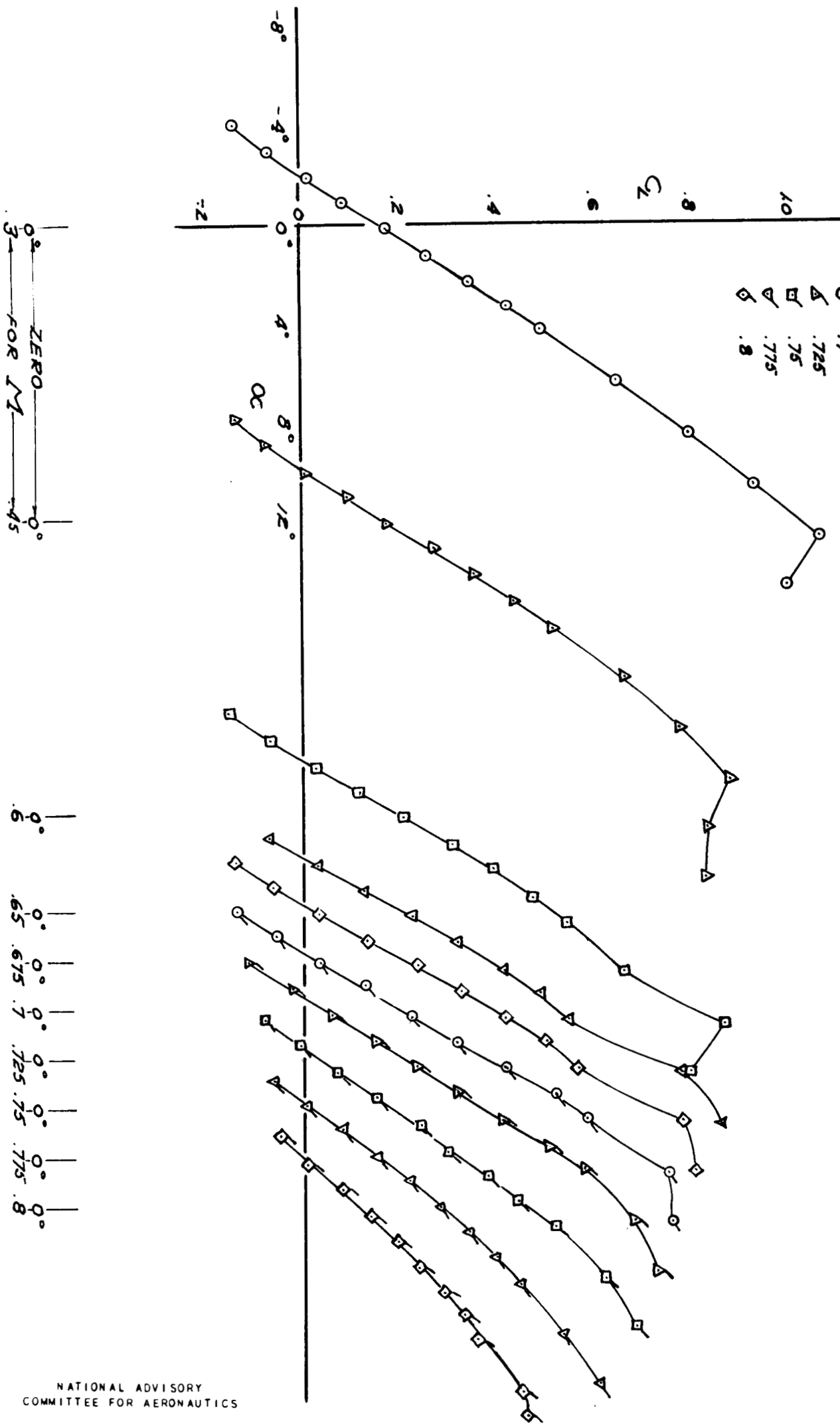

FIGURE 16:- VARIATION OF LIFT COEFFICIENT WITH ANGLE OF ATTACK FOR THE MODEL WITH AMES FILLETS MINUS THE HORIZONTAL TAIL, TWO VERTICAL TAILS AND CANOPIES.

MR No. A6D03

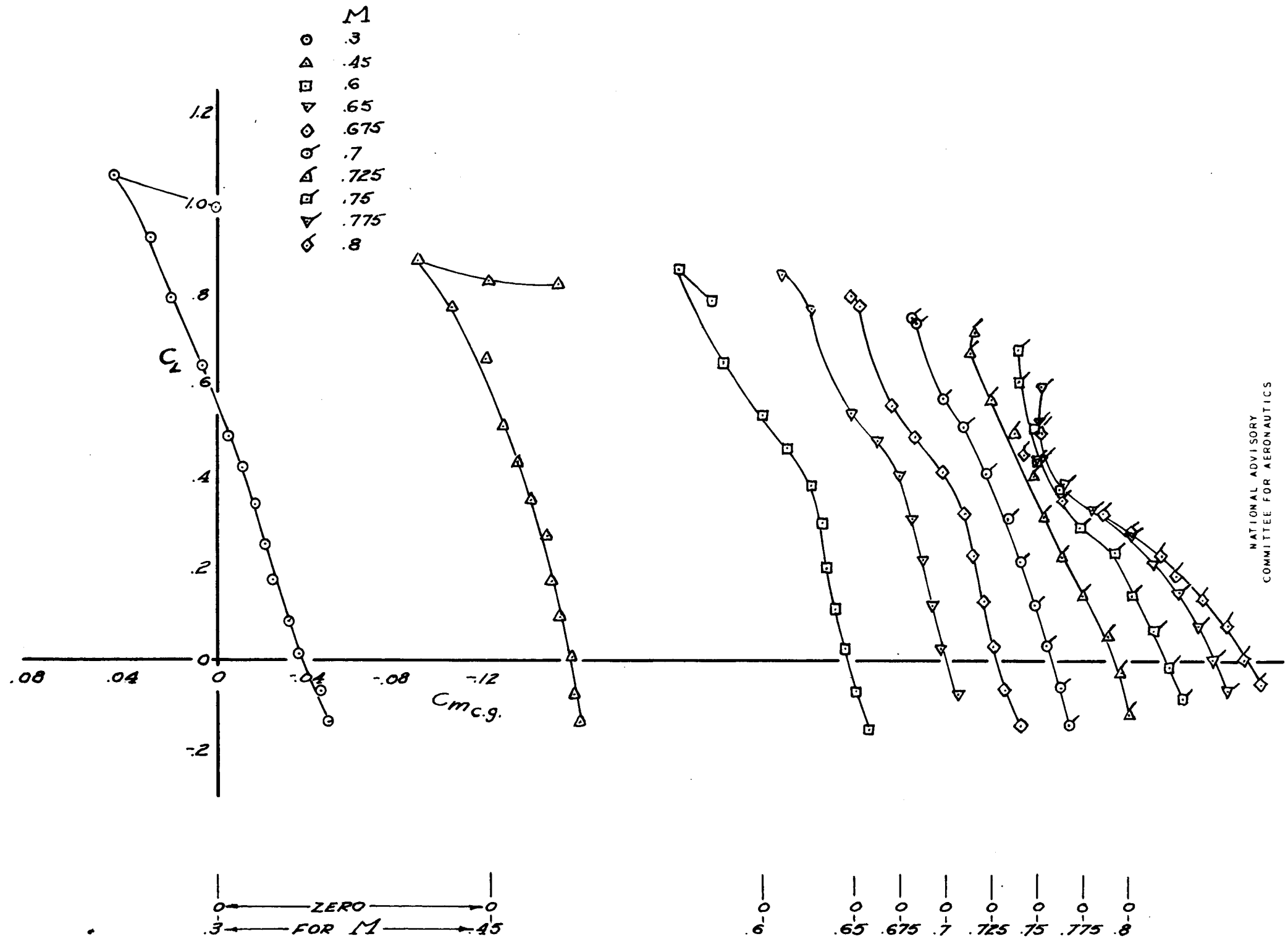

NATIONAL ADVISORY
COMMITTEE FOR AERONAUTICS

FIGURE 17:- VARIATION OF LIFT COEFFICIENT WITH PITCHING - MOMENT COEFFICIENT FOR THE MODEL WITH AMES FILLETS MINUS THE HORIZONTAL TAIL, TWO VERTICAL TAILS, AND CANOPIES.

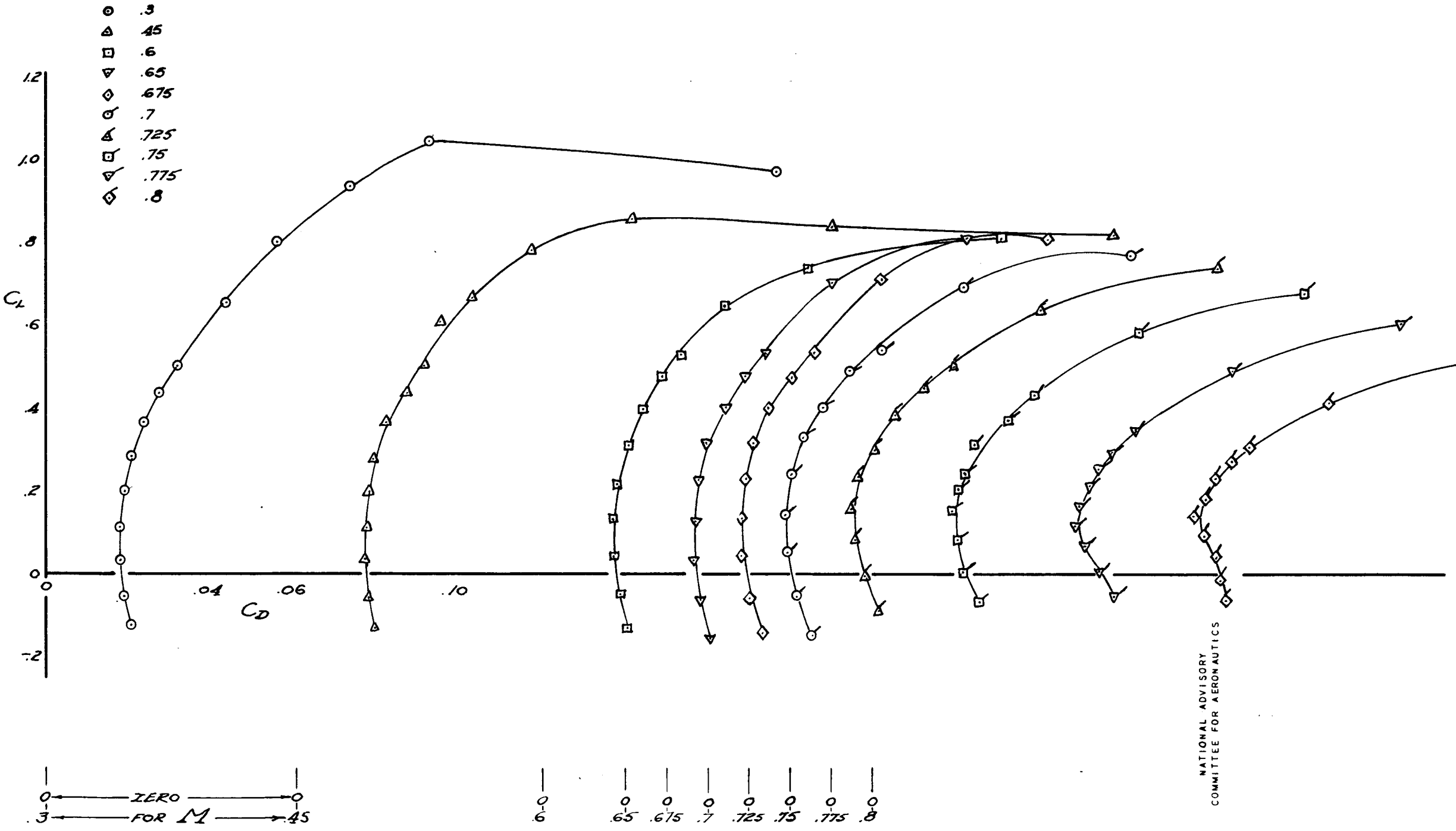

NATIONAL ADVISORY
COMMITTEE FOR AERONAUTICS

FIGURE 18:- VARIATION OF LIFT COEFFICIENT WITH DRAG COEFFICIENT FOR THE MODEL WITH AMES FILLETS MINUS THE HORIZONTAL TAIL AND TWO VERTICAL TAILS.

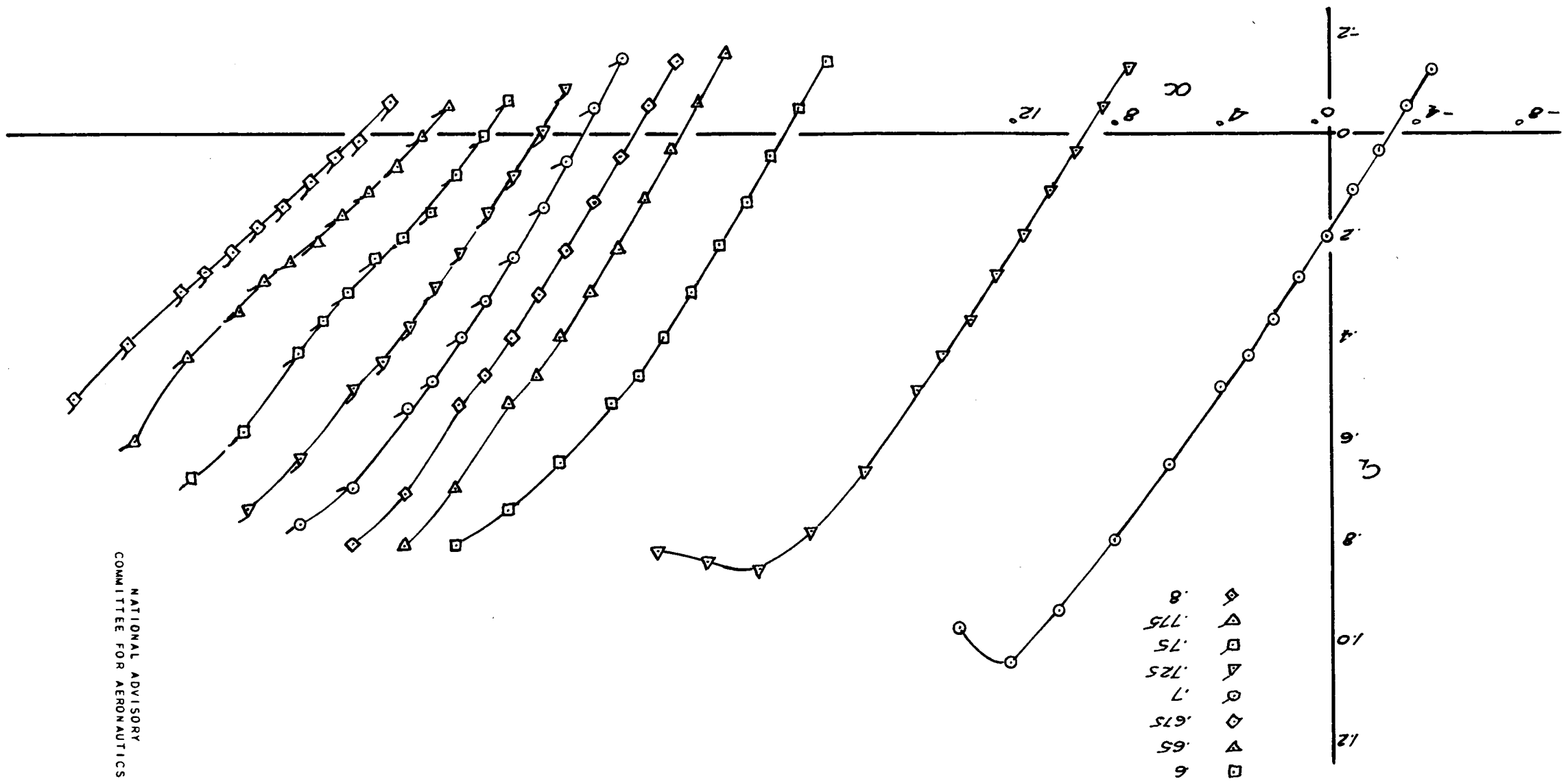

NATIONAL ADVISORY
COMMITTEE FOR AERONAUTICS

FIGURE 19:- VARIATION OF LIFT COEFFICIENT WITH ANGLE OF ATTACK FOR THE MODEL WITH AMES FILLETS MINUS THE HORIZONTAL TAIL AND TWO VERTICAL TAILS.

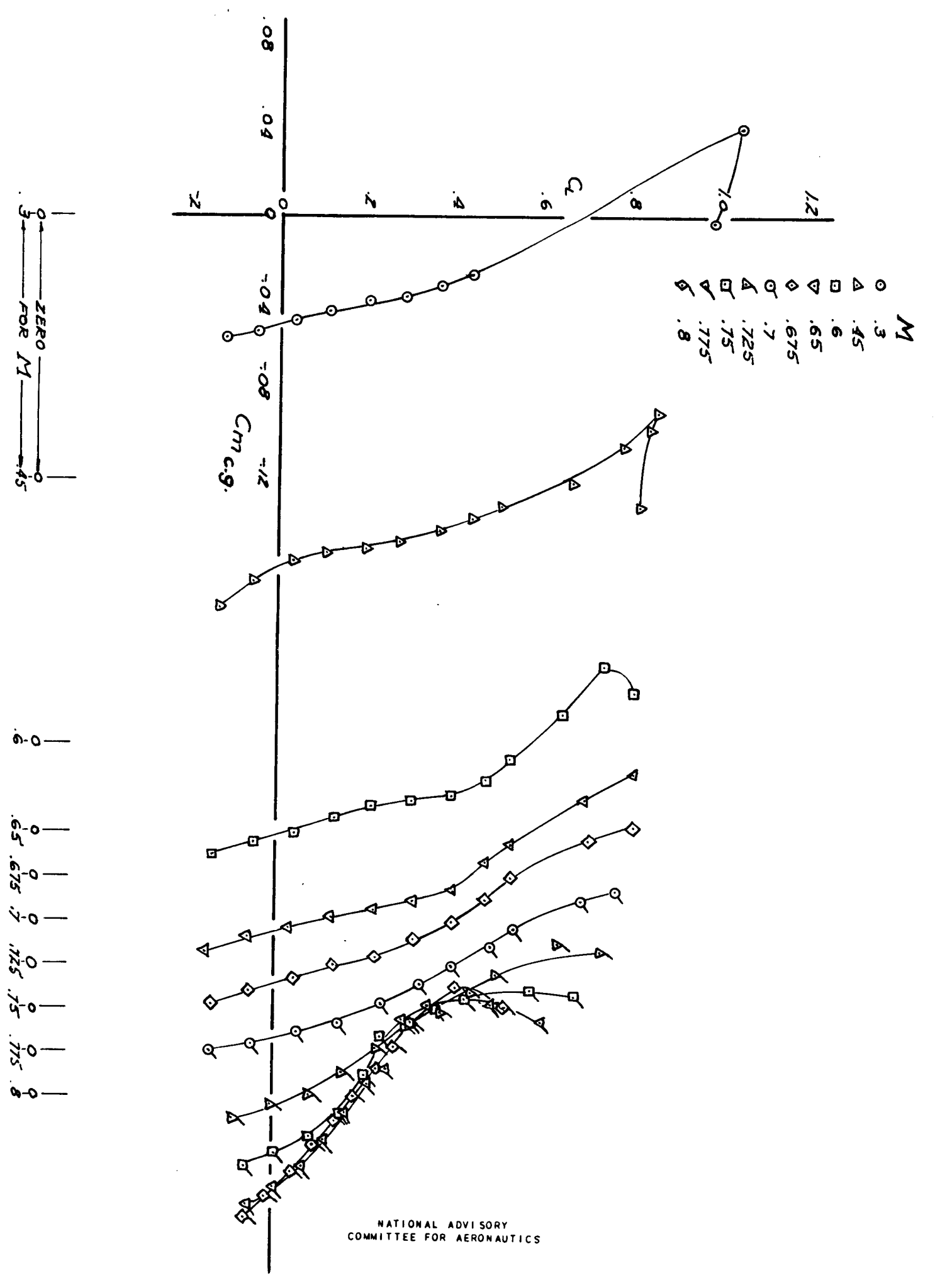

FIGURE 20:- VARIATION OF LIFT COEFFICIENT WITH PITCHING-MOMENT COEFFICIENT FOR THE MODEL WITH AMES FILLETS MINUS THE HORIZONTAL TAIL AND TWO VERTICAL TAILS.

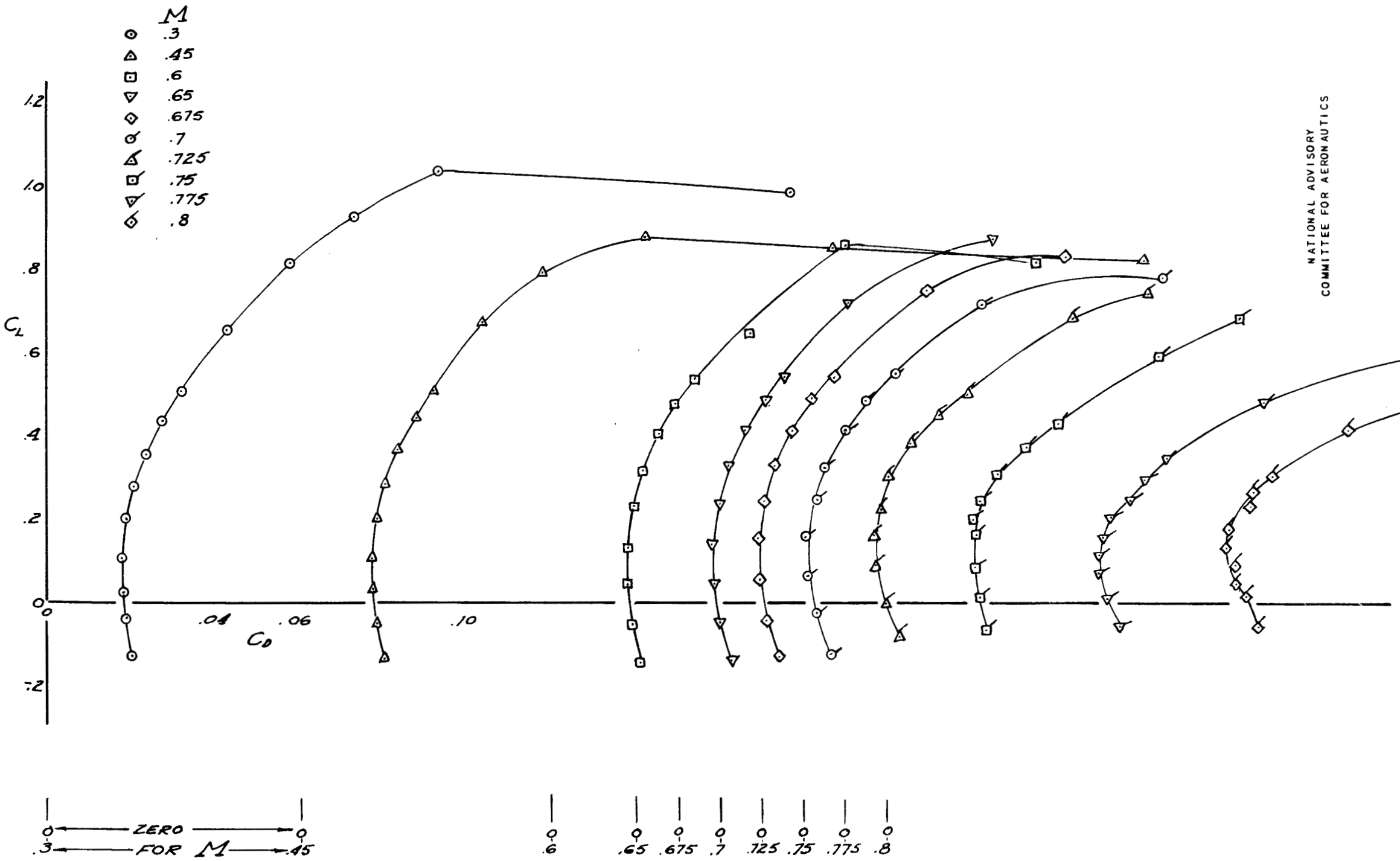

NATIONAL ADVISORY
COMMITTEE FOR AERONAUTICS

FIGURE 21:- VARIATION OF LIFT COEFFICIENT WITH DRAG COEFFICIENT FOR THE MODEL WITH AMES FILLETS MINUS THE HORIZONTAL TAIL.

MR No. A6D03

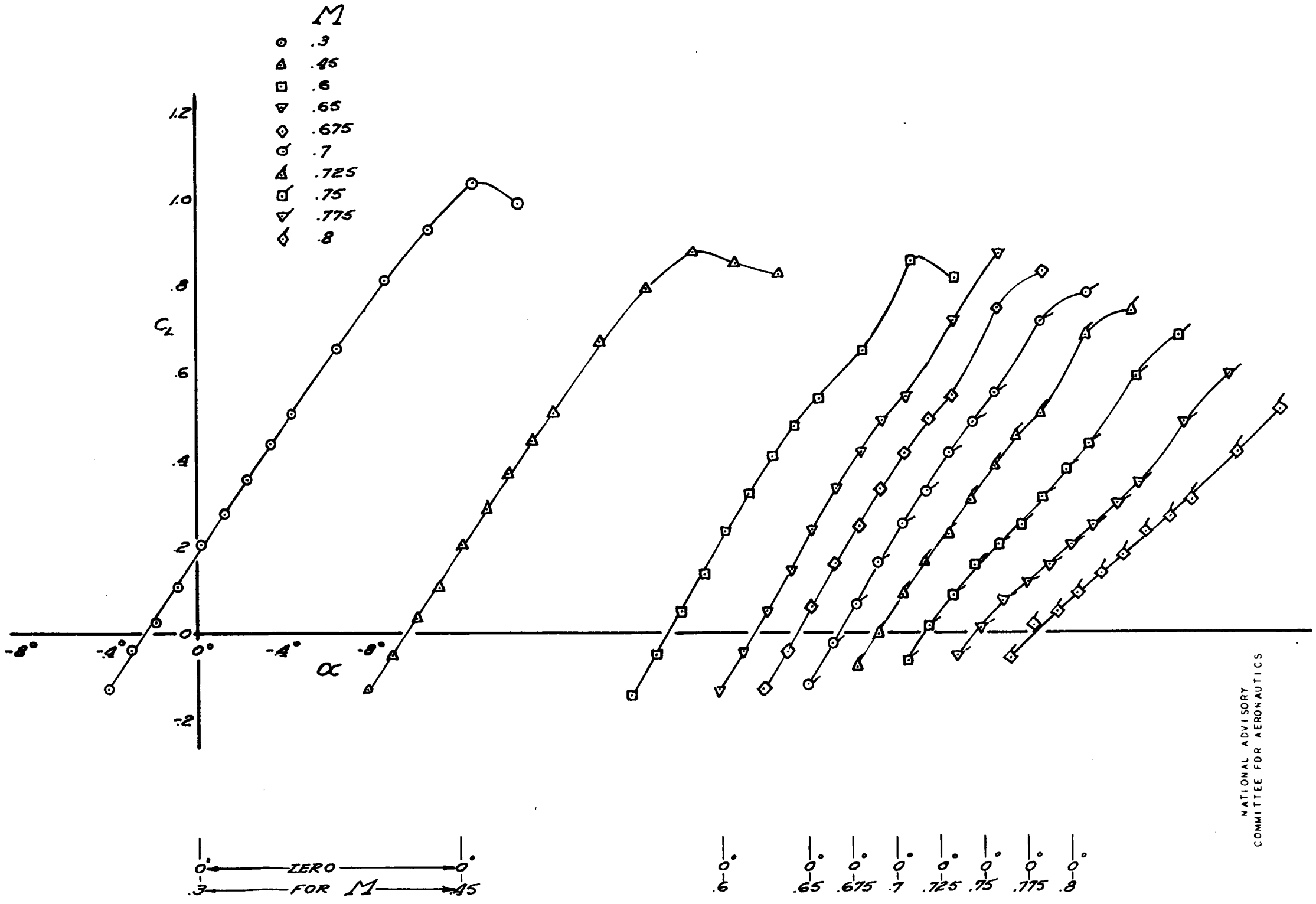

FIGURE 22:- VARIATION OF LIFT COEFFICIENT WITH ANGLE OF ATTACK FOR THE MODEL WITH AMES FILLETS MINUS THE HORIZONTAL TAIL.

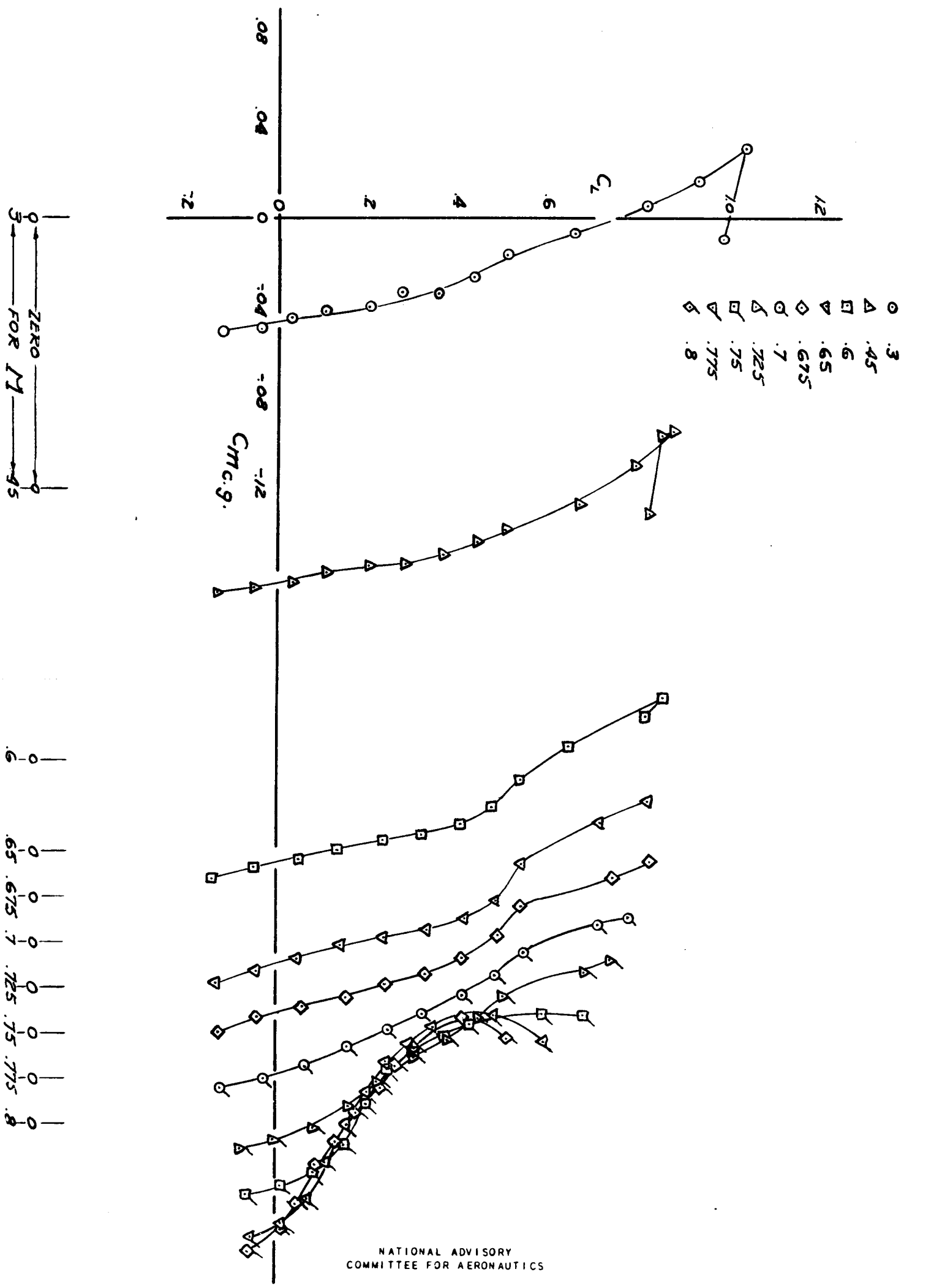

FIGURE 23:- VARIATION OF LIFT COEFFICIENT WITH PITCHING-MOMENT COEFFICIENT FOR THE MODEL WITH AMES FILLETS MINUS THE HORIZONTAL TAIL.

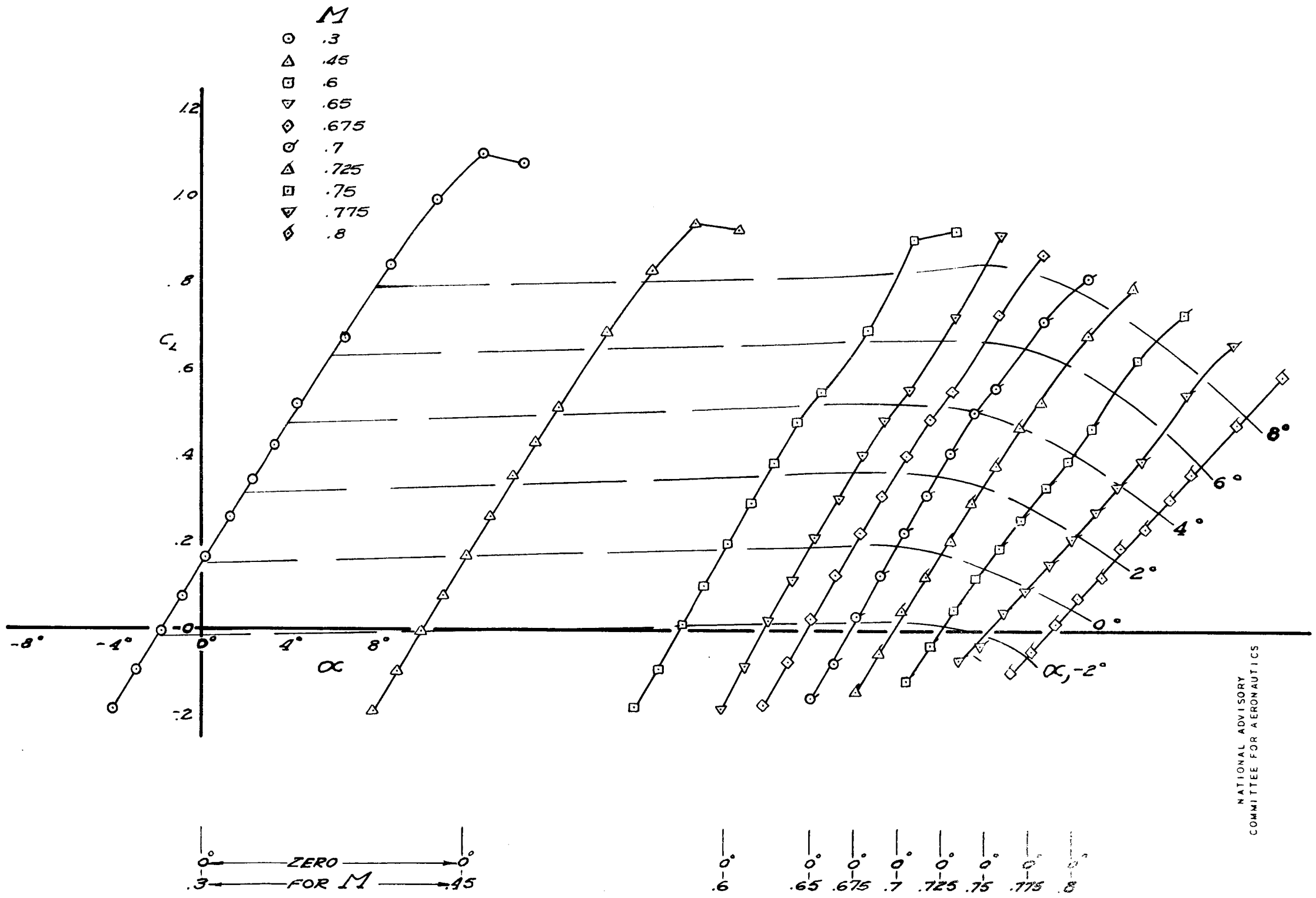

NATIONAL ADVISORY
COMMITTEE FOR AERONAUTICS

FIGURE 25.- VARIATION OF LIFT COEFFICIENT WITH ANGLE OF ATTACK FOR THE COMPLETE MODEL WITH AMES FILLETS AND AND 20-PERCENT-CHORD ELEVATOR. δ_e, 0°.

R No. A6D03

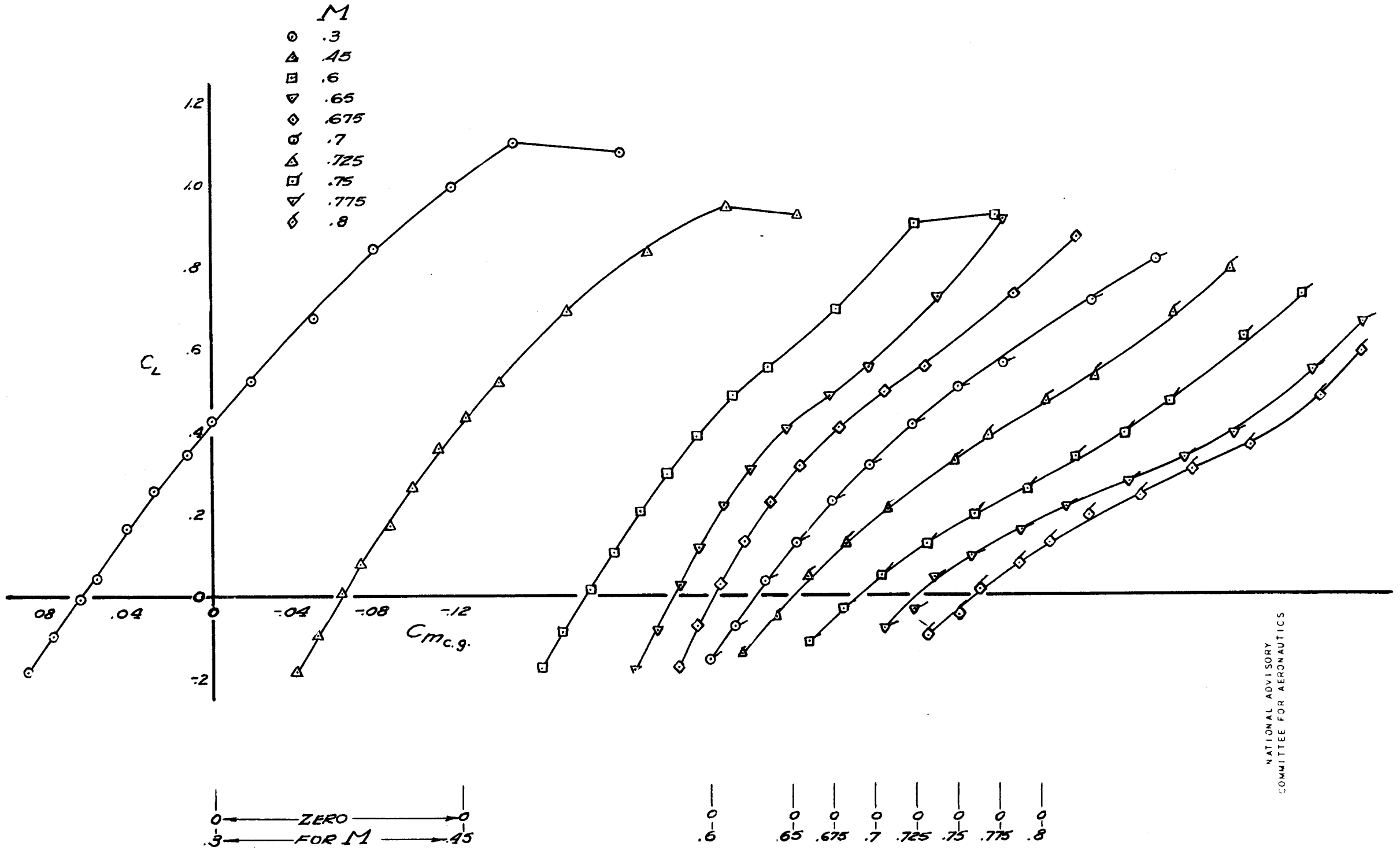

NATIONAL ADVISORY
COMMITTEE FOR AERONAUTICS

FIGURE 26:- VARIATION OF LIFT COEFFICIENT WITH PITCHING-MOMENT COEFFICIENT FOR THE COMPLETE MODEL WITH AMES FILLETS AND 20-PERCENT-CHORD ELEVATOR. δ_e, 0°.

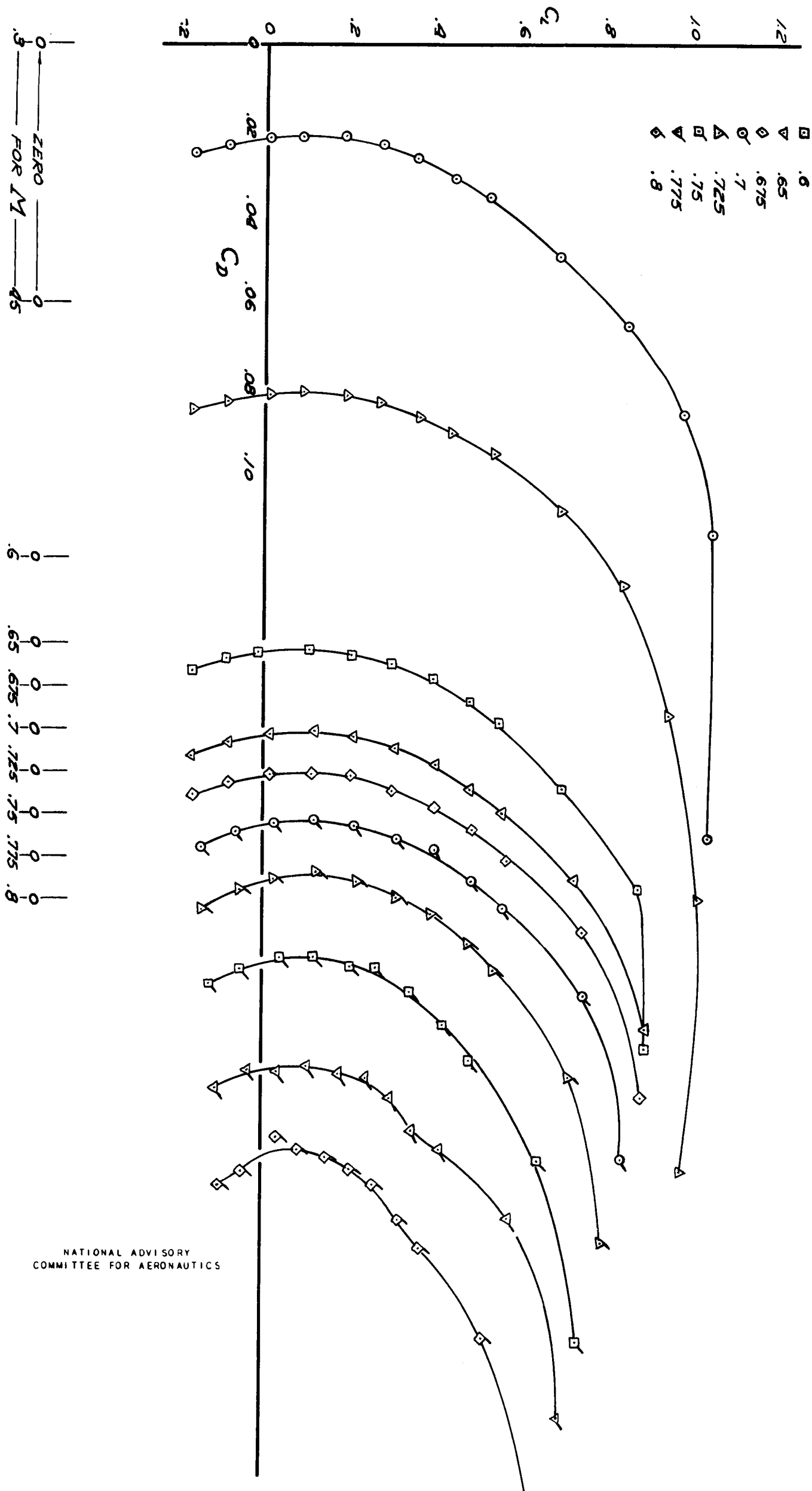

FIGURE 27:- VARIATION OF LIFT COEFFICIENT WITH DRAG COEFFICIENT FOR THE COMPLETE MODEL WITH AMES FILLETS PLUS SIX WING GUNS. δ_e, 0°.

MR No. A6D03

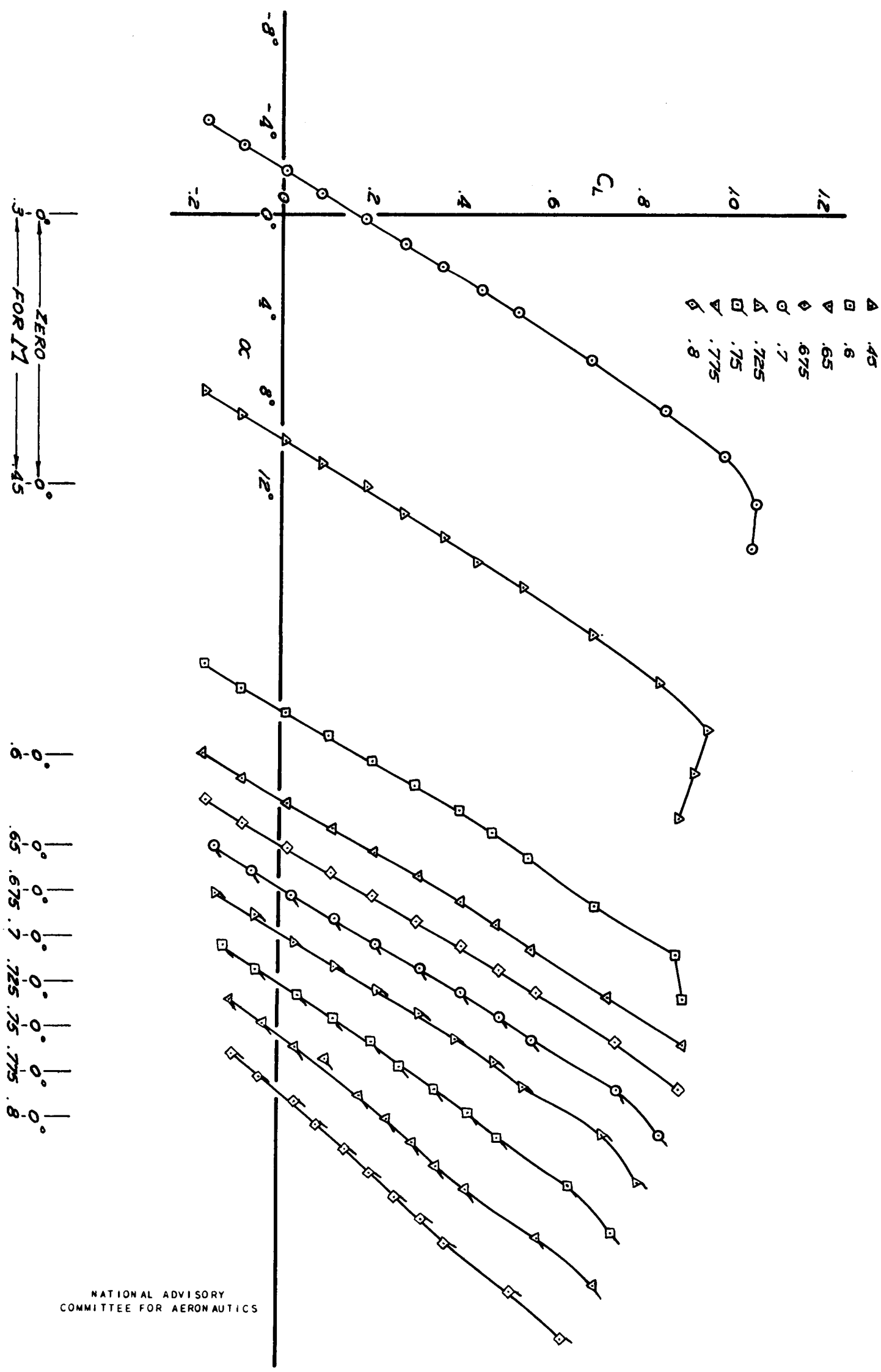

FIGURE 28:- VARIATION OF LIFT COEFFICIENT WITH ANGLE OF ATTACK FOR THE COMPLETE MODEL WITH AMES FILLETS PLUS SIX WING GUNS. δ_e, 0°.

MR No. A6D03

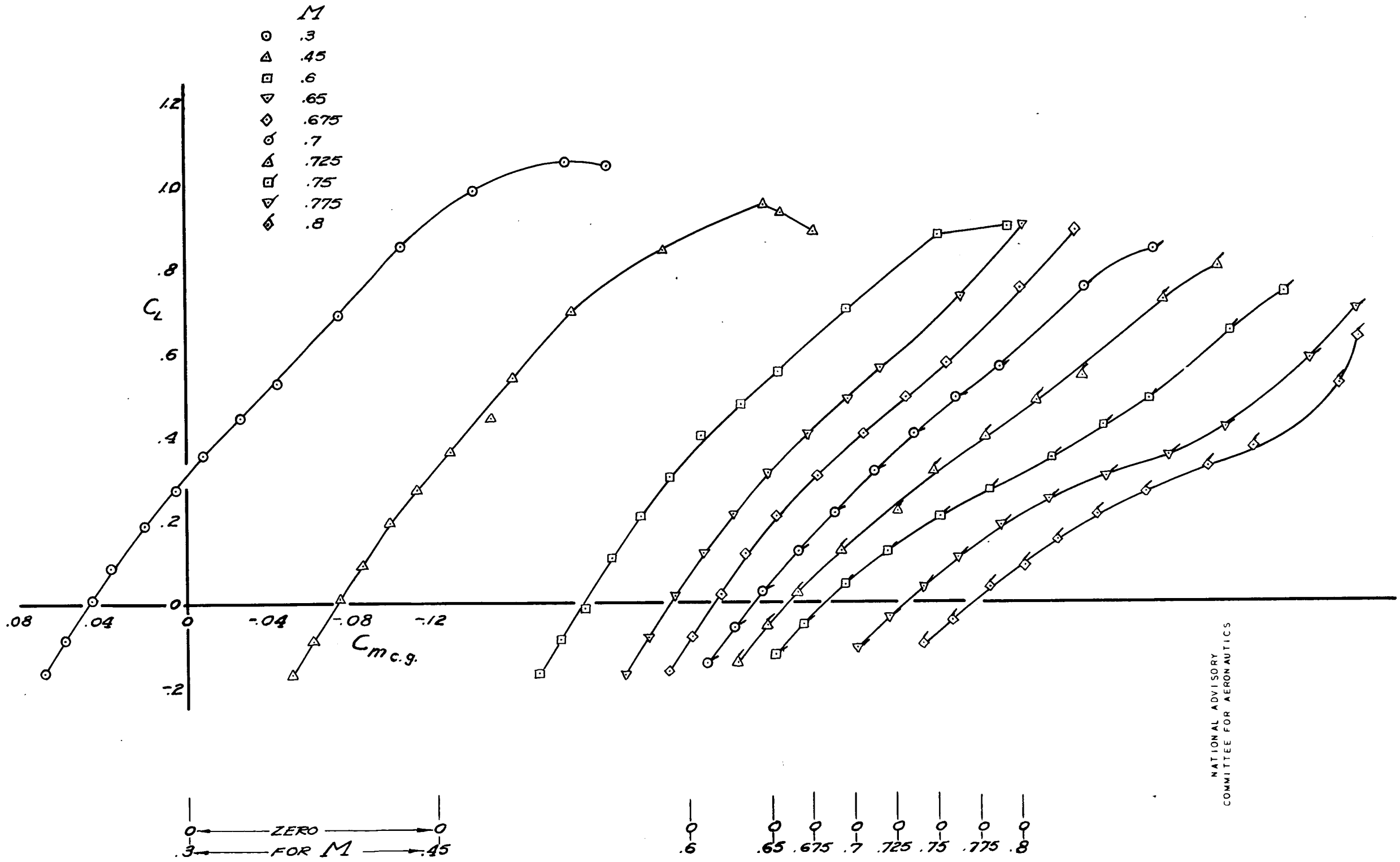

NATIONAL ADVISORY
COMMITTEE FOR AERONAUTICS

FIGURE 29:- VARIATION OF LIFT COEFFICIENT WITH PITCHING-MOMENT COEFFICIENT FOR THE COMPLETE MODEL WITH AMES FILLETS PLUS SIX WING GUNS. δ_e, 0°.

MR No. A6D03

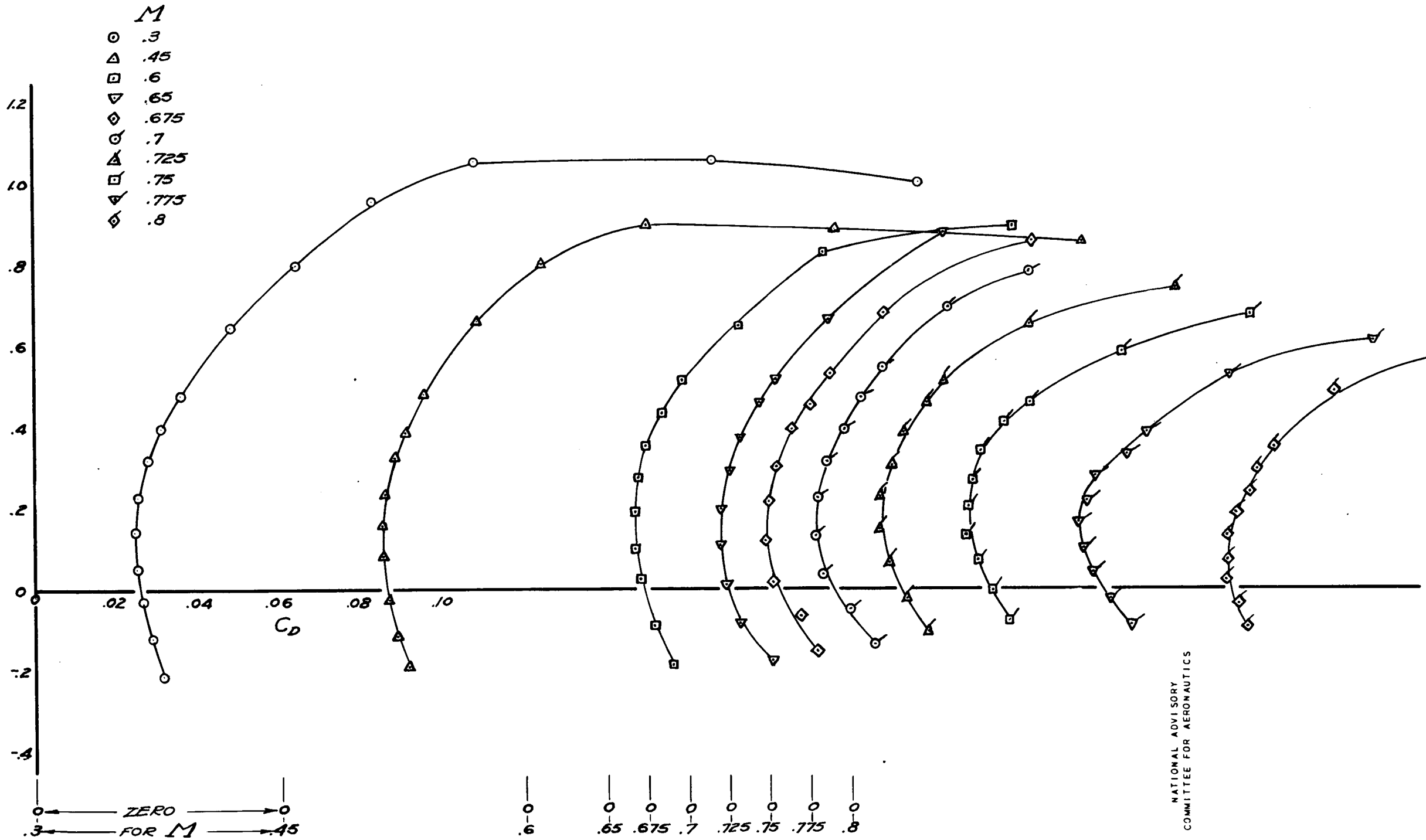

NATIONAL ADVISORY COMMITTEE FOR AERONAUTICS

FIGURE 30:- VARIATION OF LIFT COEFFICIENT WITH DRAG COEFFICIENT FOR THE COMPLETE MODEL WITH AMES FILLETS PLUS SIX WING GUNS AND EIGHT GUN NACELLE. δ_e, 0°.

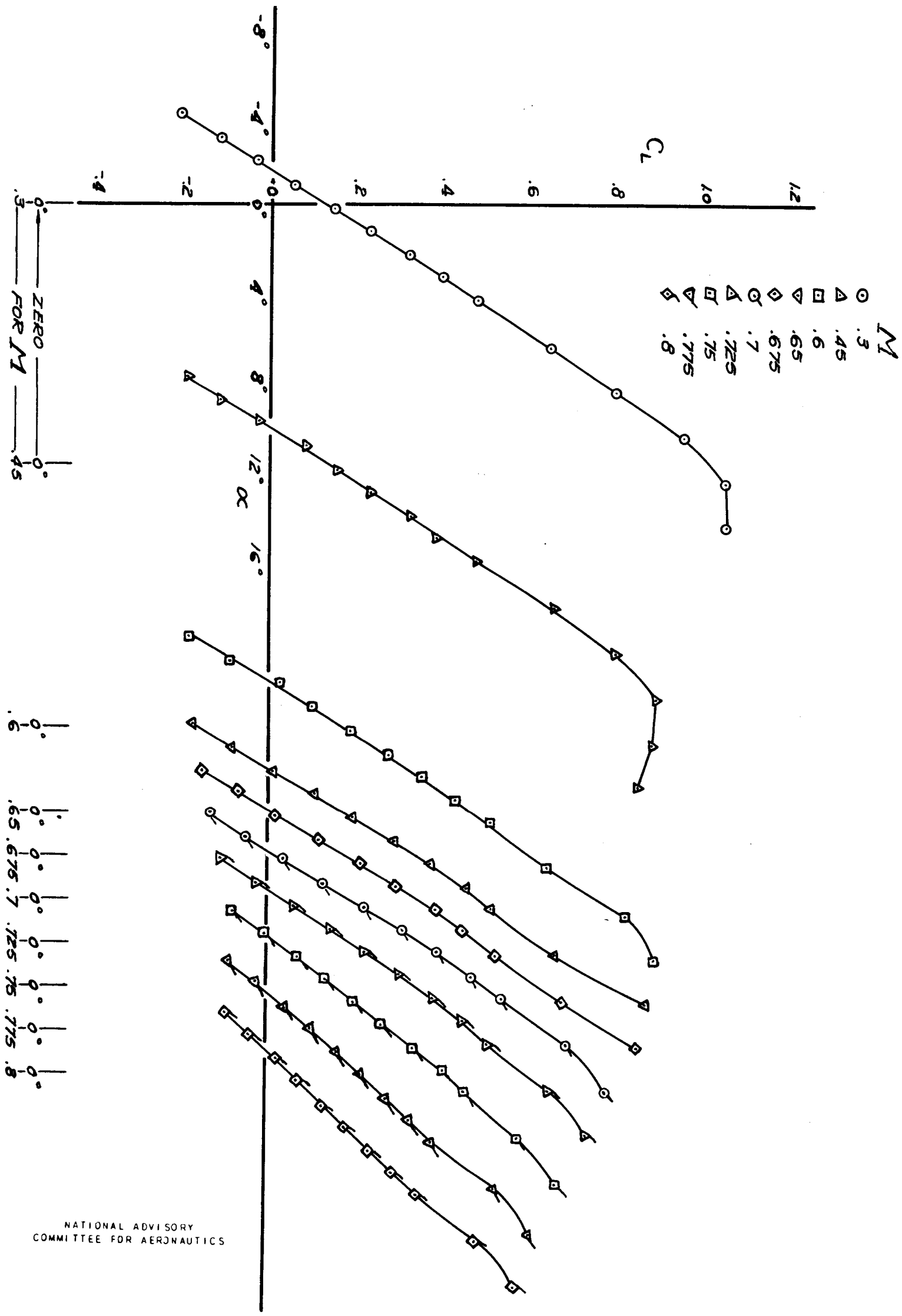

FIGURE 31:- VARIATION OF LIFT COEFFICIENT WITH ANGLE OF ATTACK FOR THE COMPLETE MODEL WITH AMES FILLETS PLUS SIX WING GUNS AND EIGHT GUN NACELLE. δ_e, 0°.

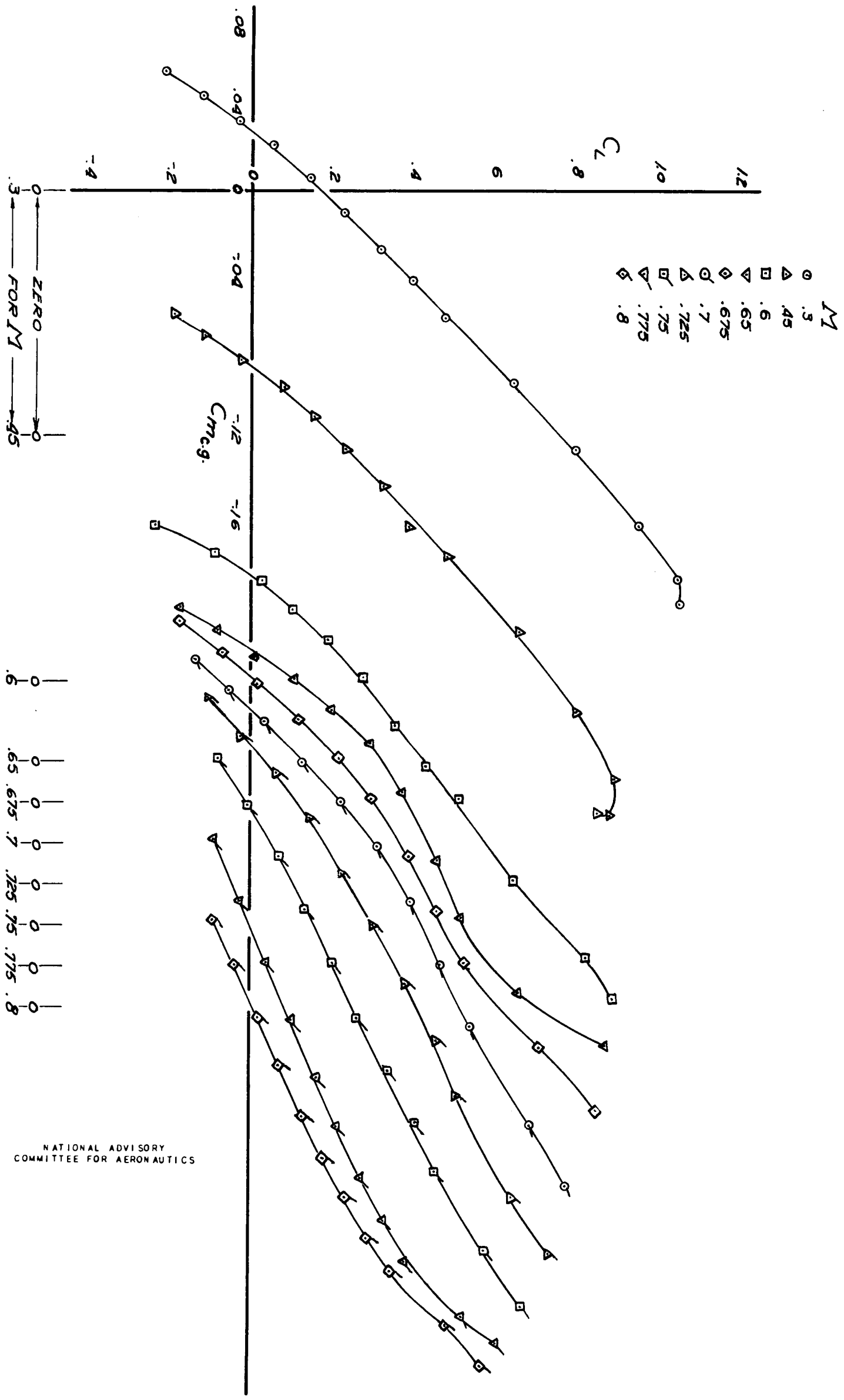

FIGURE 32:- VARIATION OF LIFT COEFFICIENT WITH PITCHING-MOMENT COEFFICIENT FOR THE COMPLETE MODEL WITH AMES FILLETS PLUS SIX WING GUNS AND EIGHT GUN NACELLE. δ_e, 0°.

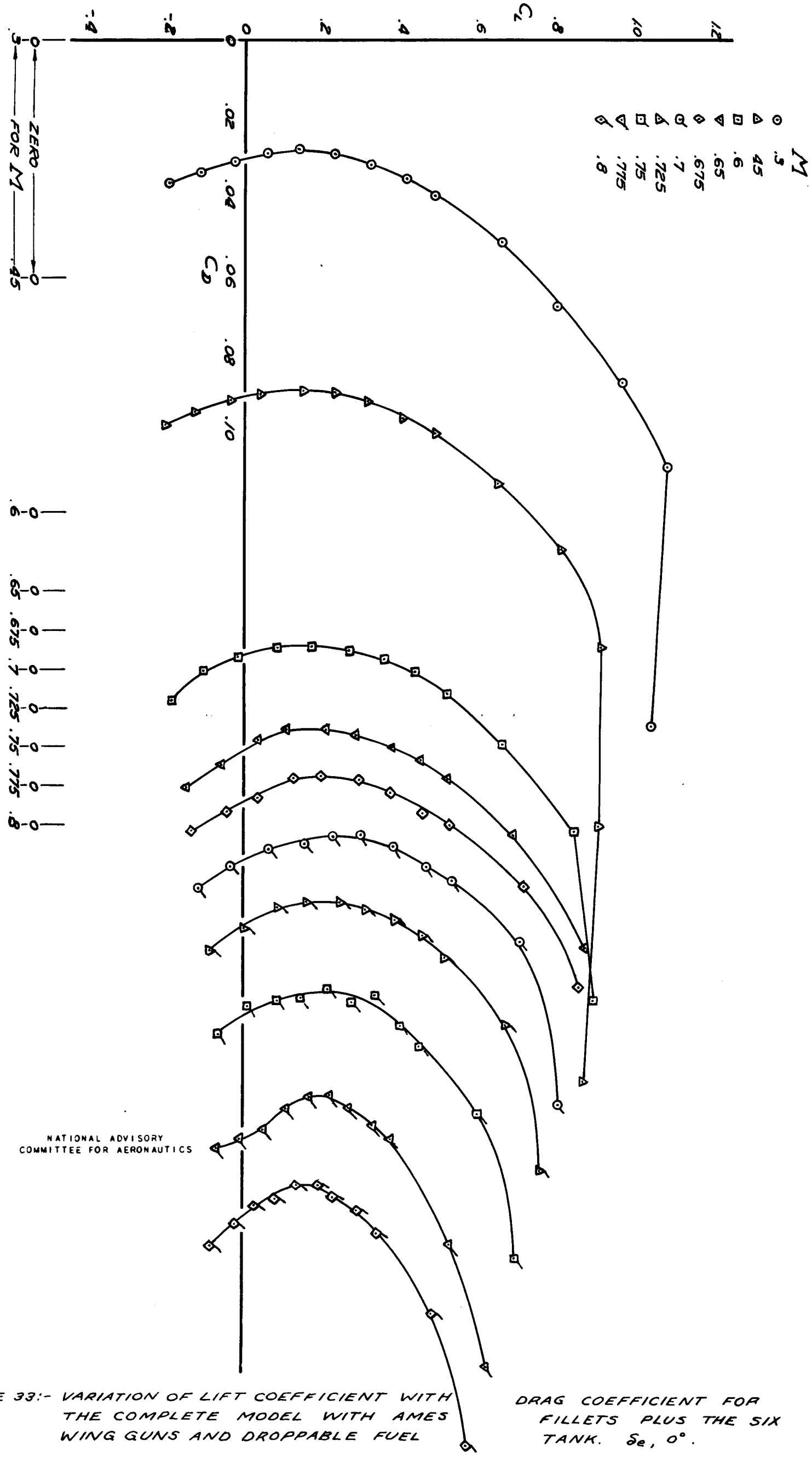

FIGURE 33:- VARIATION OF LIFT COEFFICIENT WITH DRAG COEFFICIENT FOR THE COMPLETE MODEL WITH AMES FILLETS PLUS THE SIX WING GUNS AND DROPPABLE FUEL TANK. δ_e, 0°.

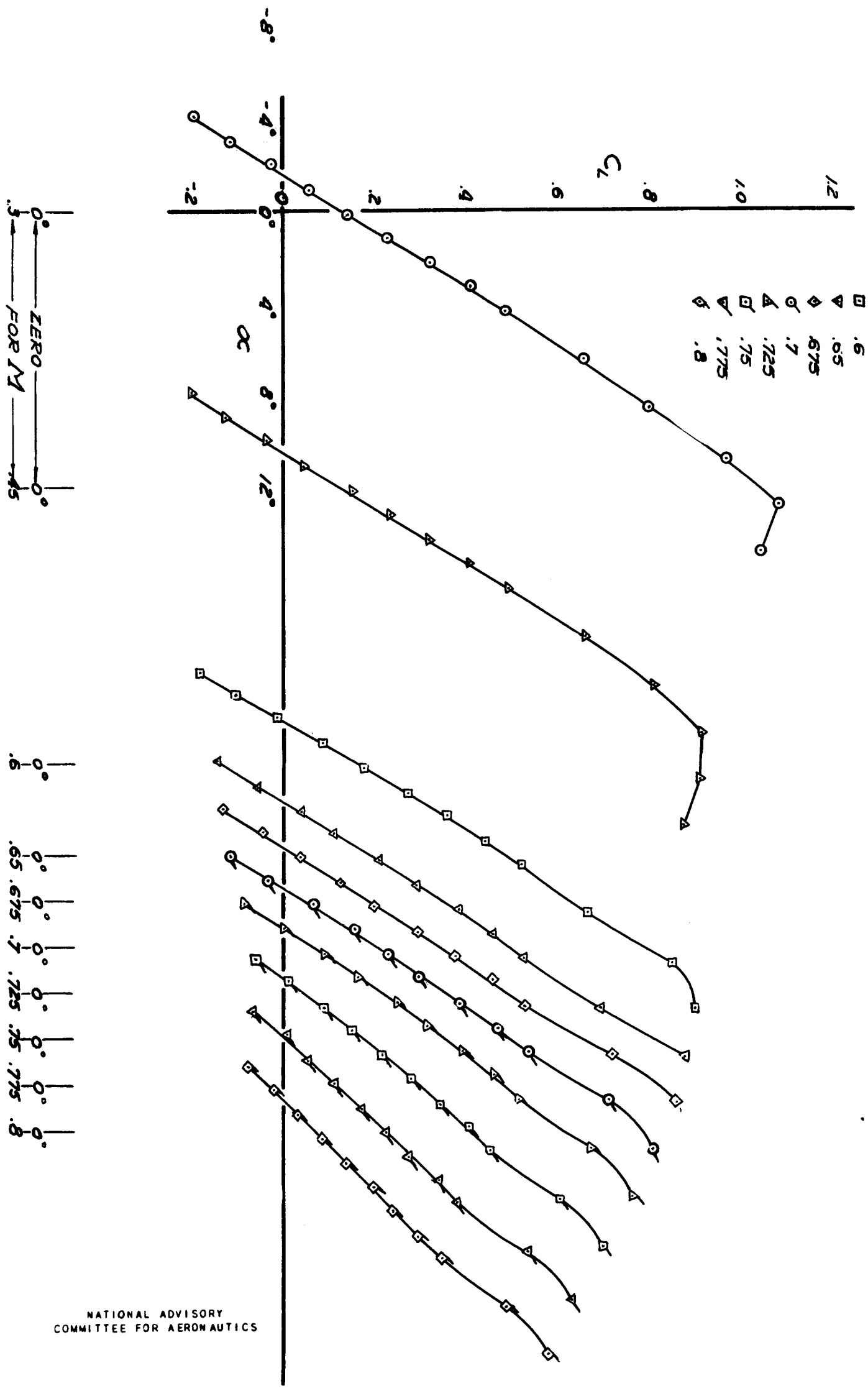

FIGURE 34:- VARIATION OF LIFT COEFFICIENT WITH ANGLE OF ATTACK FOR THE COMPLETE MODEL WITH AMES FILLETS PLUS SIX WING GUNS AND DROPPABLE FUEL TANK.

MR No. A6D03

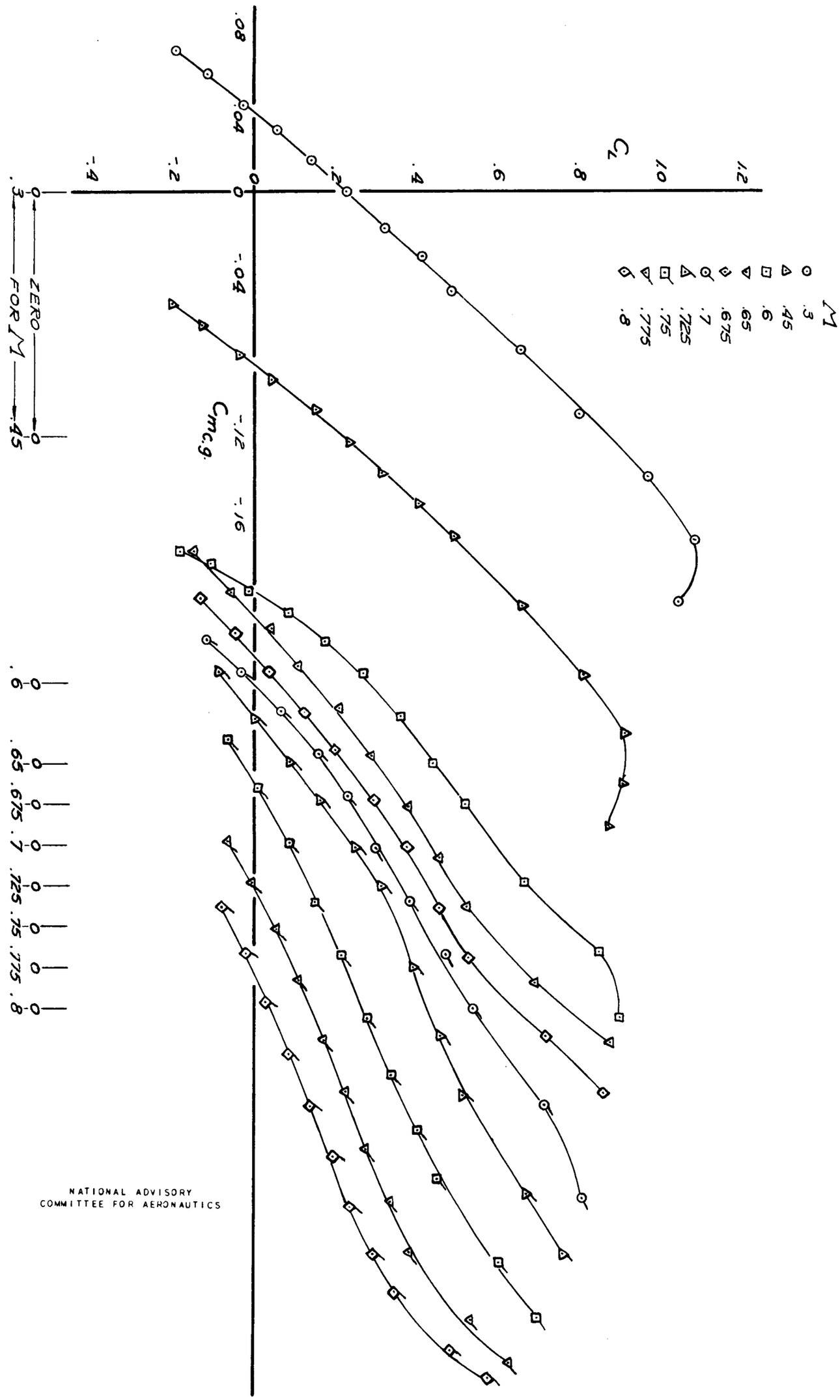

FIGURE 35:- VARIATION OF LIFT COEFFICIENT WITH PITCHING-MOMENT COEFFICIENT FOR THE COMPLETE MODEL WITH AMES FILLETS PLUS SIX WING GUNS AND DROPPABLE FUEL TANK. δ_e, 0°.

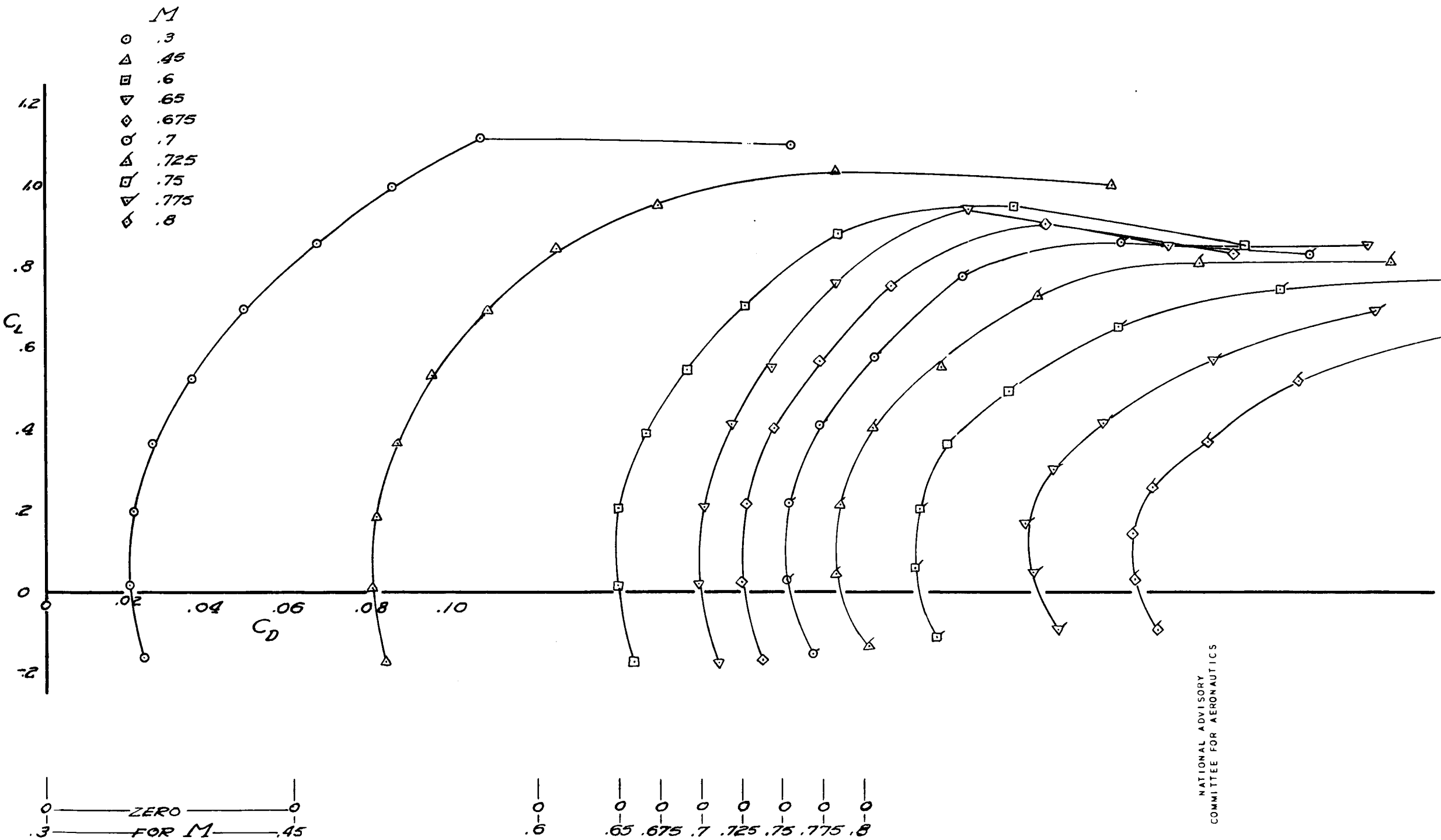

NATIONAL ADVISORY
COMMITTEE FOR AERONAUTICS

FIGURE 36:- VARIATION OF LIFT COEFFICIENT WITH DRAG COEFFICIENT FOR THE COMPLETE MODEL WITH MANUFACTURER'S FILLETS AND 32.8-PERCENT-CHORD ELEVATOR. δ_e, 0°.

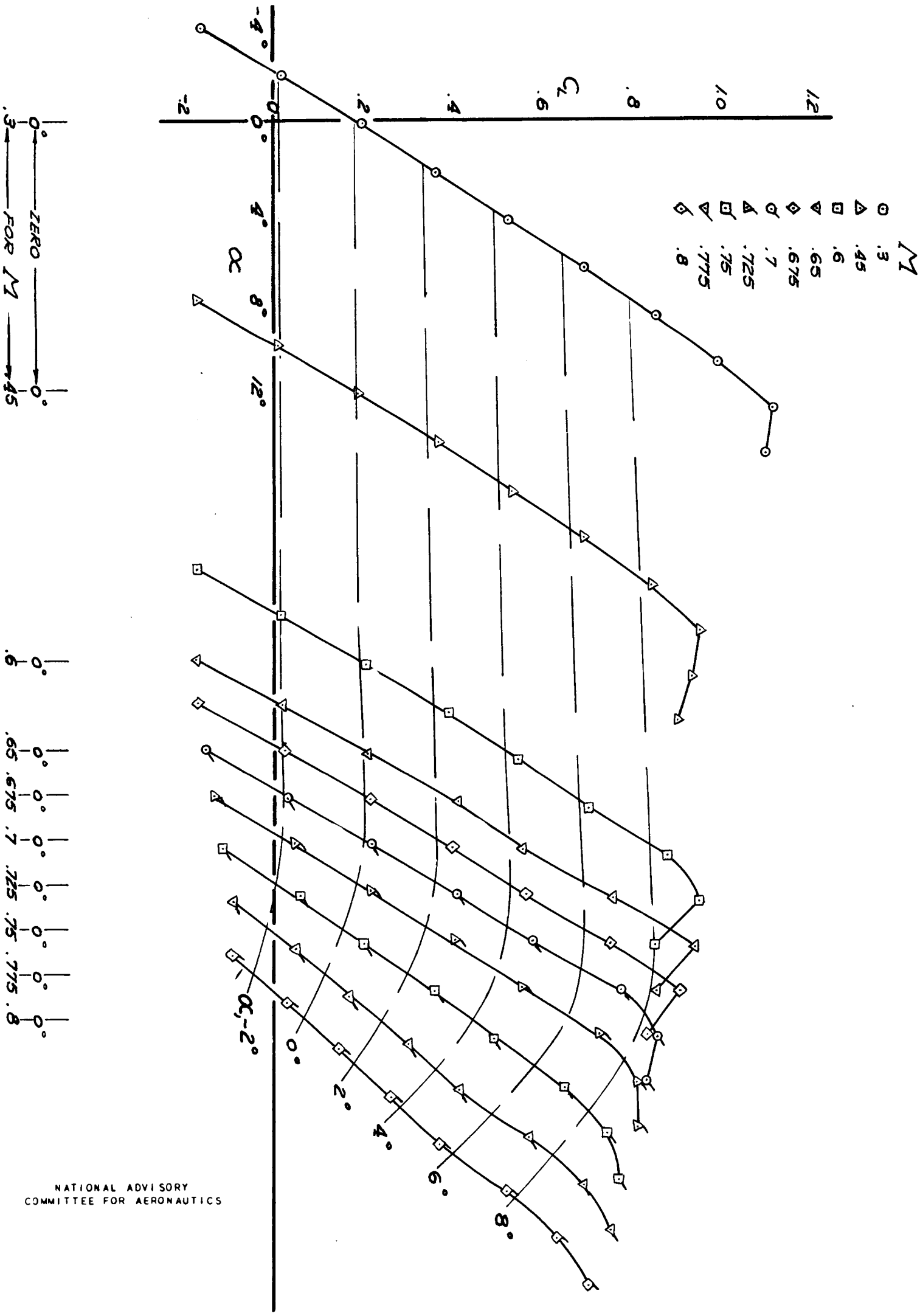

FIGURE 37:- VARIATION OF LIFT COEFFICIENT WITH ANGLE OF ATTACK FOR THE COMPLETE MODEL WITH MANUFACTURER'S FILLETS AND 32.8-PERCENT-CHORD ELEVATOR. δ_e, 0.6°.

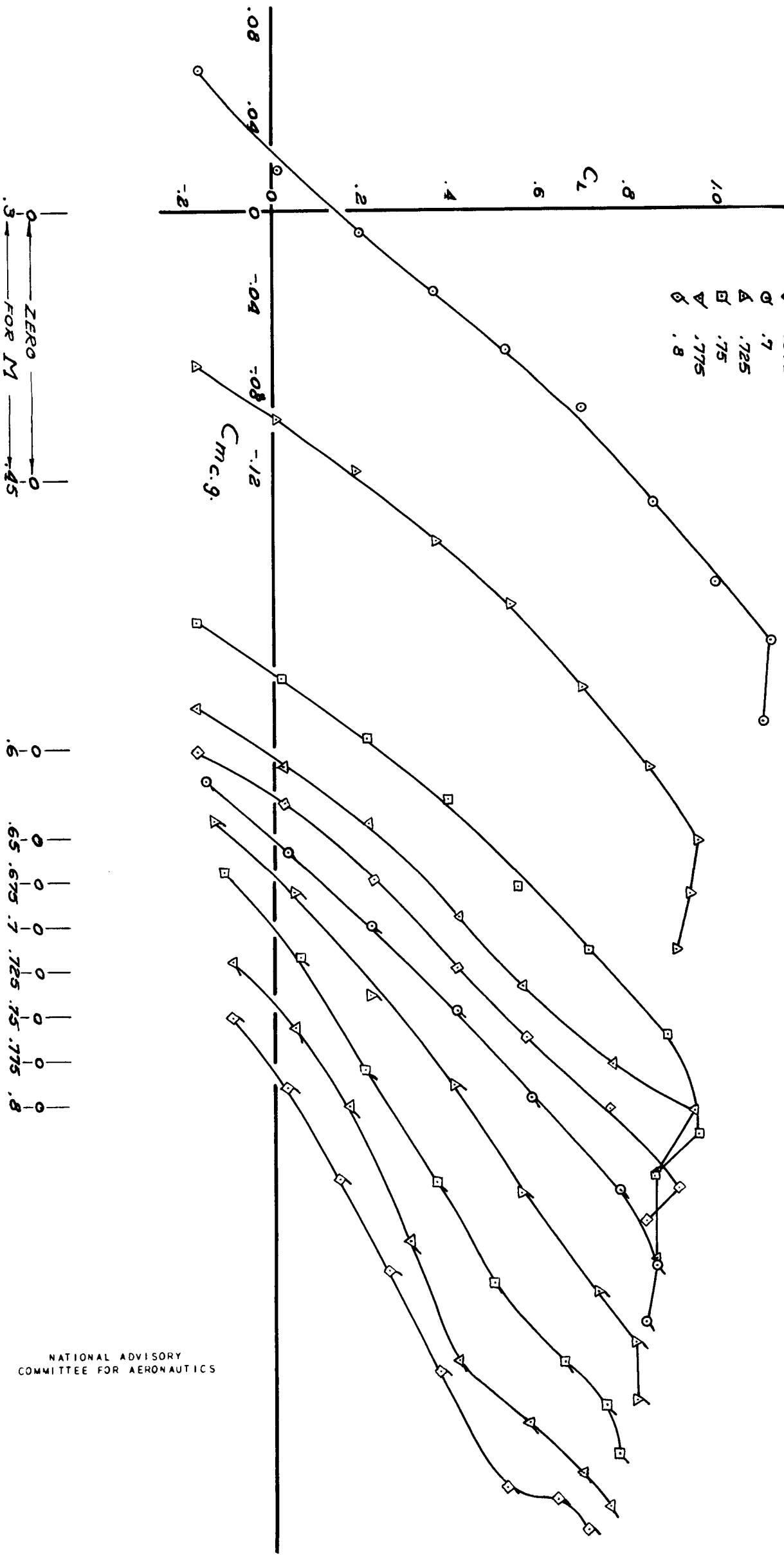

FIGURE 38:- VARIATION OF LIFT COEFFICIENT WITH PITCHING-MOMENT COEFFICIENT FOR THE COMPLETE MODEL WITH MANUFACTURER'S FILLETS AND 32.8-PERCENT CHORD ELEVATOR. δ_e, 0.6°.

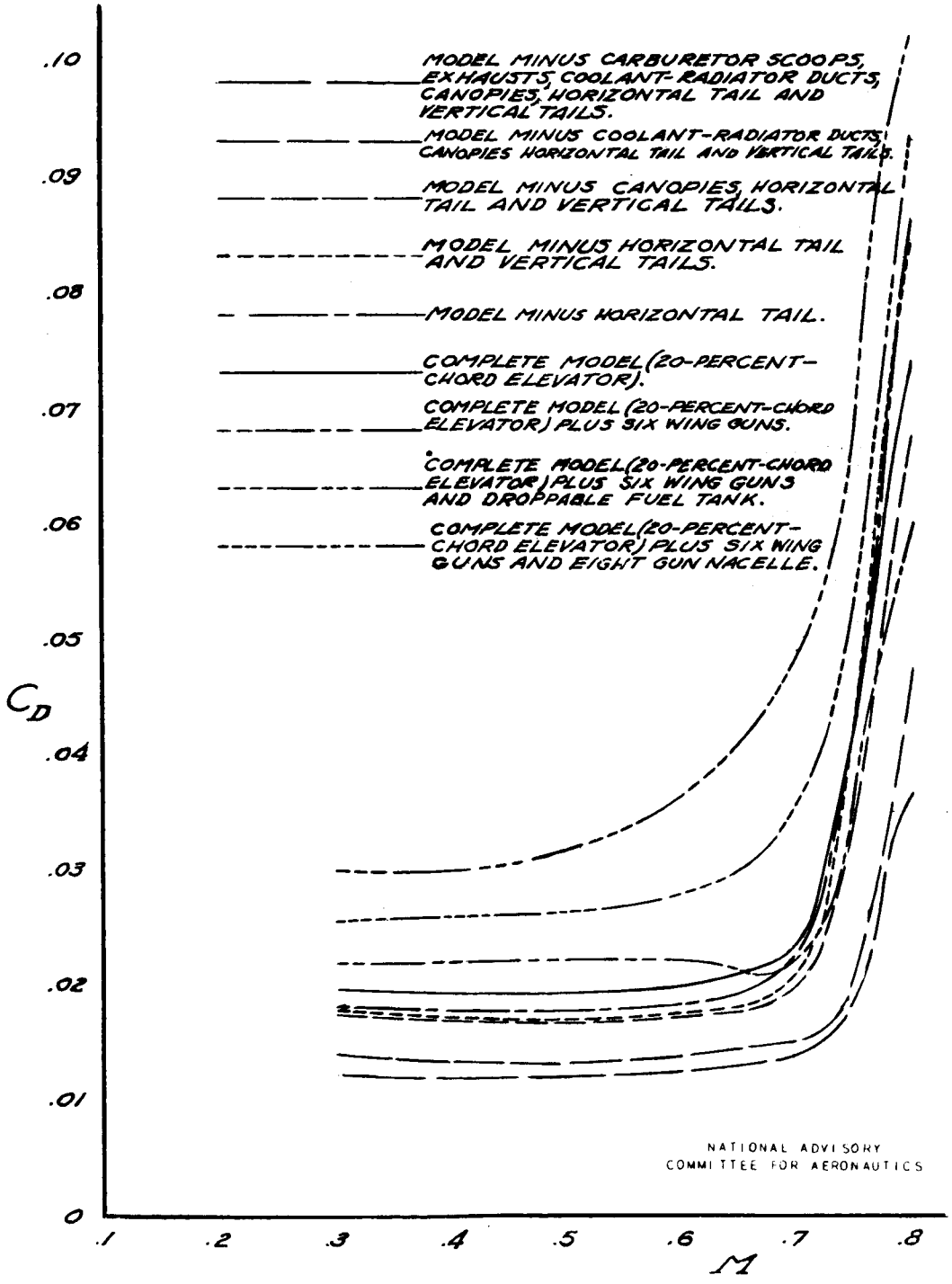

FIGURE 39.- VARIATION OF DRAG COEFFICIENT WITH MACH NUMBER FOR SEVERAL CONFIGURATIONS OF THE MODEL WITH AMES FILLETS.
C_L, 0.0 .

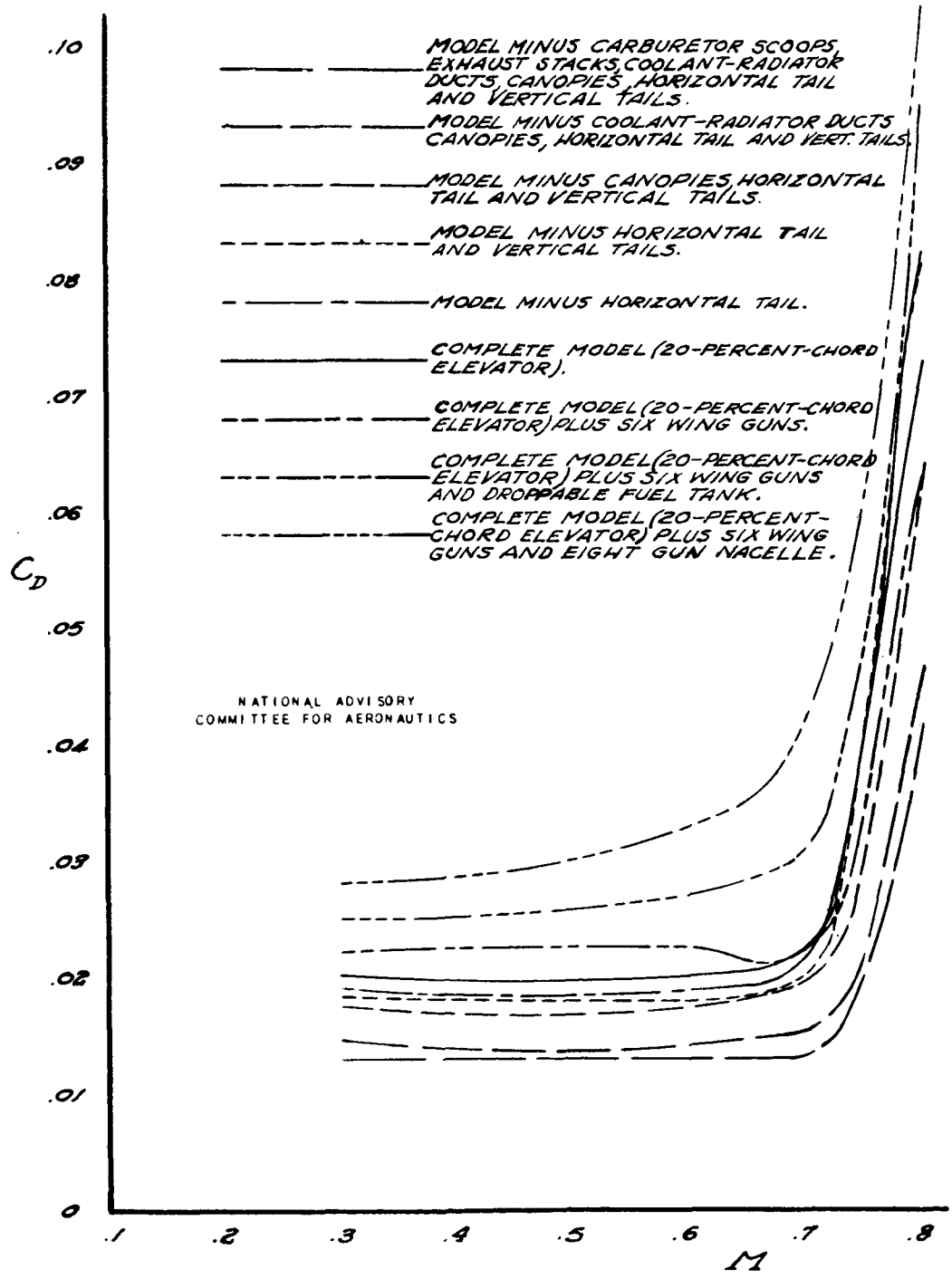

FIGURE 40:- VARIATION OF DRAG COEFFICIENT WITH MACH NUMBER FOR SEVERAL CONFIGURATIONS OF THE MODEL WITH AMES FILLETS.
C_L, 0.2.

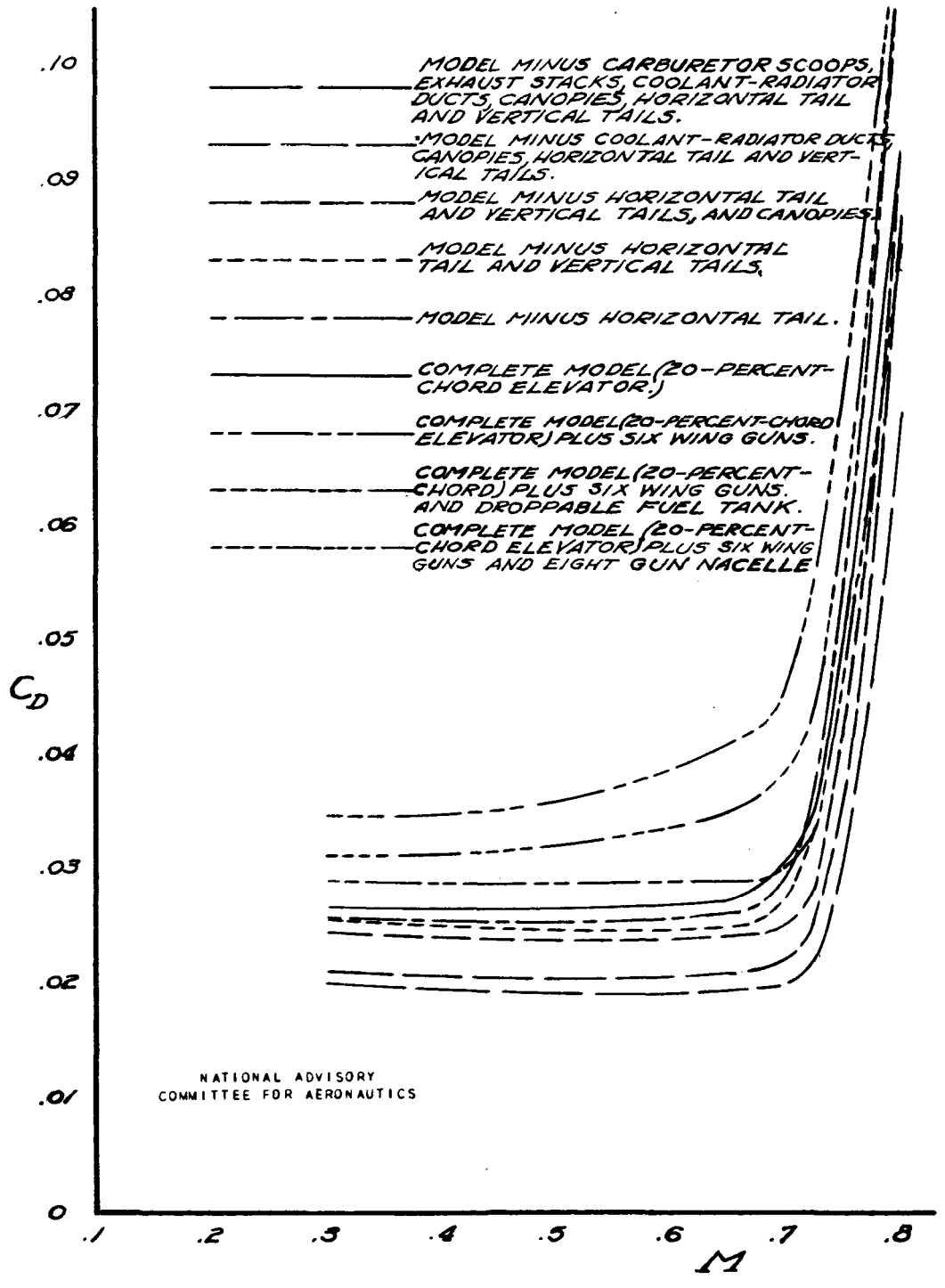

FIGURE 41.- VARIATION OF DRAG COEFFICIENT WITH MACH NUMBER FOR SEVERAL CONFIGURATIONS OF THE MODEL WITH AMES FILLETS.
C_L, 0.4.

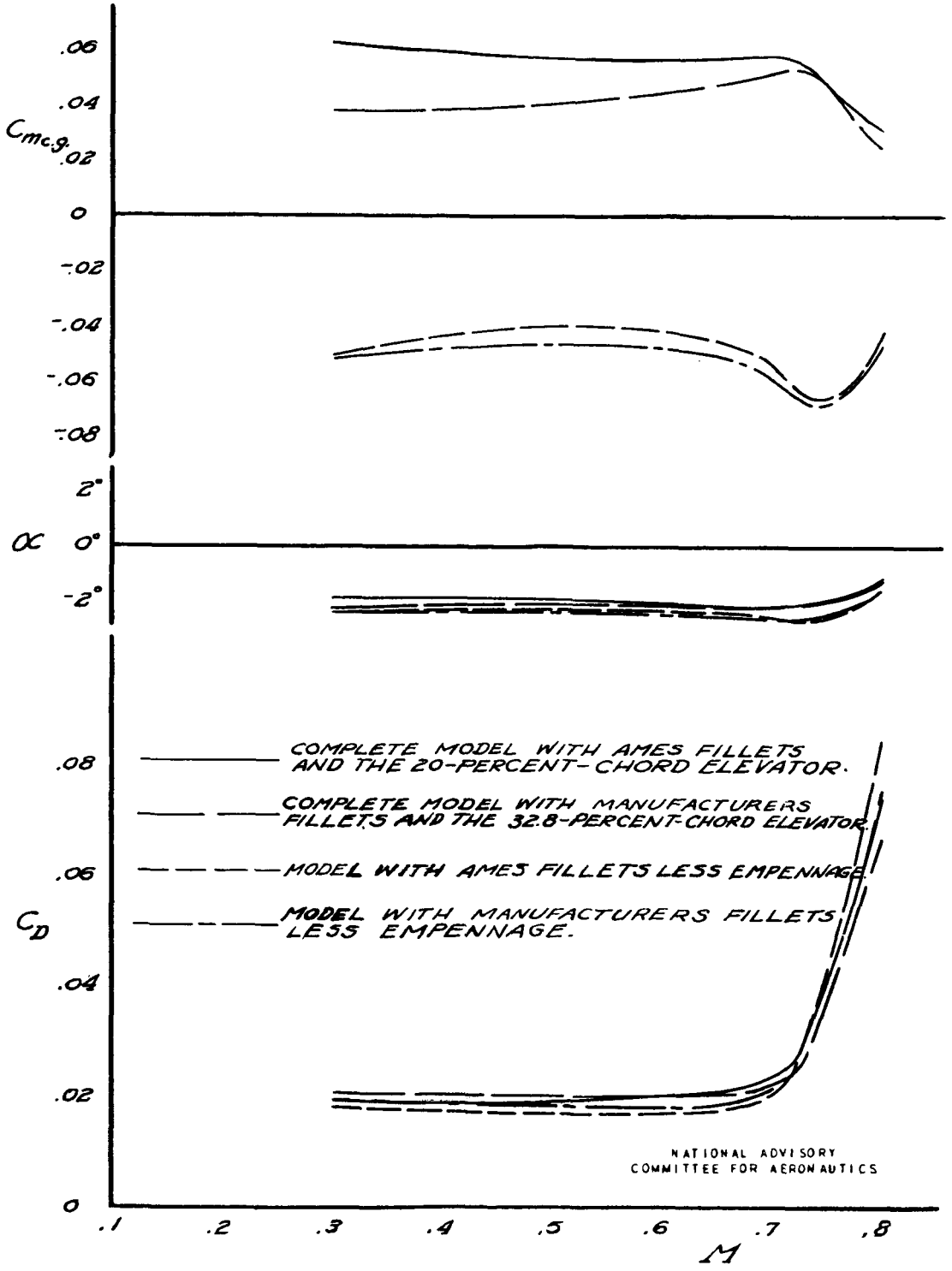

FIGURE 42.- VARIATION OF PITCHING-MOMENT COEFFICIENT, DRAG COEFFICIENT, AND ANGLE OF ATTACK WITH MACH NUMBER FOR SEVERAL CONFIGURATIONS OF THE MODEL. C_L, 0.0 .

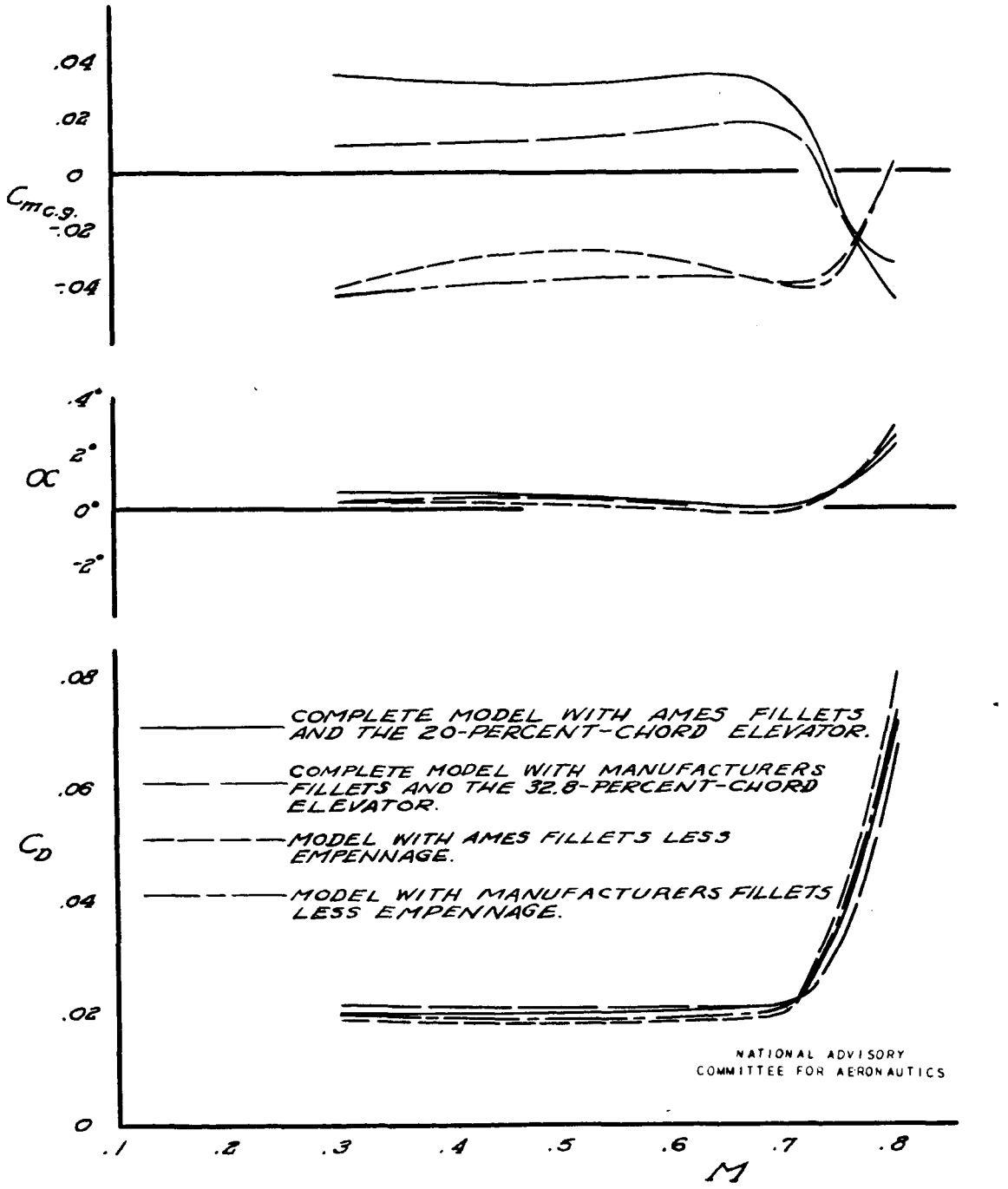

FIGURE 43:- VARIATION OF PITCHING-MOMENT COEFFICIENT, DRAG COEFFICIENT AND ANGLE OF ATTACK WITH MACH NUMBER FOR SEVERAL CONFIGURATIONS OF THE MODEL. C_L, 0.2.

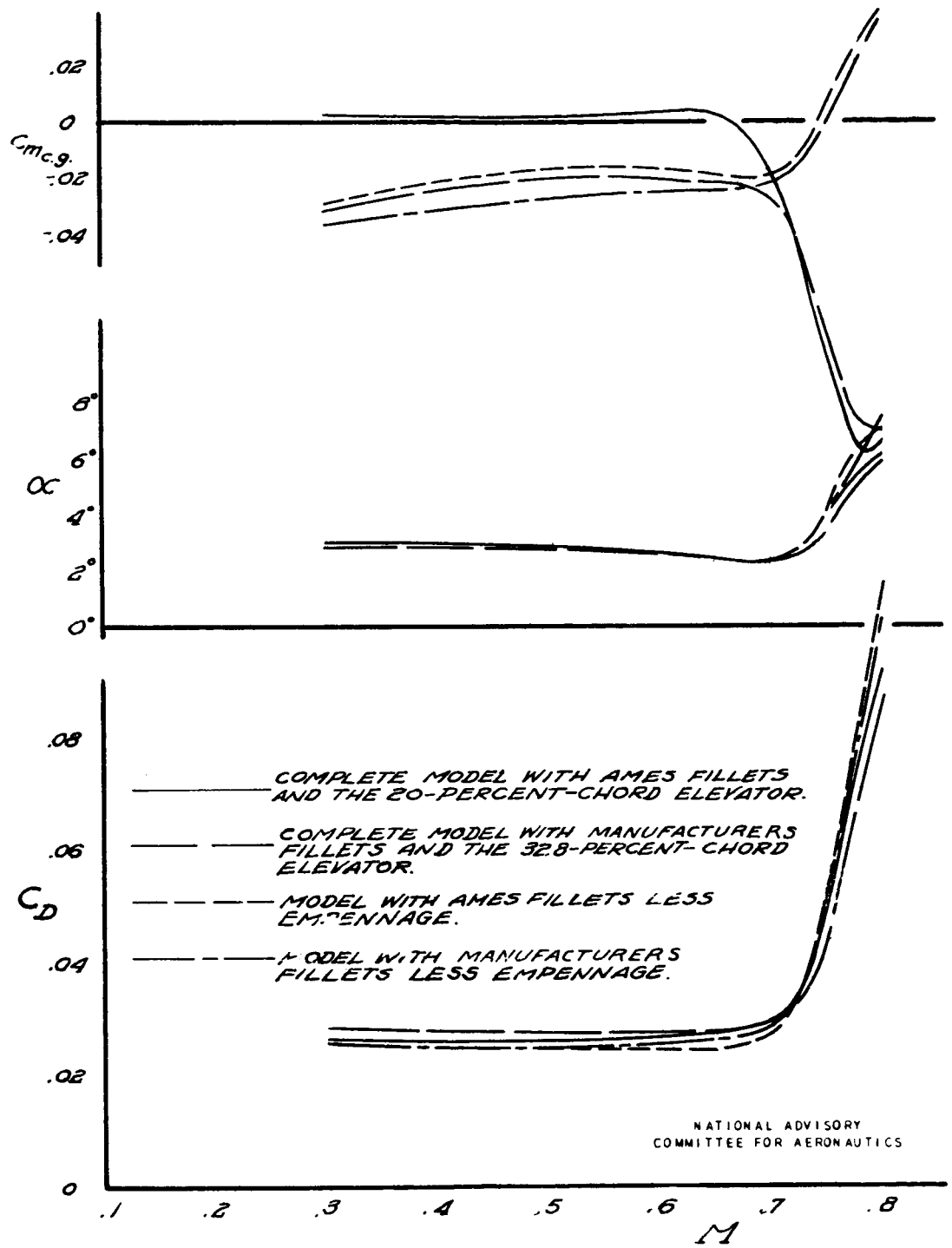

FIGURE 44:- VARIATION OF PITCHING-MOMENT COEFFICIENT, DRAG COEFFICIENT AND ANGLE OF ATTACK WITH MACH NUMBER FOR SEVERAL CONFIGURATIONS OF THE MODEL. C_L, 0.4.

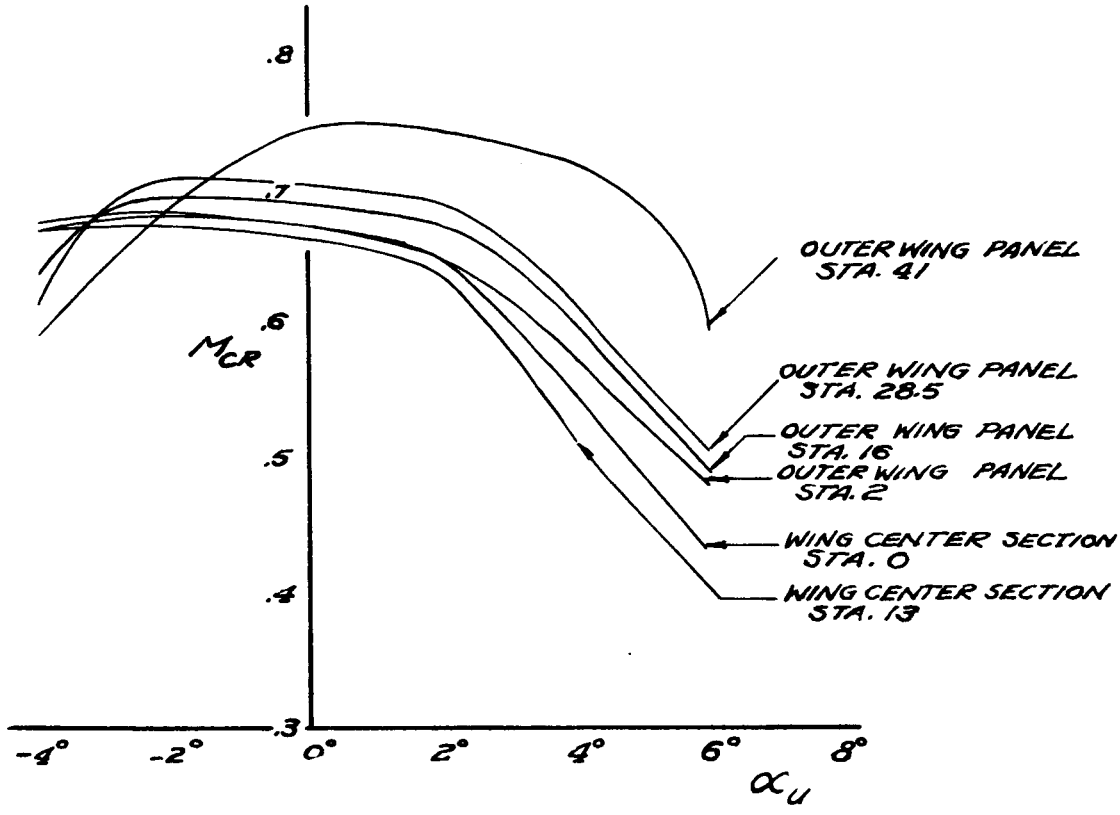

FIGURE 45:- VARIATION OF THE CRITICAL MACH NUMBER WITH ANGLE OF ATTACK FOR SEVERAL WING STATIONS ON THE MODEL WITH AMES FILLETS. δ_a, 0°; MODEL COMPLETE WITH PRESSURE-TUBE STRUT.

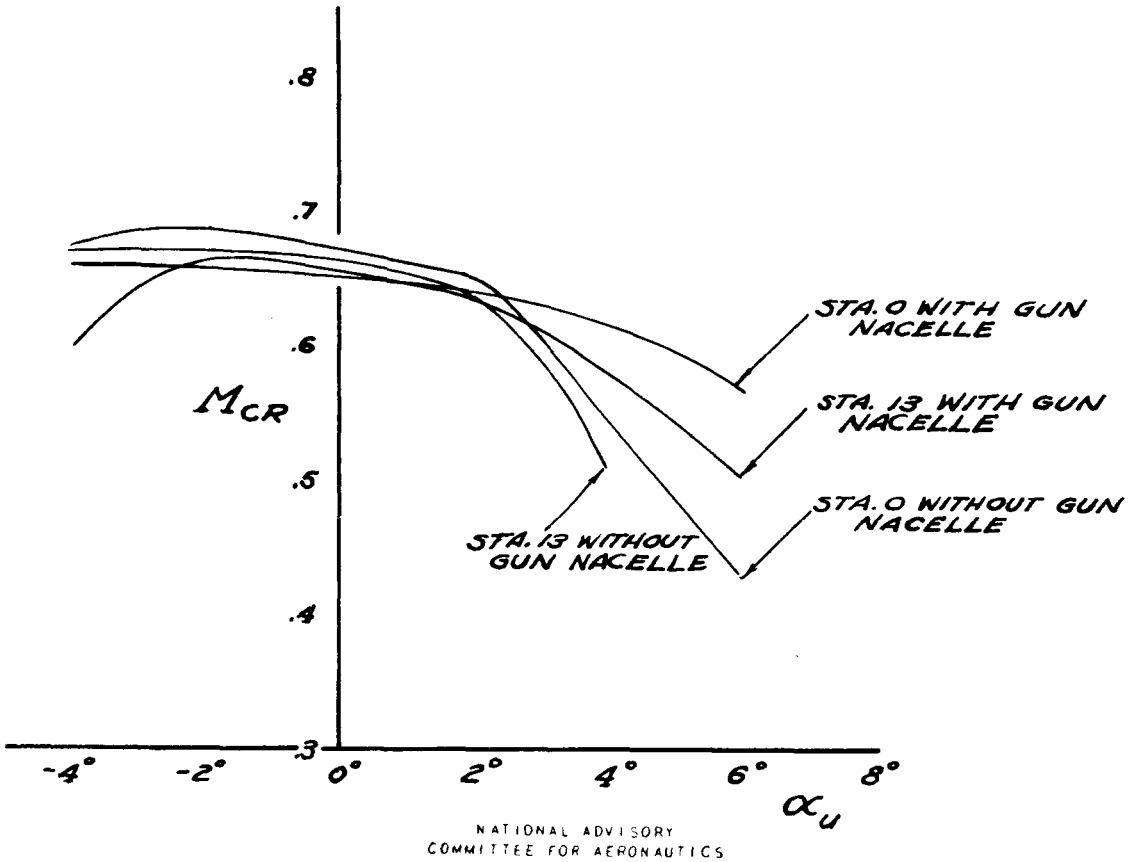

FIGURE 46:- EFFECT OF GUN NACELLE ON THE CRITICAL MACH NUMBER OF THE WING CENTER SECTION OF THE MODEL WITH AMES FILLETS. MODEL COMPLETE WITH PRESSURE-TUBE STRUT.

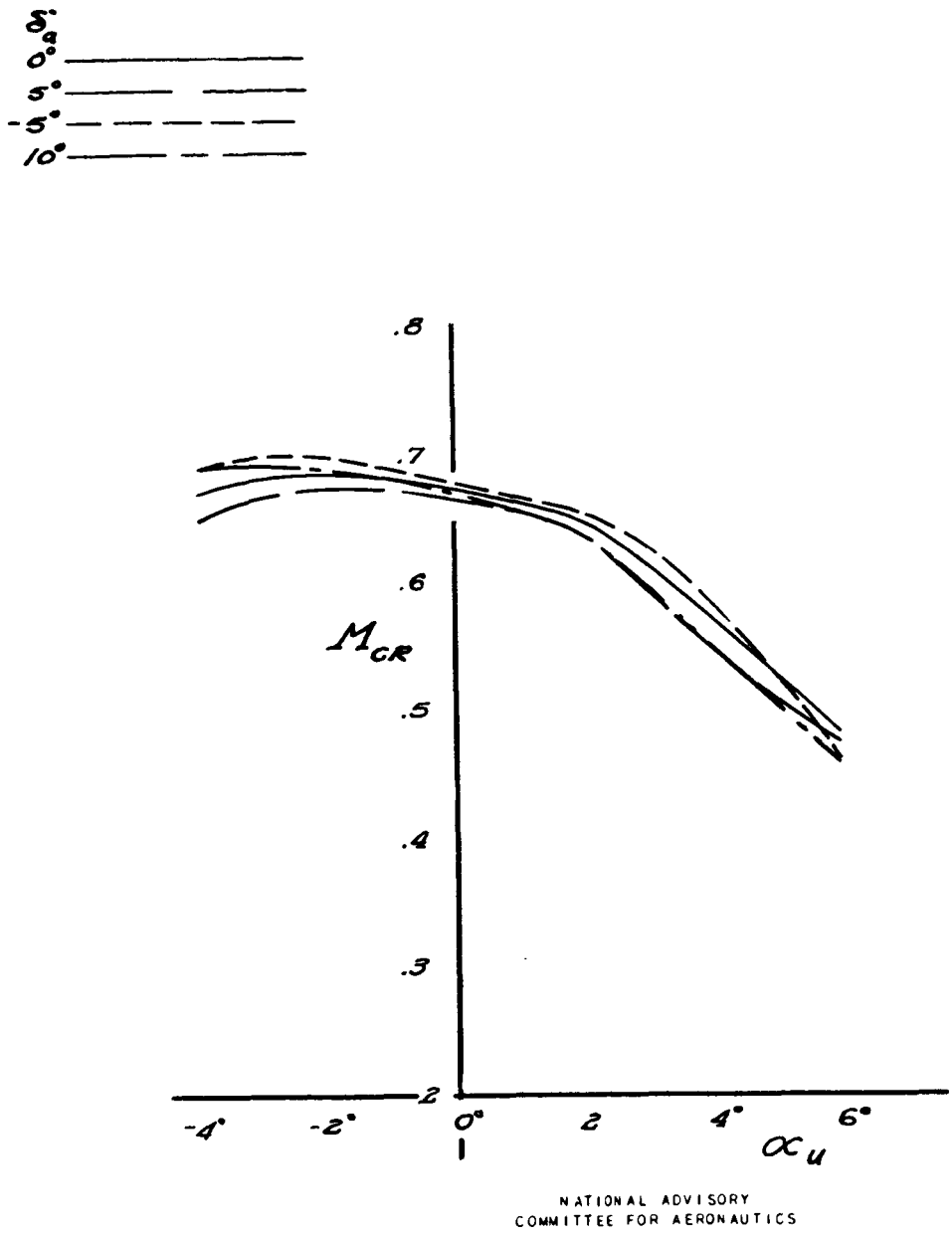

FIGURE 47:- VARIATION OF CRITICAL MACH NUMBER WITH ANGLE OF ATTACK FOR SEVERAL AILERON DEFLECTIONS ON THE MODEL WITH AMES FILLETS. MODEL COMPLETE WITH PRESSURE-TUBE STRUT. WING STATION 2.00

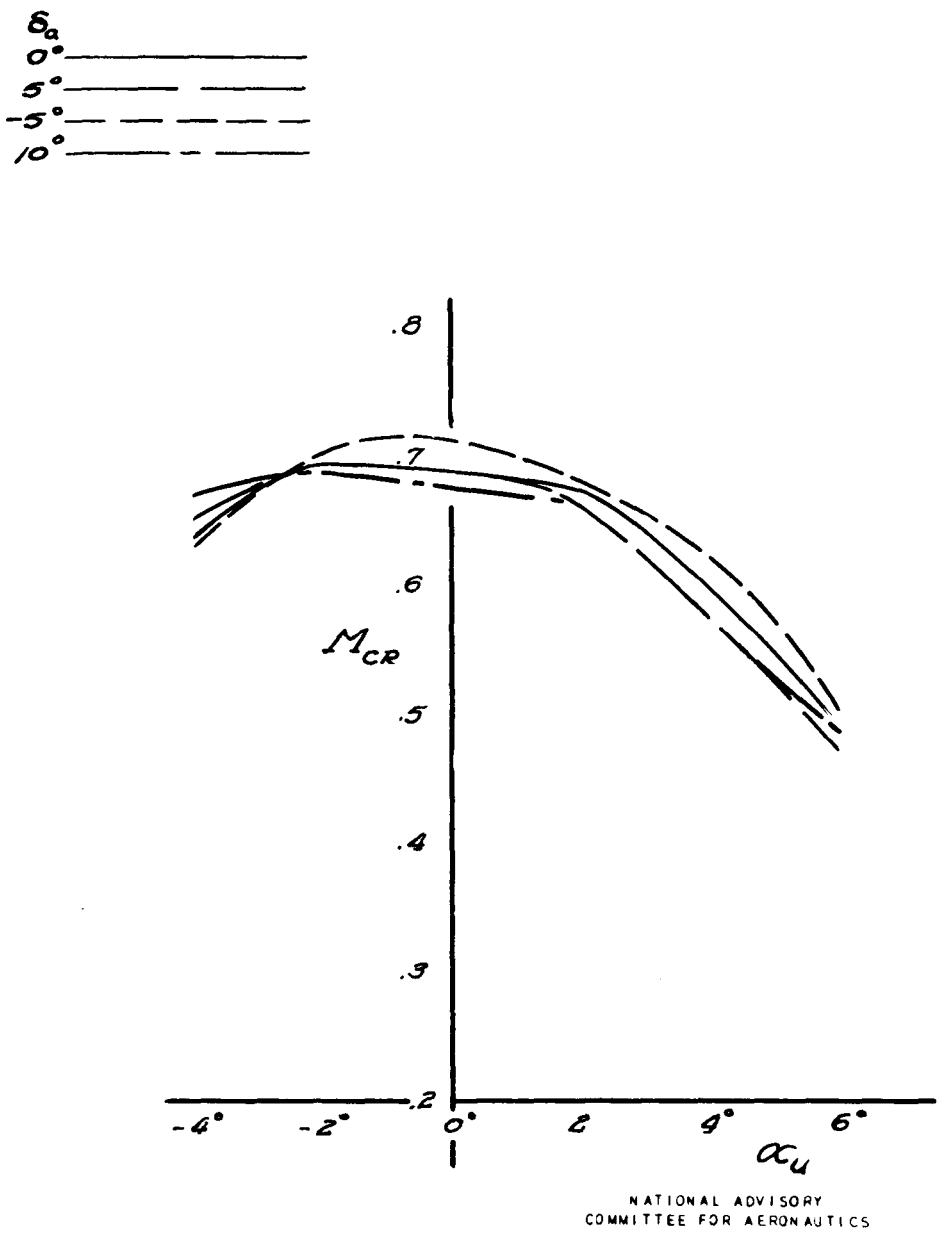

FIGURE 48:- VARIATION OF CRITICAL MACH NUMBER WITH ANGLE OF ATTACK FOR SEVERAL AILERON DEFLECTIONS ON THE MODEL WITH AMES FILLETS. MODEL COMPLETE WITH PRESSURE-TUBE STRUT. WING STATION 16.00 .

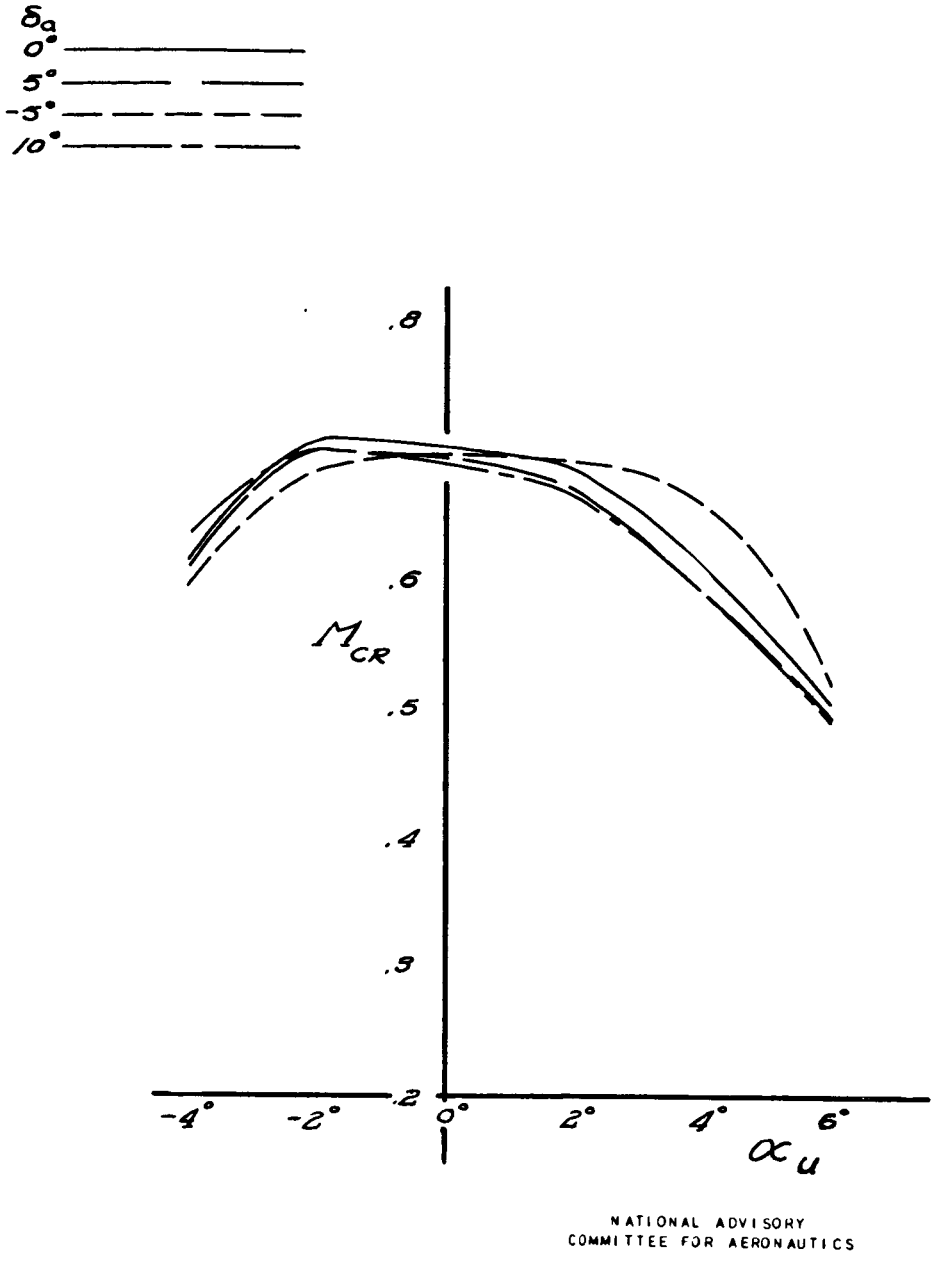

FIGURE 49:- VARIATION OF CRITICAL MACH NUMBER WITH ANGLE OF ATTACK FOR SEVERAL AILERON DEFLECTIONS ON THE MODEL WITH AMES FILLETS. MODEL COMPLETE WITH PRESSURE-TUBE STRUT. WING STATION 28.50.

MR No. A6D03

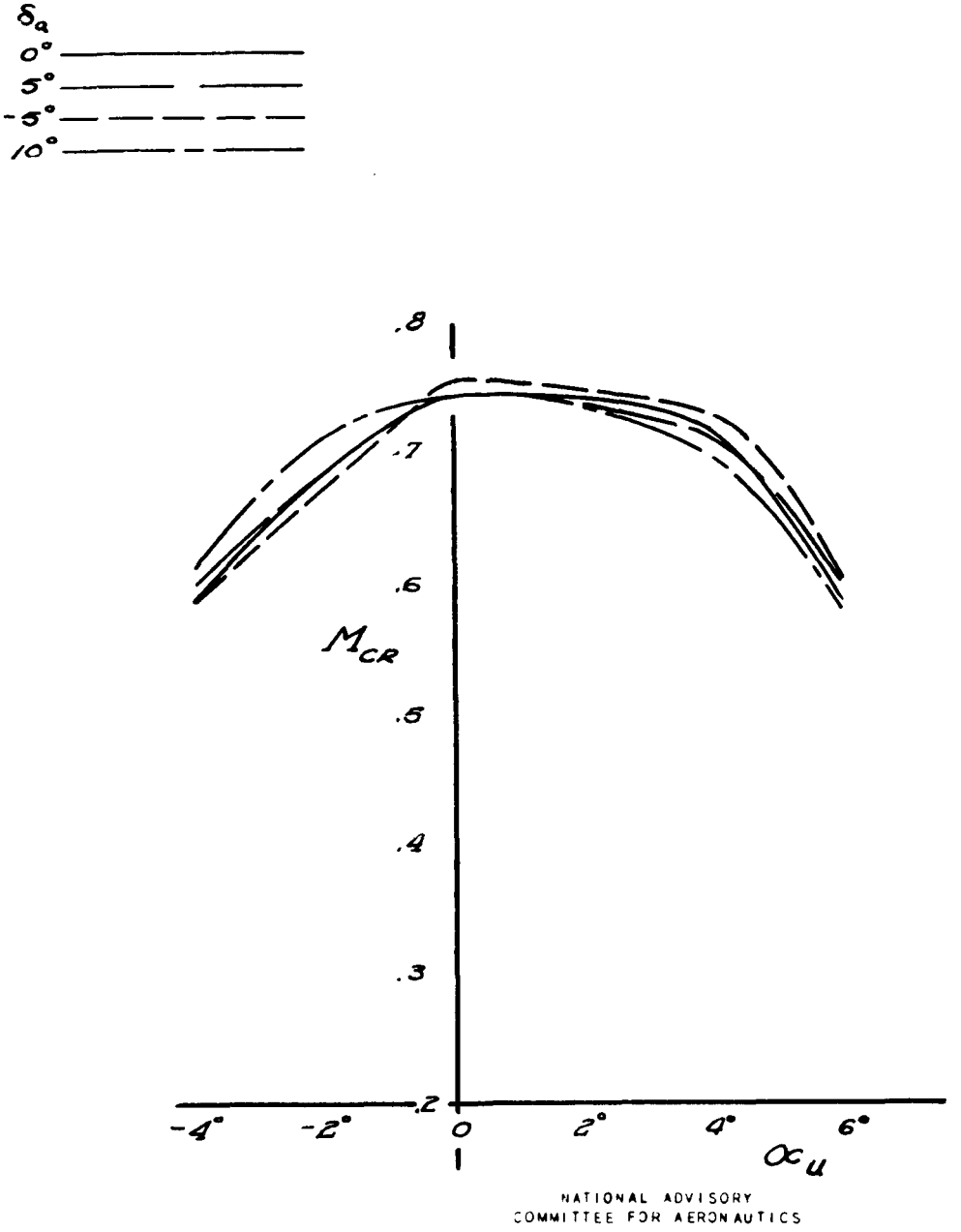

FIGURE 50:- VARIATION OF CRITICAL MACH NUMBER WITH ANGLE OF ATTACK FOR SEVERAL AILERON DEFLECTIONS ON THE MODEL WITH AMES FILLETS. MODEL COMPLETE WITH PRESSURE-TUBE STRUT. WING STATION 41.00 .

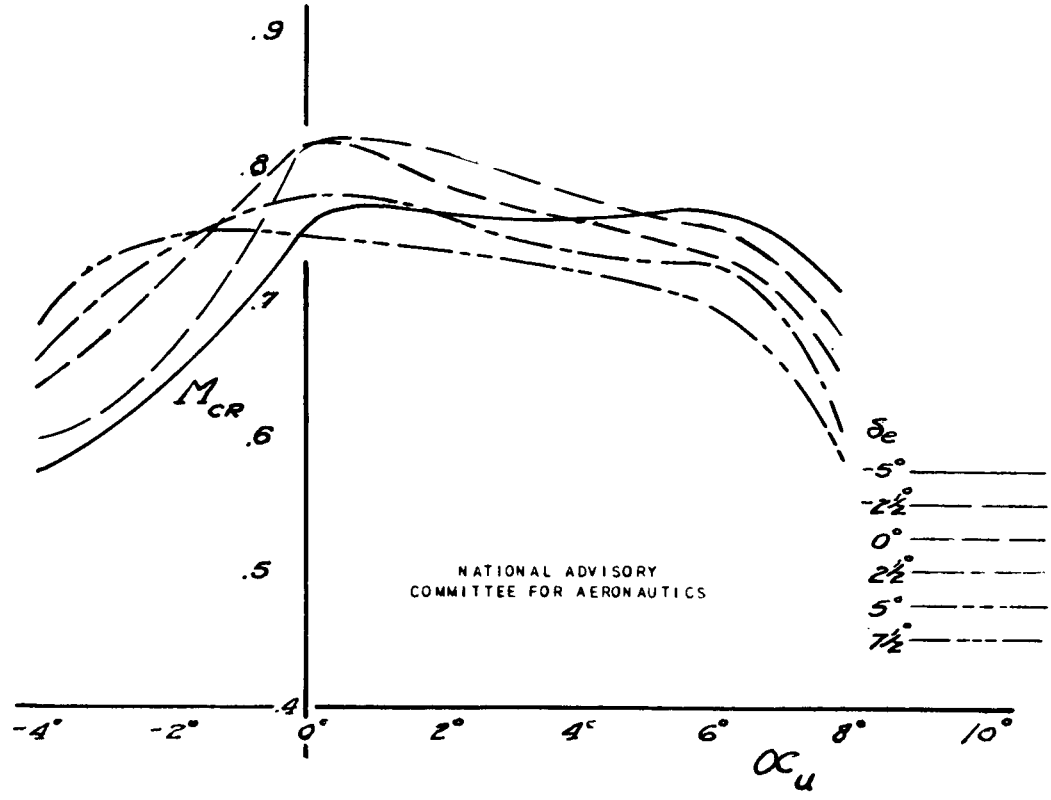

FIGURE 51:- VARIATION OF CRITICAL MACH NUMBER WITH ANGLE OF ATTACK FOR SEVERAL ELEVATOR DEFLECTIONS OF THE 32.8-PERCENT-CHORD ELEVATOR ON THE MODEL WITH THE MANUFACTURER'S FILLETS. MODEL COMPLETE WITH PRESSURE-TUBE STRUT. HORIZONTAL-TAIL STATION 3.00.

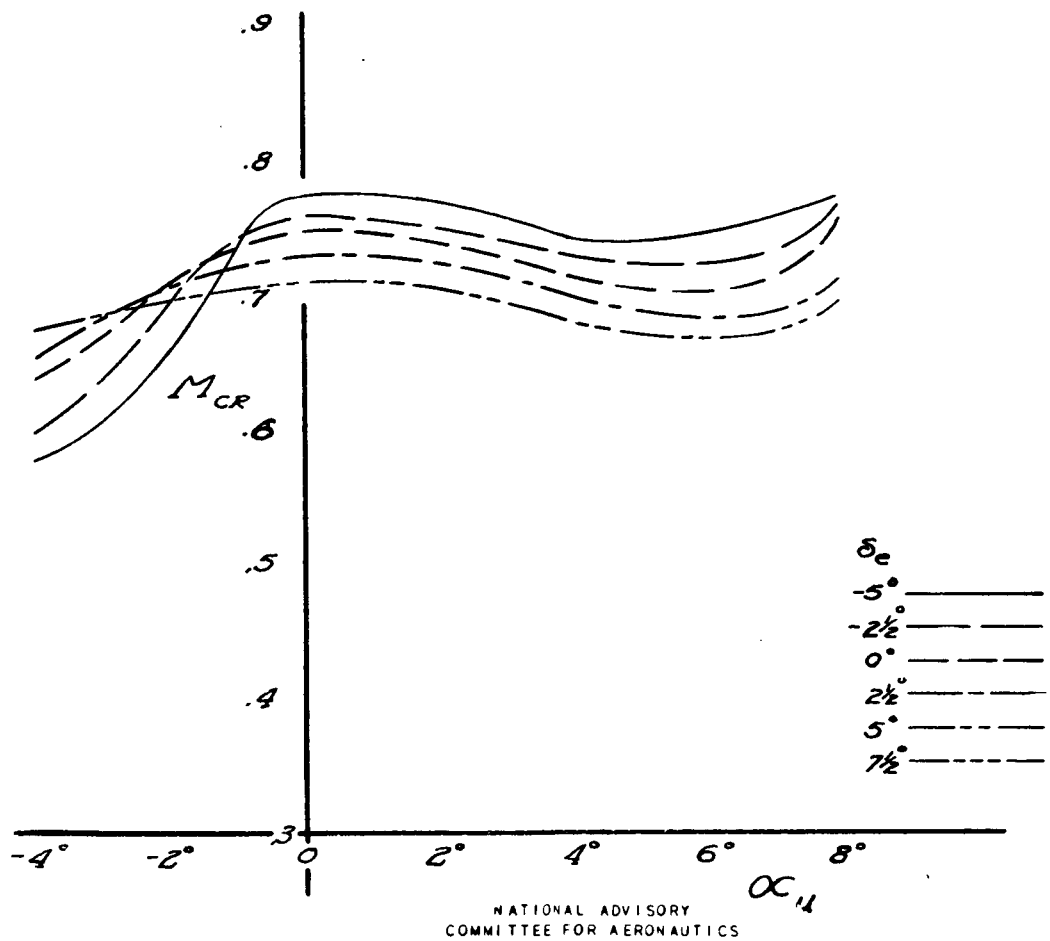

FIGURE 52:- VARIATION OF CRITICAL MACH NUMBER WITH ANGLE OF ATTACK FOR SEVERAL ELEVATOR DEFLECTIONS OF THE 32.8-PERCENT-CHORD ELEVATOR ON THE MODEL WITH THE MANUFACTURER'S FILLETS. MODEL COMPLETE WITH PRESSURE-TUBE STRUT. HORIZONTAL TAIL STATION 16.42.

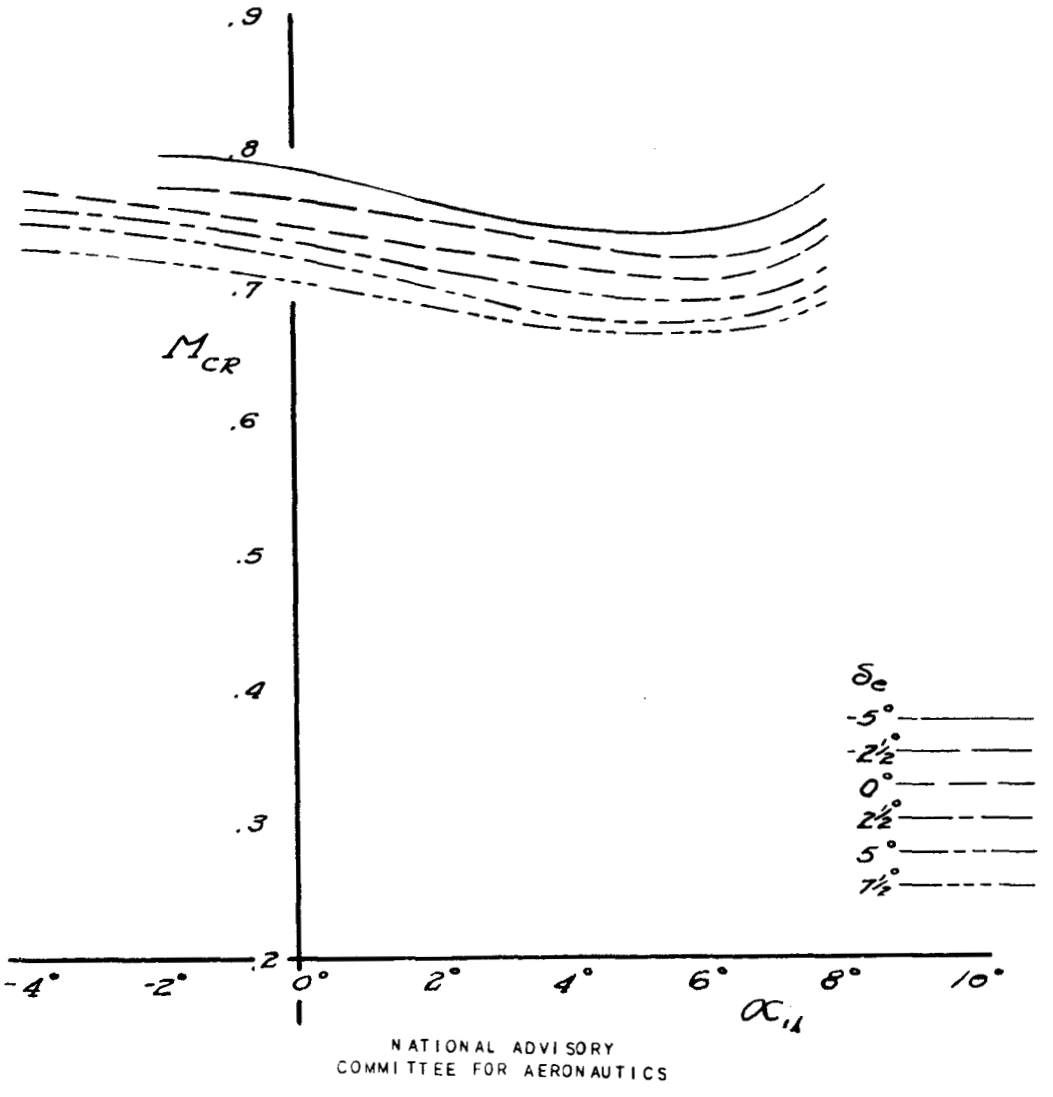

FIGURE 53.- VARIATION OF CRITICAL MACH NUMBER WITH ANGLE OF ATTACK FOR SEVERAL ELEVATOR DEFLECTIONS OF THE 32.8-PERCENT-CHORD ELEVATOR ON THE MODEL WITH THE MANUFACTURER'S FILLETS. MODEL COMPLETE WITH PRESSURE-TUBE STRUT. VERTICAL TAIL STATION 8.884.

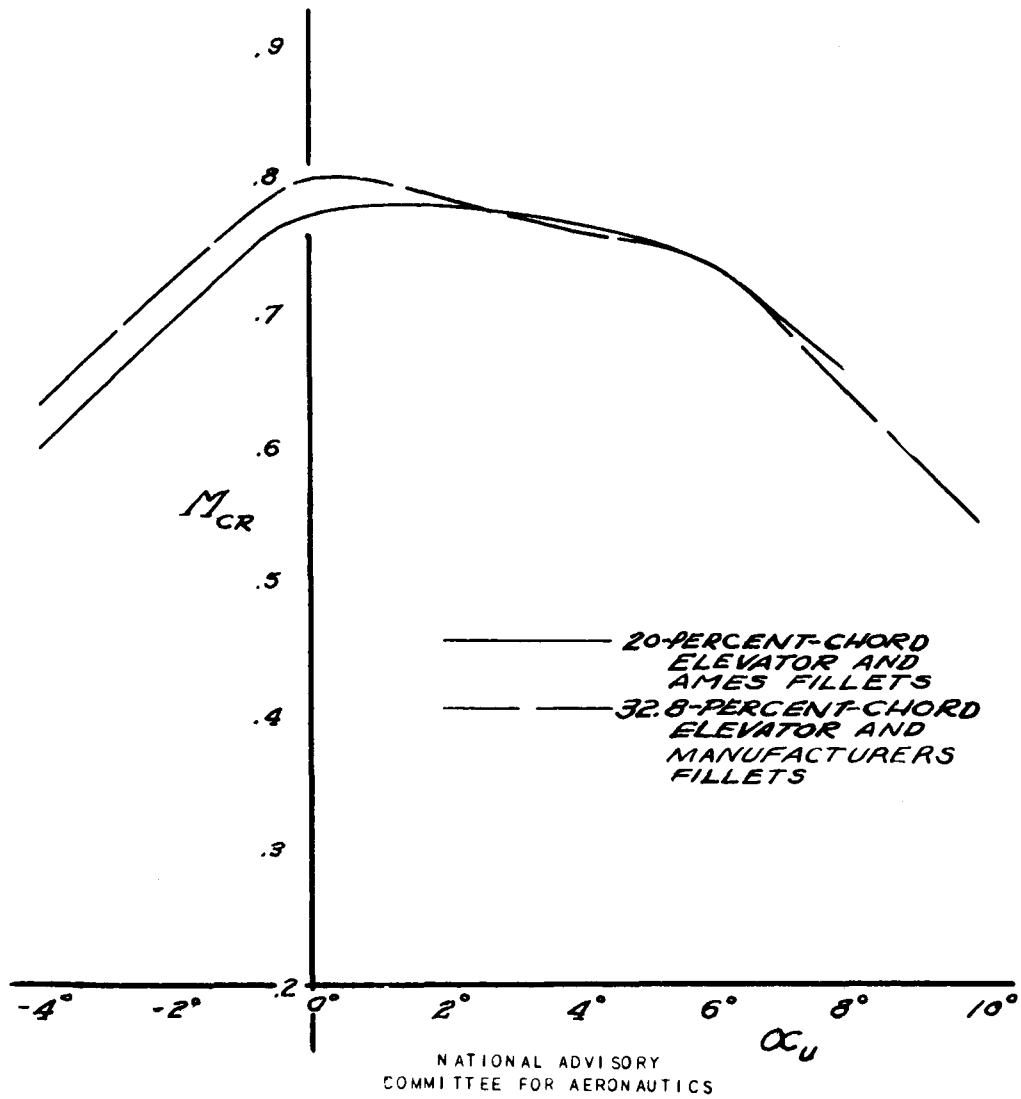

FIGURE 54:- VARIATION OF THE CRITICAL MACH NUMBER WITH ANGLE OF ATTACK FOR TWO DIFFERENT PERCENT-CHORD ELEVATORS ON THE MODEL. MODEL COMPLETE WITH PRESSURE-TUBE STRUT. HORIZONTAL-TAIL STATION 3.00 .

MR No. A6D03

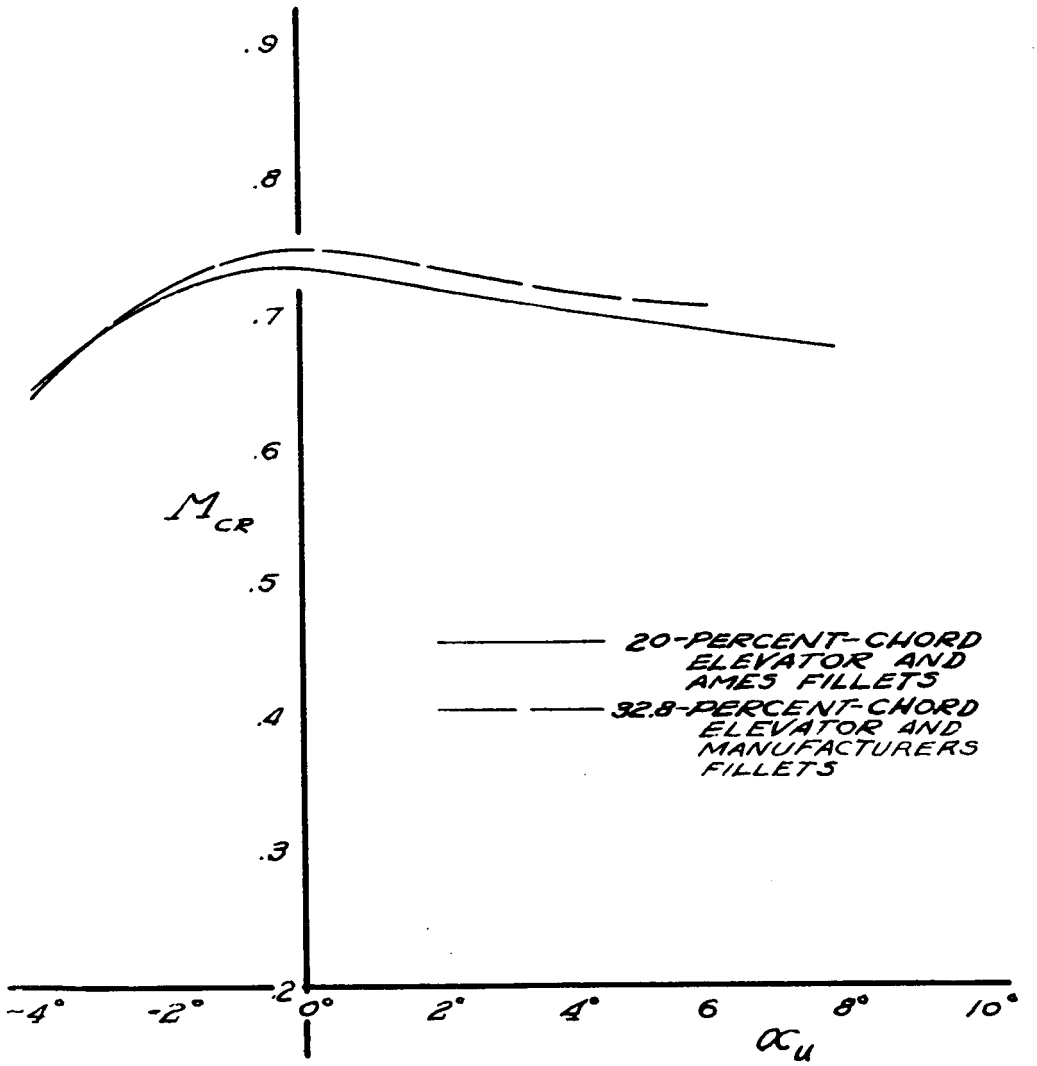

FIGURE 55:- VARIATION OF CRITICAL MACH NUMBER WITH ANGLE OF ATTACK FOR TWO DIFFERENT PERCENT-CHORD ELEVATORS ON THE MODEL. MODEL COMPLETE WITH PRESSURE-TUBE STRUT; HORIZONTAL-TAIL STATION 16.42 .

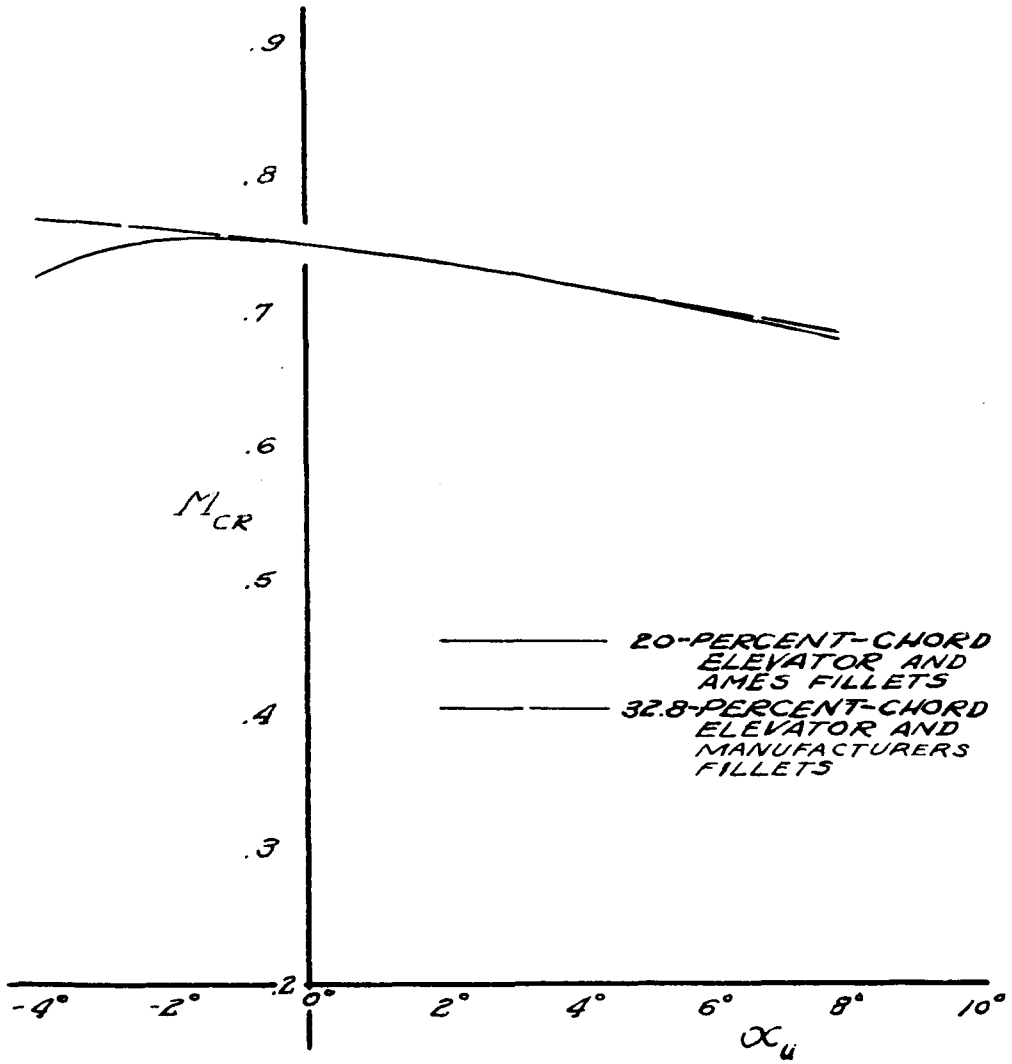

FIGURE 56:- VARIATION OF CRITICAL MACH NUMBER WITH ANGLE OF ATTACK FOR TWO DIFFERENT PERCENT-CHORD ELEVATORS ON THE MODEL. MODEL COMPLETE WITH PRESSURE-TUBE STRUT. VERTICAL-TAIL STATION 8.89 .

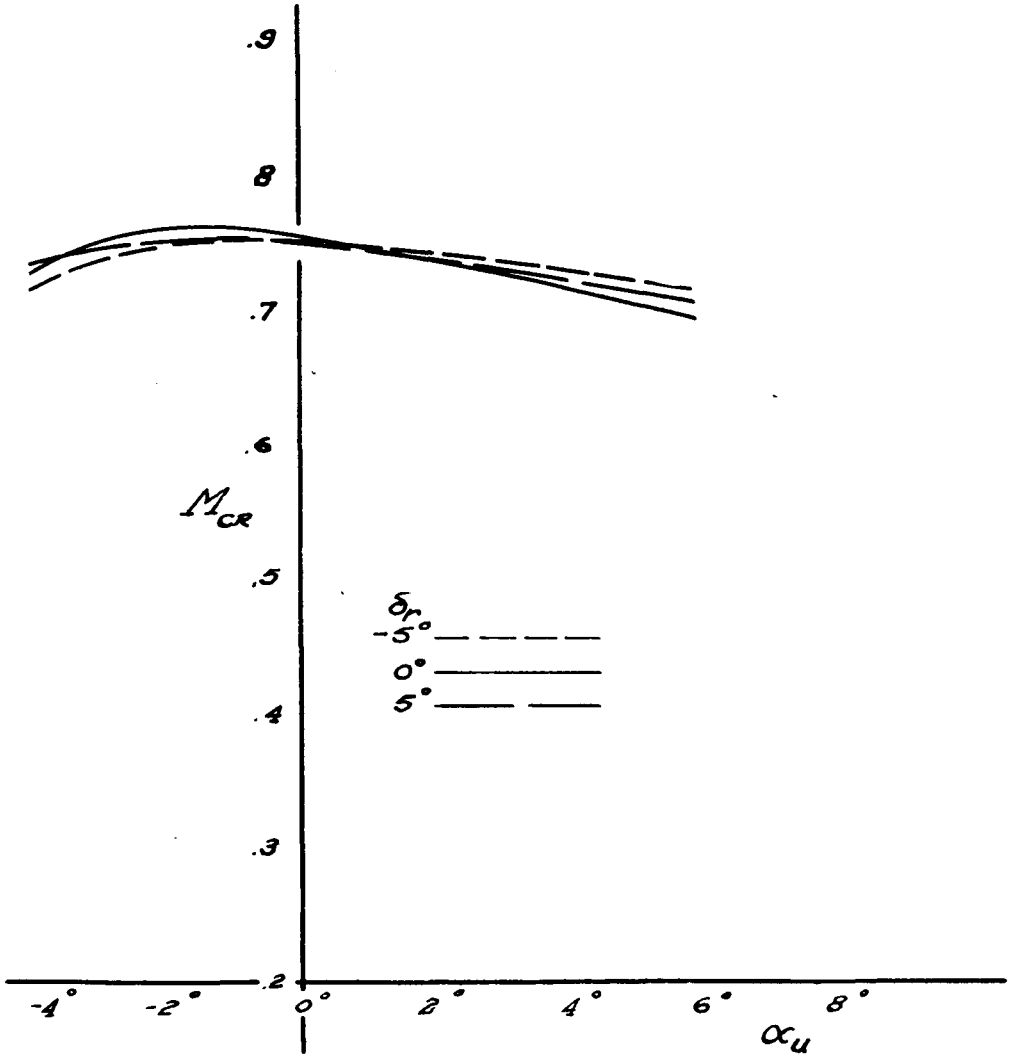

FIGURE 57:- VARIATION OF CRITICAL MACH NUMBER WITH ANGLE OF ATTACK FOR SEVERAL RUDDER DEFLECTIONS ON THE MODEL. MODEL COMPLETE WITH AMES FILLETS AND PRESSURE-TUBE STRUT. VERTICAL TAIL STATION 8.884.

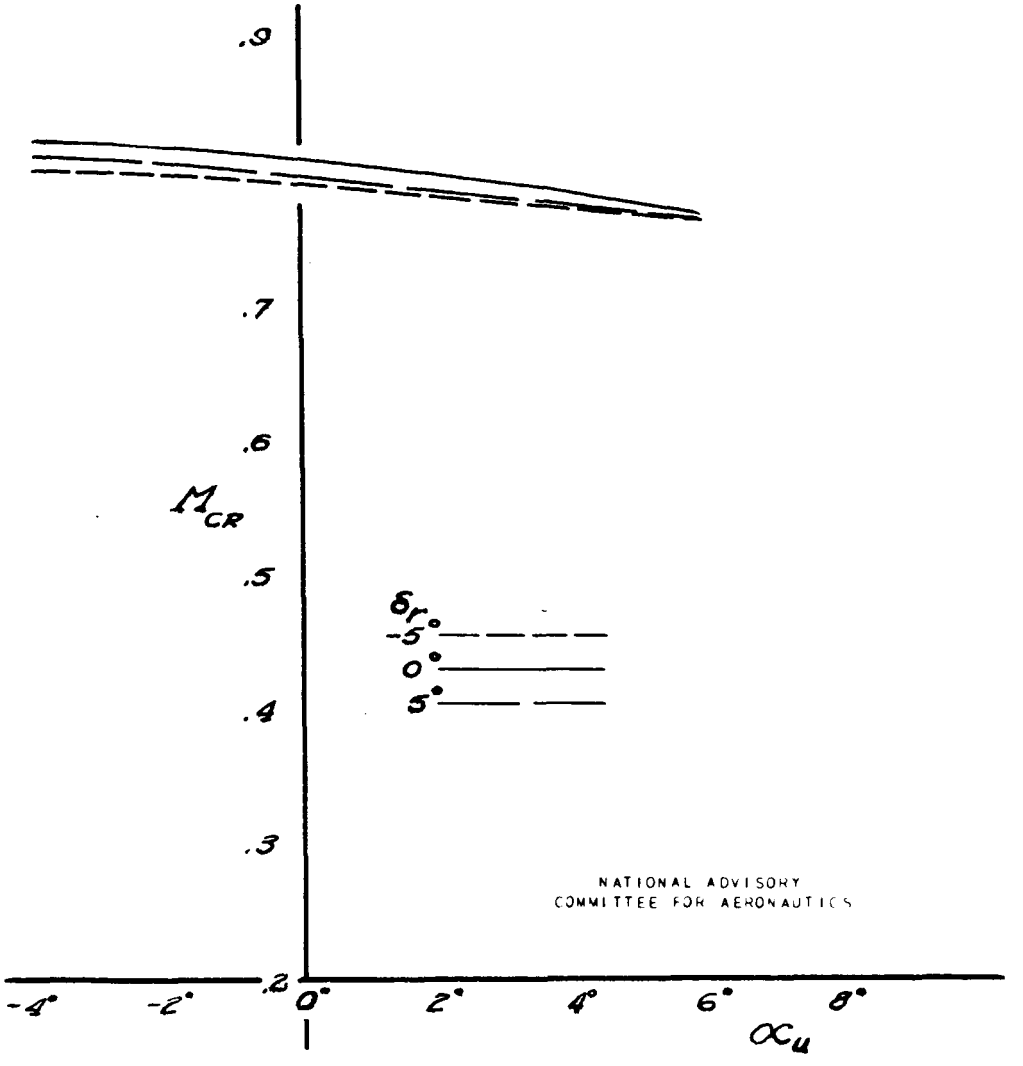

FIGURE 58:- VARIATION OF CRITICAL MACH NUMBER WITH ANGLE OF ATTACK FOR SEVERAL RUDDER DEFLECTIONS ON THE MODEL. MODEL COMPLETE WITH AMES FILLETS AND PRESSURE-TUBE STRUT. VERTICAL-TAIL STATION 16.60.

MR No. A6D03

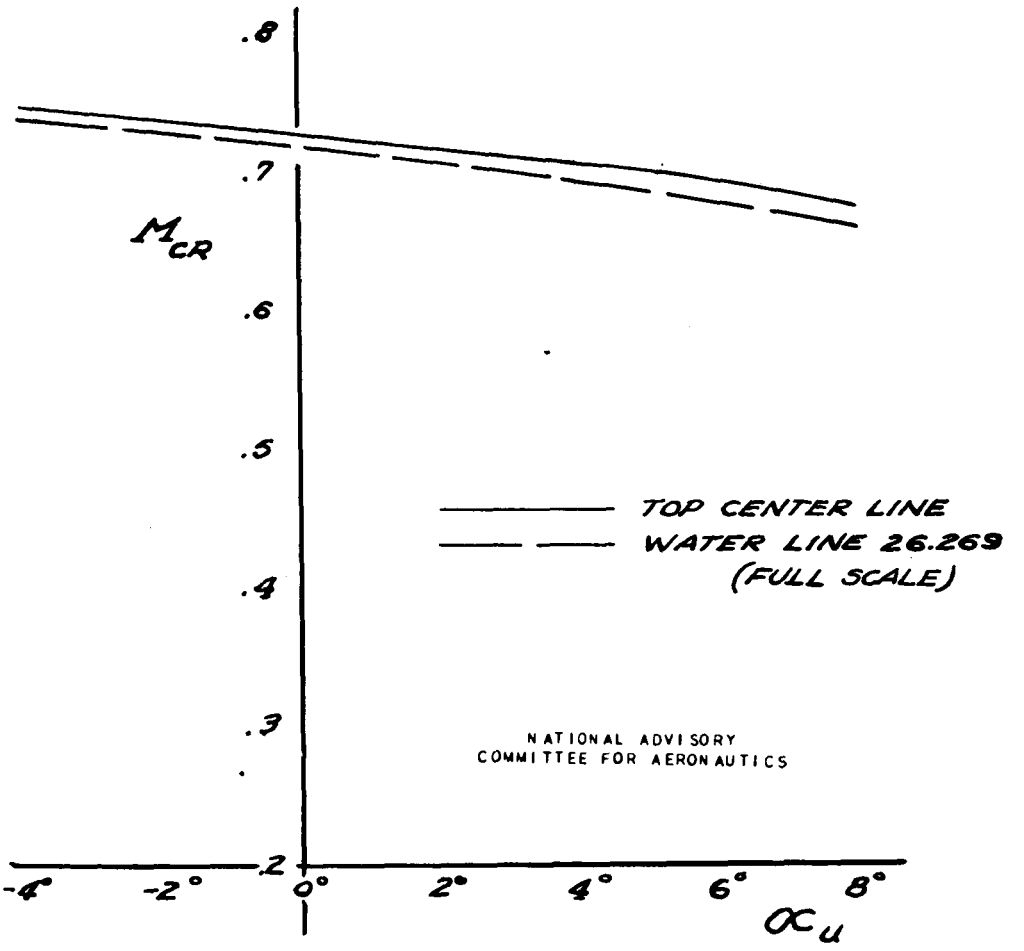

FIGURE 59:- VARIATION OF CRITICAL MACH NUMBER WITH ANGLE OF ATTACK OVER THE CANOPY OF THE MODEL. MODEL COMPLETE WITH AMES FILLETS AND PRESSURE-TUBE STRUT.

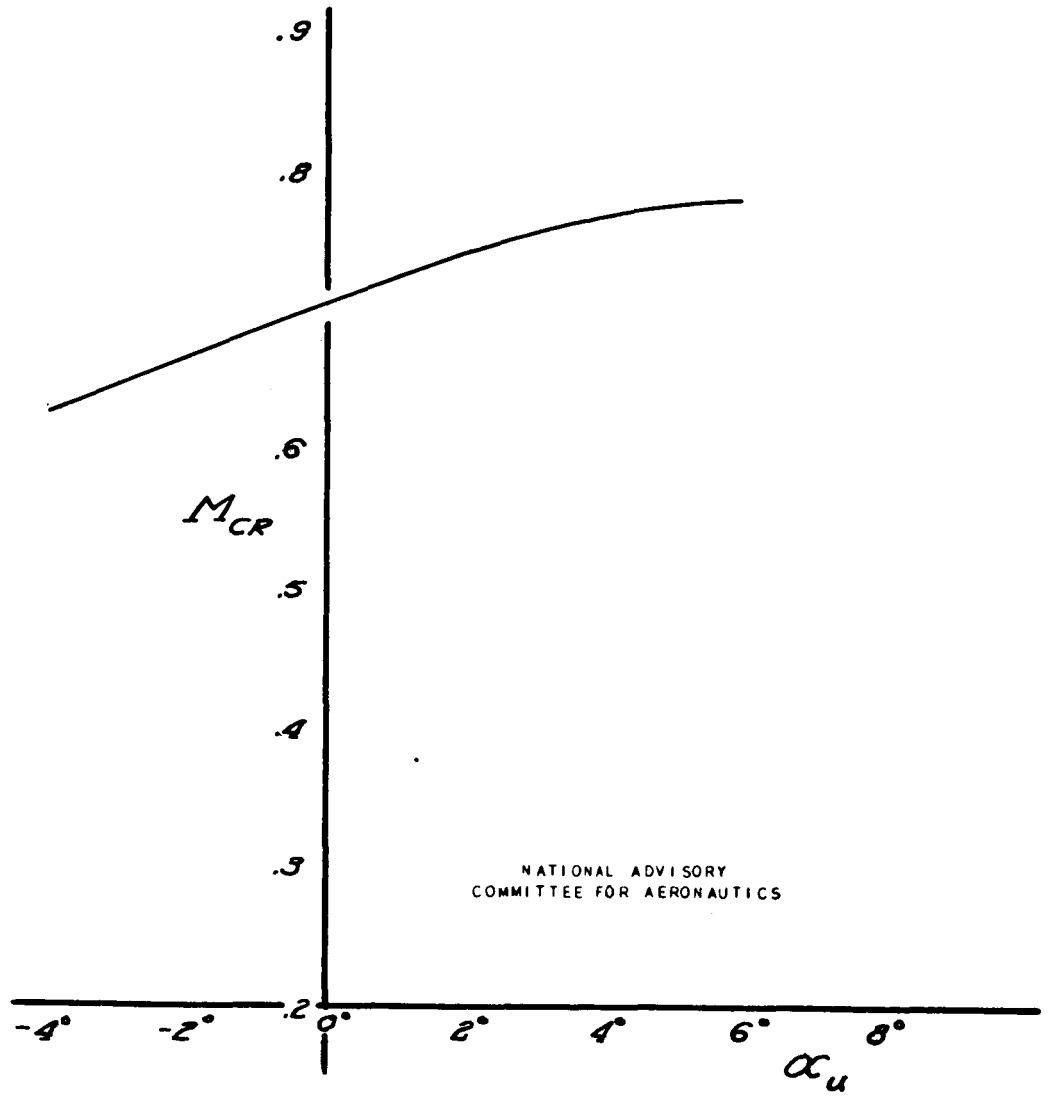

FIGURE 60:- VARIATION OF CRITICAL MACH NUMBER WITH ANGLE OF ATTACK OVER THE ENTRANCE OF THE COOLANT-RADIATOR DUCT ON THE MODEL. MODEL COMPLETE WITH AMES FILLETS AND PRESSURE-TUBE STRUT.